Distribution Agreement

In presenting this thesis or dissertation as a partial fulfillment of the requirements for an advanced degree from Emory University, I hereby grant to Emory University and its agents the non-exclusive license to archive, make accessible, and display my thesis or dissertation in whole or in part in all forms of media, now or hereafter known, including display on the world wide web. I understand that I may select some access restrictions as part of the online submission of this thesis or dissertation. I retain all ownership rights to the copyright of the thesis or dissertation. I also retain the right to use in future works (such as articles or books) all or part of this thesis or dissertation.

Signature:

_____ _____
Phil K. Byun   Date

The Taiman transcriptional coactivator engages Toll signals to promote apoptosis and inter-tissue invasion in *Drosophila*

By

Phil K. Byun

Doctor of Philosophy

Genetics and Molecular Biology
Graduate Division of Biological and Biomedical Sciences
Laney Graduate School
Emory University

_____
Kenneth Moberg, Ph.D.
Advisor

_____
David Katz, Ph.D.
Committee Member

_____
Renee Read, Ph.D.
Committee Member

_____
Iain Shepherd, Ph.D.
Committee Member

_____
Paula Vertino, Ph.D.
Committee Member

Accepted:

_____
Lisa A. Tedesco, Ph.D.
Dean of the James T. Laney School of Graduate Studies

_____
Date

The Taiman transcriptional coactivator engages Toll signals to promote apoptosis and inter-tissue invasion in *Drosophila*

By

Phil K. Byun
B.S., University of Illinois at Urbana-Champaign 2006

Kenneth H. Moberg, Ph.D.
Advisor

An abstract of
A dissertation submitted to the Faculty of the
James T. Laney School of Graduate Studies of Emory University
in partial fulfillment of the requirements for the degree of Doctor of Philosophy in the
Genetics and Molecular Biology,
Graduate Division of Biological and Biomedical Sciences
2018

Abstract

The Taiman transcriptional coactivator engages Toll signals to promote apoptosis and inter-tissue invasion in *Drosophila*

Tissue morphogenesis and remodeling is a tightly choreographed phenomenon fundamental to the development of multicellular organisms. Among the numerous developmental cues that can guide morphogenesis, steroid hormones stand out as distinct from local morphogen gradients for their ability to cause organism-wide transcriptional changes in response to systemic hormonal pulses. In *Drosophila*, the steroid hormone ecdysone (Ec) controls a number of tissue morphogenic events such as fusion of the thoracic discs into an intact dorsal thorax, activation and movement of hemocytes and immune cells, and overall cell growth. Ec exerts these effects by binding to its cognate receptor, the Ec receptor (EcR). Activation of EcR homologs in humans, such as the estrogen and androgen receptors, is often associated with invasive cancers. We have discovered that ectopic expression of an EcR co-activator called *taiman* (*tai*) can transform a normal wing epithelial to invade and penetrate the neighboring thorax. This unique and novel phenotype can be modified using alleles of known genetic interactors of *tai* such as *EcR, yorkie* (*yki*; the nuclear effector of the Hippo pathway), *pvf2* and *pvf3* (PDGF/VEGF related proteins 2 and 3). To ascertain a more complete landscape of the transcriptional changes induced by *tai* expression in invasive wing cells, we performed two different screens: (1) a genetic suppressor screen using genetic deficiencies (deletions) that tile across the entire *Drosophila* 2nd chromosome, (2) and an RNA-sequencing (RNA-seq) analysis of transcripts altered in Tai-expressing pupal wing cells relative to control wings cells. These parallel screens revealed that the Toll and immune

deficient (IMD) pathways, which control expression of innate immunity and apoptotic genes, are active in Tai-expressing cells. Each of these pathways is activated by binding of ligand to cell-surface receptors: the Toll family of receptors is bound by secreted, processed Spätzle (Spz) ligands, and transmembrane peptidoglycan recognition proteins (PGRPs) serve as IMD receptors. We find that Tai expression in wing cells elicits a systemic Toll/IMD response in the absence of a pathogen, a phenomenon referred to as "sterile inflammation" that is often associated with locally invasive *Drosophila* tumors. Based upon published work linking Toll and IMD pathways to competitive killing of neighboring cells by faster growing "super-competitors" that overexpress dMyc, we posited that Tai-expressing wing cells express immune ligands, specifically the Spz proteins, and "kill" their way through the thoracic epidermis and into underlying tissue by activating Toll in these cells. Consistent with this hypothesis, a Toll/IMD reporter is activated in thoracic cells adjacent to invasive Tai-expressing wing cells and this correlates spatially with elevated apoptosis. Moreover, loss of function alleles of factors that act downstream of the Toll receptor dominantly suppress Tai-driven wing invasion. Intriguingly, a strong loss-of-function allele of the IMD pathway inhibitor *caspar* (*casp*) dominantly suppressed Tai invasion, implying that elevated IMD activity can prevent invasion. Upon further investigation, I found that Tai-expression hyper-sensitizes wing cells to *casp* dosage, and that *casp* heterozygosity causes Tai-expressing cells to undergo apoptosis, which in turn prevents them from invading thoracic tissue. These data led to my model that Tai-expressing cells elevate expression of Spz proteins, which kill neighboring cells, and Casp, which protects Tai cells from Spz-mediated death. When Casp is reduced, Tai-expressing cells succumb to Toll-driven cell death. In summary,

these studies show a novel inter-tissue invasion model driven by an EcR co-activator Taiman that non-autonomously induces Toll-mediated killing of neighboring cells but the differing threshold for IMD activation protects Tai-expressing cells from apoptotic fate. Similar mechanism of local invasion is seen in human cancers where pro-inflammatory signals have been linked to invasive behavior of cancer cells, including breast and prostate. In the future, this novel aspect of Tai function may provide insight into immune-based interactions that contribute to the competitive advantage of human tumors overexpressing Tai homologs.

The Taiman transcriptional coactivator engages Toll signals to promote apoptosis and inter-tissue invasion in *Drosophila*

By

Phil K. Byun
B.S., University of Illinois at Urbana-Champaign 2006

Kenneth H. Moberg, Ph.D.
Advisor

A dissertation submitted to the Faculty of the
James T. Laney School of Graduate Studies of Emory University
in partial fulfillment of the requirements for the degree of Doctor of Philosophy in the
Genetics and Molecular Biology,
Graduate Division of Biological and Biomedical Sciences
2018

A few words of reflection and gratitude

My father is an engineer. He has a master's degree in engineering from Yonsei University in South Korea, one of the most prestigious schools in Korea. He has never lost being the top of his class. He worked for a prominent company that makes cellphones and home appliances. When he got offered a position in Chicago, he left his own country and moved his family to Illinois, and when the company told him to go back to Korea, he resigned and started a dry-cleaning business. All of that, so that I could get an education in the US. When he found out I got accepted to Emory for graduate school, he told my mom that he had achieved his American dream. I am not writing to say anything about me or that our family story is anything unique. If anything, it is the opposite. Our family history is a part of every immigrant family's story that comes to the US, looking for a better opportunity. I wanted my parents' story to be written here in the beginning of my dissertation, so I would never forget. So that, at the end of the day, when all is said and done, I should just feel lucky that I was able to get here and move forward, do the thing I love the most.

What Ken said to me a couple years ago still rings in my ear almost weekly. 'Take care of your science, and it will take care of you'. I am extremely lucky to have met Ken and been trained under him. I could not ask for a better mentor. He is an incredible teacher and always demonstrates his ideals, rather than being pedantic or condescending. Of course, he is skilled, he is knowledgeable, and he is experienced. But what I respect the most about Ken is his attitude about science, his humility and his expectation to be surprised by nature, never thinking he is above nature.

I want to thank all my lab mates, both past and present. I especially want to thank Dr. Seth Kelly, Dr. Jacob Kagey, Dr. Brian Robinson, Dr. Danny Barron, Dr. Rick Bienkowski, Dr. Can Zhang, and Dr. Joanna Wardwell-Ozgo, for all of whom I have tremendous respect. Seth and Jacob have talked about teaching and research with such passion that all of it rubbed off on me. Can is a solid rock in the lab, the master of everything technique related, and a brilliant scientist who gives the best advice. Joanna is an amazing friend and mentor, both in science, in life, and in faith.

I want to thank all my committee members, Dr. Paula Vertino, Dr. David Katz, Dr. Renee Read, and Dr. Iain Shepherd. They have all been so valuable in pushing the project forward and asking me tough questions. I also want to thank the GMB program, all the faculty, all my colleagues who have gone before and are coming up.

Lastly, I want to thank my family, especially my wife Minhae who has lived up to her wedding vows to the tee, stayed up late nights waiting for me to get home, visiting me in lab with food, and taking care of my sanity when everything seemed to go crazy. I love you so much.

To my family
whose sacrifice and love
I will never be able to repay

Soli Deo Gloria!
Galatians 1:5

Table of Contents

Chapter 1

Introduction

Cellular movement and tissue invasion as a biological question

The dynamic interactions between cells and the extracellular environment can result in the movement of cells through the surrounding environment. The pathways and proteins that are involved in this complex process can act cell-autonomously or non-cell autonomously on surrounding cells and extracellular matrix to allow for the movement of cells. This process is necessary for normal development. During gastrulation, embryonic epiblast cells delaminate and invade dorsally into the hypoblast cell layer. This also occurs in embryonic patterning and convergent extension when the intercalating cells elongate along an axis [1-3].

The phenomenon of invasion can occur as a single cell invasion or as part of a group, or 'collective'. One of the most well studied examples of single cell migration is the epithelial-to-mesenchymal transition (EMT), which was first observed during sea urchin gastrulation. During this process, ectodermal cells within the primitive streak lose their epithelial shape, detach from neighbors and become mesenchymal [4]. Individual mesenchymal cells extend filopodial extensions to pull themselves towards the underlying hypoblast [5]. Studies of collective cell migration have been accelerated by the genetic analysis of invasive behavior of a group of follicle cells in the *Drosophila* ovary border cells (BCs) [6]. These studies have revealed that collective invasion is a complex phenomenon that requires communication between cells within the group, as well as between cells and the extracellular environment [7]. For example, collectively invading cells must maintain adhesion between themselves while maintaining an invasive, mesenchymal-like state [8]. A complex set of cell-cell communication arrays and signaling pathways are required to govern tissue invasion and to respond to extracellular

cues such as chemoattractants that guide the invasive behavior of single cells or clusters of cells.

The same secreted proteins and signaling pathways that are involved in developmental invasion are also involved in the pathological invasion of cancer cells into adjacent tissues and organs [9, 10]. Invasion is an early and obligate step for the metastasis of cancer cells throughout the body. Recent studies have found that metastatic cancer cells share key traits with cells in developmentally programed forms of collective cell migration [11]. The traditional understanding of metastasis favored a model by which individual epithelial cells lose adhesion and polarity and increase expression of matrix metalloproteinases (MMPs) that breakdown the extracellular matrix (ECM) and the basement membrane. However, *in vivo* observation of cancer cell invasion finds groups of cells that express few of the classic markers of metastasis [11]. Migrating groups of cancer cells can be heterogenous and include tumor-associated macrophages that provide cytokines and nutrients that modulate the ability of the cells to invade the surrounding tissue [12, 13]. The study of relationship between immunity and oncogenesis is a blooming field and has the potential to provide an additional perspective into how cancer cells become metastatic [14].

In this dissertation, I examine the genetic and molecular mechanism behind epithelial tissue invasion driven by steroid hormone receptor co-activator *taiman* (*tai*) in the model organism *Drosophila melanogaster*. *tai* encodes a well conserved transcriptional regulatory protein that serves as a co-factor for the ectysteroid hormone receptor EcR (ecdysone receptor). It was first described as a necessary gene for the proper migration of BCs in *Drosophila* [15]. Here, I will describe my unexpected

discovery that Tai expression is sufficient to transform normally sessile wing epithelial cells into an invasive tissue that penetrates into the adjacent thorax. I will present evidence describing molecular mechanism behind this invasion, which links Tai to Toll-induced cell competition within the context of a pathologic model of tissue invasion. This work may serve as a model to understand the role of Tai human homologs in locally invasive cancers. The following is an introduction to the terms and concepts used in this dissertation.

Features of *Drosophila melanogaster*

Before discussing how *Drosophila* has been used, and is still being used, to uncover the genetic mechanism behind cell motility and tissue invasion, a short description of what makes *Drosophila melanogaster* such an attractive genetic model system is appropriate. With six Nobel Prizes and countless seminal discoveries, *Drosophila* melanogaster has proved to be one of the best genetic systems used for the investigation of many biological processes. One of its best features is its short life cycle and fecundity. Coupled with tractable, visually apparent phenotypes, genetic analysis using *Drosophila* is easily managed. From genetics standpoint, flies share more than 70% of the disease-causing genes in humans and has been successfully used to model human disease because *Drosophila* exhibit many of the parallel disease-driven phenotypes as humans. Lastly, the vast amount of genetic tool-kits allows for tissue specific and temporally controlled genetic alterations.

Border cell migration and cancer metastasis

Drosophila eggs develop inside an egg chamber made up of supporting polyploid cells called nurse cells, surrounded by follicle cells that line the exterior. Upon a developmental cue at the end of egg development (stage 8), a pair of pole cells located at the anterior end of the egg chamber recruit 4-8 neighboring follicle cells to form a migrating cluster of cells termed border cells (BC) [16]. These cells begin to move at the start of stage 9 and by the end of stage 10 of egg development, the border cell cluster arrives near the egg [17]. The purpose of border cell migration is to create an entry way through which a sperm fertilizes the egg. Thus, a common phenotype that that results from defective border cell migration is female infertility [6].

From a cursory view of the border cell migration, it resembles how cancer cells become motile and invade the surrounding tissues and enter the bloodstream. However, the molecular markers of border cell migration do not resemble known metastatic, neoplastic markers of cancer cells [11]. One of the main characteristics of neoplasia is the loss of cadherins and loss of adhesion. In contrast, there is an increase in the expression of cadherins and cell adhesion in BC migration [18]. In fact, cadherins are required for directionality; cadherin loss leads to border cell clusters unable to properly migrate towards the oocyte resulting in BC migrations toward the edges of the egg chamber [18-20]. Similarly, the loss of polarity seen in neoplasia is not seen in border cell cluster. Yet, the border cell clusters appear mesenchymal with cytoplasmic extensions, while simultaneously maintaining strong adhesion with the pole cells (**Figure 1.1**). Therefore, BC migration falls into a different category of cell motility called collective cell migration and is a good example of cluster cell migration where the adhesion within the

cluster is maintained, and the leader cell directs the group toward a certain direction provided by an external stimulus (i.e. Pvf1; *Drosophila* homolog of human PDGF/VEGF) [21]. Another example of collective migration is the branching of *Drosophila* trachea directed by fibroblast growth factor receptor (FGF) gene *branchless* (*bnl*) and FGF receptor *breathless* (*btl*), which guides the invasion of tracheal tissue into flight muscles [22]. *btl* is a downstream target of C/EBP gene *slow border cells* (*slbo*) and is required for BC migration as well [23]. Wound healing is yet not example of collective migration where two sheets of epithelia migrate towards each other to close the wound [11]. Collective migration events appear vastly different from single-cell invasion of cancer cells. Nonetheless, pathways implicated in controlling border cell migration and other examples of collective cell migration such as the Notch pathway, the PDGF/VEGF-like pathway, and the JAK/STAT pathway have strong links to oncogenesis and cancer metastasis (**Figure 1.1**) [6, 20, 23-29].

Studies into cancer microenvironment, a heterogeneous tumor mass made up of mixture of tumors cells and various host cell types, reveal that some cancer cells gain the ability to invade via tumor-associated macrophages that are part of the tumor microenvironment rather than becoming invasive on its own [30, 31][[12, 13]. This suggests that oncogenic tissue invasion has a significant overlap with collective cell migration mechanistically. Therefore, investigations into how cancer cells adopt the mechanism of collective cell migration in relation to their environment is an important area of research pertaining to metastasis.
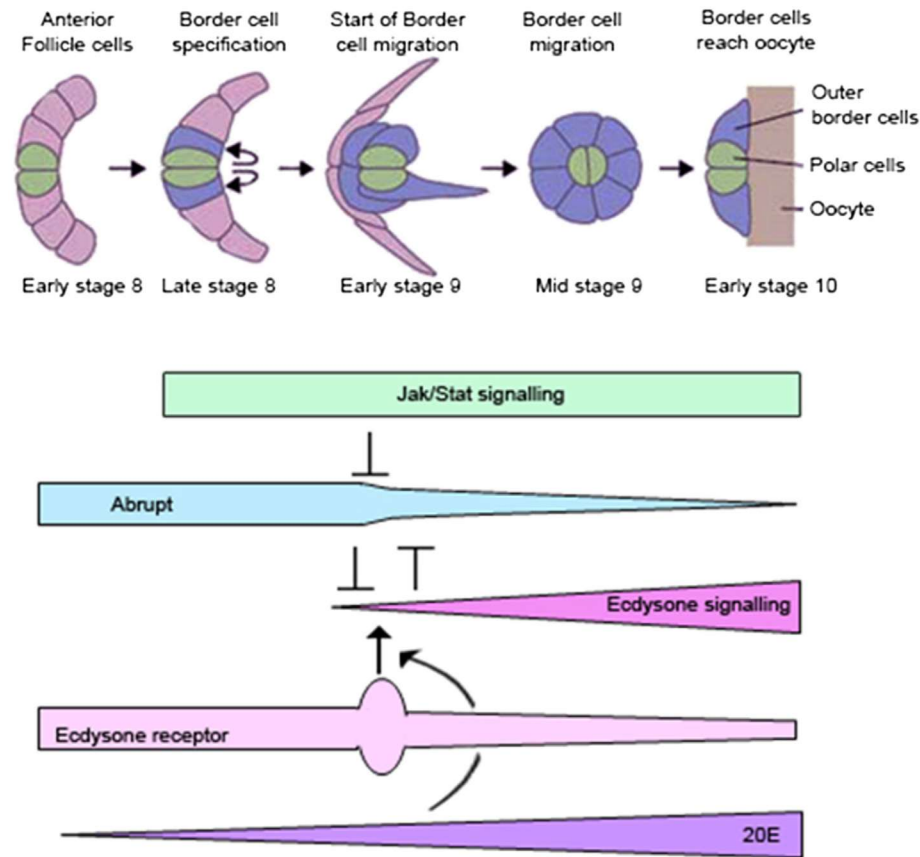
Figure 1.1 Border cell migration in *Drosophila* egg development.
Diagram of stages of border cell migration and various inputs that control it. Determination starts in the early stage 8 and delamination starts early stage 9. By stage 10, border cell cluster has arrived at the oocyte. This process is an interplay between the JAK/STAT pathway and the EcR. While the increase in ecdysone signaling is required, JAK/STAT provides de-repression of ecdysone signaling via inhibiting Abrupt. Abrupt is a BTB-POZ domain protein that binds to Taiman for inhibition and decreases Ecdysone signaling output [32]

Figure is adapted from [33]

Taiman and Ecdysone Receptor

An important pathway that governs border cell migration is the *Drosophila* steroid hormone ecdysone signaling pathway which includes the hormone ecdysone, its receptor, Ecdysone Receptor (EcR), and the EcR co-activator Taiman (*tai)*. Before *tai* was identified and mapped, the requirement of steroid hormone signaling in border cell migration was unknown. In *Drosophila*, a pulse of ecdysone that occurs during stage 8 of egg development was discovered to be the developmental cue that initiates border cell migration mechanism [34]. Moreover, pole cells synthesize their own titer of ecdysone by upregulating a series of cytochrome P450 enzymes that belong to a group of genes called the Halloween genes, which converts cholesterol to ecdysone [35-37]. The final enzyme in the pathway is a gene called *shade* which converts ecdysone to 20-hydroxyecdysone, an active form of ecdysone that can bind the EcR and activate gene transcription [37]. EcR forms a heterodimer with Ultraspiracle (Usp) protein, a *Drosophila* homolog of mammalian retinoid-X receptor (**Figure 1.2**) [38]. In the presence of ecdysone, Tai binds to EcR via the two LxxLL domains and recruits additional factors such as histone acetylases to active gene transcription [15]. In the absence of ecdysone, however, EcR complex tightly bound to the nuclear corepressor Smrter (Smr) which indirectly binds to histone deacetylases [39]. This potent repression complex is involved with the regression of chromosomal puffs seen in polytene chromosomes.

Interestingly, *tai* is a homolog of human oncogene Amplified in Breast Cancer 1 (AIB1), also known as steroid receptor co-activator 3 (SRC-3) and related to SRC-1 and -2 [15]. In normal human development and function, SRCs are extensively involved in metabolic control of various organs: controlling food intake signal in the brain,

gluconeogenesis in the liver, fat absorption and fat metabolism in the intestine and the skeletal muscle, and generating heat in adipocytes [40, 41]. In disease, SRC family members as well as steroid hormone receptors (e.g. androgen, estrogen, progesterone, and testosterone receptors) are well-known for their oncogenic effects [40, 42, 43]. In fact, a common and effective treatment for estrogen receptor positive tumors is tamoxifen, an estrogen analogue that binds to the estrogen receptor and inhibits its activity [44]. However, in estrogen receptor negative cancers (ER-), which tend to be more advanced and aggressive, the tumors are tamoxifen resistant. This resistance coincides with heightened SRC activity in tumors and the ability to no longer require hormone titer for oncogenesis [45-48]. How hormone related cancers become steroid hormone independent and how SRC activity contributes to this progression is not well characterized and is an active area of cancer research.

A possible mechanism is the coupling of steroid hormone pathway with the Hippo pathway. Recent publications describe the cooperation of the EcR pathway and the Hippo tumor suppressor pathway, through the co-activator Yorkie (Yki) and its binding partner Scalloped (Sd) in *Drosophila* to drive tissue overgrowth [49, 50]. The physical interaction between Yki and Tai links these two DNA binding complexes at shared target loci and is also required for novel targets of Yki. Evidence suggests that this relationship may be conserved in humans. In human prostate cancers the androgen receptor and YAP1 (mammalian Yki) interact and is responsible for the switch from androgen dependent tumors to androgen independent, castration resistant tumors (chemical or surgical castration is a common treatment for prostate cancers) [51]. Therefore, *Drosophila* is a

powerful model system to elucidate the developmental and pathological consequence of

steroid hormone signaling.
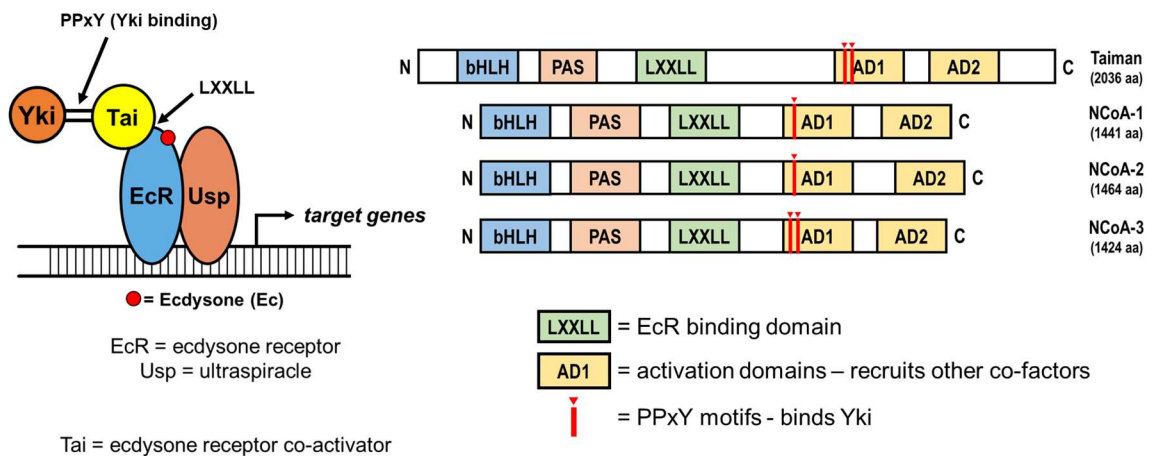
Figure 1.2 Taiman and the Ecdysone Receptor.
In the presence of ecdysone hormone, Tai binds to the EcR via LxxLL domain. EcR transcription complex consists for EcR and Usp heterodimer that sigs on target genes. *Drosophila* Tai is highly homologous to vertebrate NCoA (or SRC) proteins, consistent in the pertinent domains for regulation and activation.

Tissue fusion

Tissue fusion is a developmental phenomenon where neighboring tissues fuse to create one cohesive body structure. These developmental timed fusion events allow for sophisticated organ structures that cannot be achieved via one type of tissue alone. Optic cup, palate, heart, neural tube, and eyelids all require tissue fusion [52]. In *Drosophila*, tissue fusion allows dorsal closure during embryonic development as well as the formation of the thorax which is the result two thoracic discs during pupal metamorphosis fusing together [53]. The thorax closure (disc fusion) is partially controlled by a gene *broad* [54]. Flies with mutations in the *broad* locus has a number of developmental defects including disc fusion defects. The *broad* locus is a well-known target of the ecdysone/EcR target. Interestingly, many of the tissue fusion events coincide with high-titer of ecdysone in the animal. Considering that tissue rearrangement and disc fusion require various cellular mechanisms such as adhesion, migration, and apoptosis, it is logical to conclude that ecdysone signaling would, at least in part, control disc fusion [55]. Not all tissue fusion events are benign, however, some can be pathologic like in the case of locally invasive tumor tissue spreading into adjacent normal tissue in late stage cancers [56].

The Hippo pathway

The Hippo pathway is a highly conserved tumor suppressor pathway most known for its role in growth control (**Figure 1.3**) [57]. Since its discovery in the early 1990s, its implication in various biological processes is expansive, ranging from stem cell maintenance, wound healing, to the immune system [58-60]. Main components of the pathway include the kinase cascade of Salvador (Sav), Warts (Wts), Hippo (Hpo), and the downstream nuclear effectors Yki and Sd that sit on target loci to turn on transcription (**Figure 1.4**) [61]. Upstream regulators of the Hippo pathway include but are not limited to mechanical tension, loss of contact inhibition, and loss of apical polarity [62, 63]. In the absence of any stimulus, Wts kinase phosphorylates Yki on multiple serine sites causing Yki sequestration to the cytoplasm for degradation [64]. In the presence of upstream stimuli, Wts is phosphorylated by Sav and Hpo complex, leading to its inactivity. Yki, free of phosphorylation, is enters the nucleus for gene activation. Mutations that converts key serine residue to alanine (Serine111, S168, and S250; S168 mutation has the strongest effect) result in a constitutively active form of Yki which is unable to be phosphorylated by Wts kinase [65, 66]. This chronic activity is pathological. Transgenic expression of the constitutively active form of Yki in the *Drosophila* eye leads to a gross overgrowth of the tissue [65].

In the nucleus, the co-activator Yki binds several transcription factors including Sd, Teashirt, and Homothorax to drive the expression of pro-proliferative and pro-survival genes which include *dmyc, cyclin E, diap1,* pro-proliferative microRNA *bantam,* and its upstream inhibitor *expanded* [67, 68]. Additionally, Yki binds the steroid hormone receptor co-activator Tai and their physical binding is necessary for novel targets: *piwi,*

nanos, and *dilp8* [49]. *Nanos* and *piwi* are required for germline stem cell maintenance [69, 70]. *Drosophila* insulin-like peptide 8 (Dilp8) is expressed by an injured tissue to delay the developmental timing until the damaged tissue can be repaired [71, 72]. Developing tissues coordinate proper symmetry by secreting Dilp8. Mutant animals exhibit fluctuating asymmetry phenotype where the wings of the same animal are different sizes [73]. Interestingly, Yki and Tai can function differently in varying cellular contexts. They can cooperate to regulate in growth control, but in BC migration, Yki activity is antagonistic by negatively regulating JAK/STAT ligand Upd which disrupts actin polymerization. [74, 75].
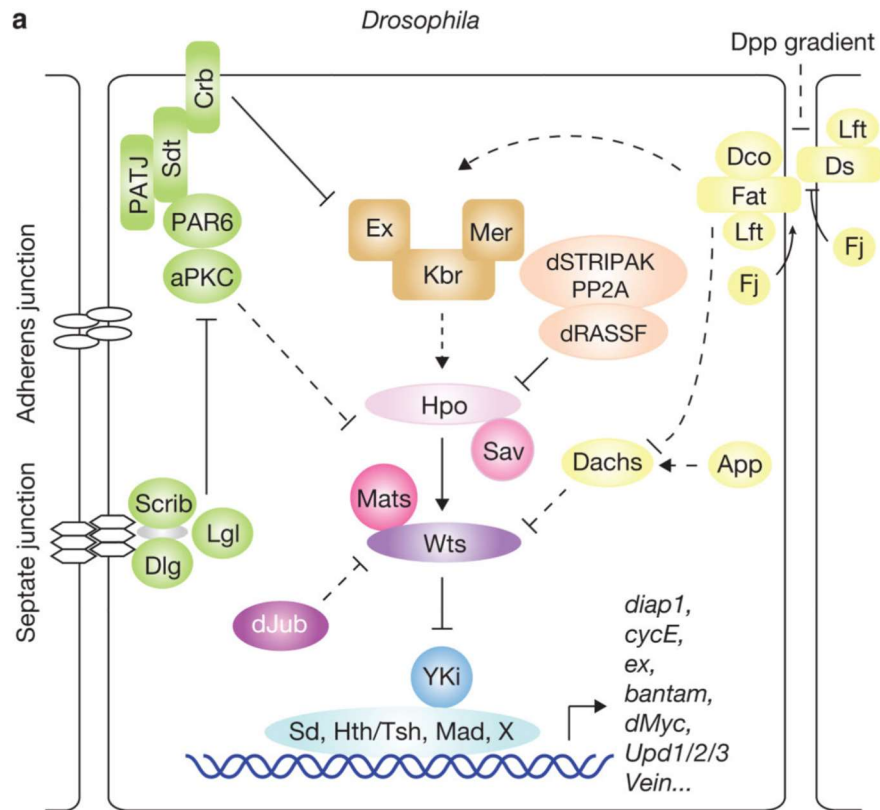
Figure 1.3 the Hippo tumor suppressor pathway
The core kinase cassette consists of Sav, Hpo, Mats, and Wts that phosphorylate Yki for cytoplasmic retention and eventually degradation. Upon external stimuli such as the loss of apical polarity (Crb), activity of Wts can no longer be sustained and un-phosphorylated Yki enter the nucleus for gene activation. Yki has multiple binding partners in the nucleus to turn on various pro-proliferative and pro-survival genes including *diap1, cycE, ex,* and *bantam.*

Figure adapted from [76]

Apoptosis and caspases in *Drosophila*

Proper organ size control is the balance between cell growth and cell death, more specifically, programmed cell suicide called apoptosis. The first step in oncogenesis is initiated by pushing the balance towards cell growth and inhibiting cell death. This is illustrated by the fact that almost all cancers lose both copies of pro-apoptotic factor *p53* [77]. One of the well-known Yki targets is *Drosophila* inhibitor of apoptosis 1 (*diap1*) [78] which inhibits both the initiating caspase Dronc and effector caspases Drice and DCP-1 by direct binding [79, 80]. Interestingly, both caspases and caspase inhibitors are constitutively expressed in most cell types. Therefore, in response to pro-death signal, caspase inhibitors must be inhibited to allow for the activation of caspases. The pro-apoptotic genes *grim, reaper,* and *hid* all reside in a conserved regulatory region [81, 82] and their gene products inhibit Diap1 to promote apoptosis (**Figure 1.4**).

The biological relevance of caspases goes beyond their role in apoptosis and they have well defined functions in non-apoptotic processes, most notably in border cell migration [29, 83]. In a screen that aimed to discover genes in Rac-dependent motility (BC migration is a Rac-dependent motility), the overexpression of Diap1 (expressed by *thread* locus) rescued motility defect in Rac dominant negative allele, suggesting that Diap1 promotes motility [29]. This effect is caused by the inhibition of Dronc by Diap1, though the basal level of Dronc activity also seems to be required for proper Rac activity and border cell migration. The apoptosis independent roles of caspases and Diap1 are important elements to consider when examining the upregulation of Diap1 expression by Tai or Yki, in that, it could be functionally relevant beyond being a pro-survival cue.
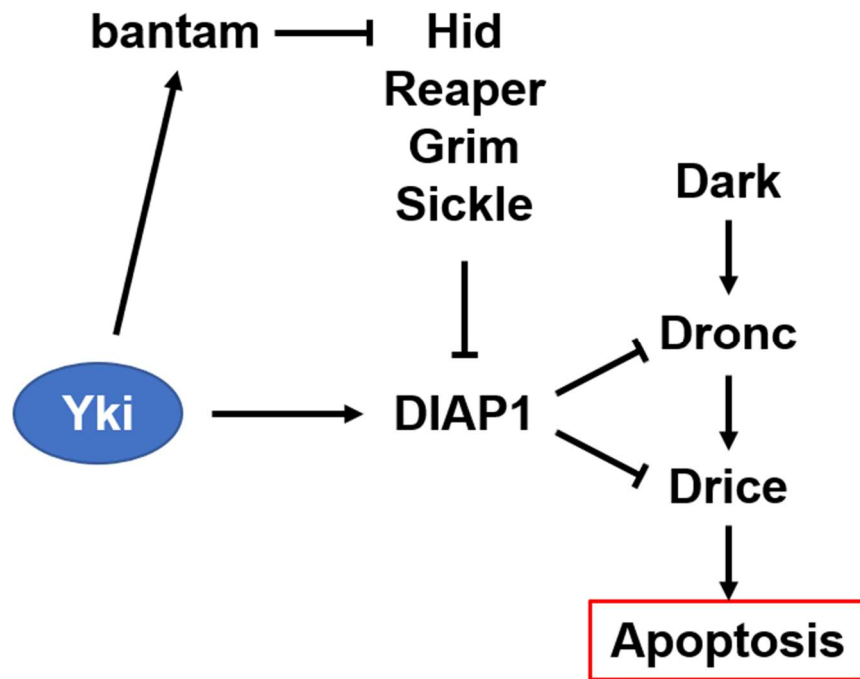
Figure 1.4 Regulation of Apoptosis in *Drosophila*
DIAP1 protein is ubiquitously expressed in most cell types, keeping the initiating caspase
Dronc and effector caspase Drice/DCP-1 off. Upon apoptotic stimuli, pro-apoptotic
factors such as Hid, Reaper, Grim, and Sickle inhibit DIAP1, releasing Dronc and
Drice/DCP-1 from inhibition, leading to apoptosis. Nuclear effector of the Hippo
pathway Yki turns on *diap1* and *bantam* pro-survival miRNA which inhibits pro-
apoptotic factors.

Innate immunity in *Drosophila*

Drosophila has been successfully used to uncover the mechanisms of innate immunity because of it lacks the complexity of an adaptive immunity found in mammals. In *Drosophila,* as with most living organisms, the first line of defense is the epidermis, the larval and adult cuticle. Once microbes are detected, a systemic immune response results in the production of antimicrobial peptides (AMPs) in the fat body, a major lymphatic tissue in *Drosophila*. This activation promotes hemocyte proliferation and differentiation (cells of hematopoietic lineage) to clear the infection through phagocytosis or encapsulation coupled with melanization [84-86]. In *Drosophila*, innate immunity is governed by the Toll and IMD pathways, the two NF-κB signal transduction pathways with their own recognition patterns. (**Figure 1.5**) [87]

The Toll pathway components were initially discovered as factors that affected dorsoventral axis formation. The downstream effector of Toll pathway *dorsal* (*dl*) is named so because the loss of function mutation of *dorsal* led to the dorsalisation of the entire embryo with no ventrally fated cells [84, 88, 89]. However, it was soon realized that the Toll pathway is a crucial part of innate immunity [90]. The Toll pathway recognizes fungal and Gram-positive bacterial infections [85]. Distinct from its vertebrate relatives, Toll receptor does not directly bind components of pathogens but instead bind to a cleaved form of cysteine-knot ligand Spätzle (Spz) [91]. Spz protein exist in the extracellular membrane as pro-Spz which is then cleaved by the serine protease Spz processing enzyme (SPE) upon microbial detection. This process is inhibited by the serine protease inhibitor Necrotic (Nec) [92]. *nec* loss of function leads to hyperactivation of Toll signaling and melanized spots throughout the animal. In the case of Toll

activation, inhibitor of NF-κB (IκB) family protein Cactus is degraded, which allows Dl and Dorsal related immunity factor (Dif) to enter the nucleus to turn on gene targets such as the antimicrobial peptide Drosomycin (Drs) [93, 94].

The mediation between pathogen recognition and immune response is done through hemocytes. There are three types of hemocytes in *Drosophila*: lamellocytes which encapsulate and melanize foreign tissue, plasmatocytes for phagocytosis, and crystal cells for oxidative enzymes [95]. Once hemocytes recognize the presence of pathogens, a forward feedback loop is activated. Hemocytes express Spz and signal to the fat body for increased production of AMPs, which in turn, promotes Spz expression. Hemocytes also receive signals from the JNK pathway and the Notch pathway for differentiation and proliferation [96, 97].

Unlike the Toll pathway, which functions in innate immunity and developmental patterning, the IMD pathway solely functions to defend against Gram-negative bacterial infection. The main receptor for the IMD pathway is peptidoglycan recognition protein-LC (PRGP-LC) but other PGRPs can activate the IMD pathway [98]. Upon its activation, the transcription factor Relish (Rel) enter the nucleus for gene activation. Interestingly, for Rel to be activated, it must be phosphorylated and cleaved. This cleavage is carried out by the caspase Dredd and is inhibited by is Caspar (Casp, **Figure 1.5**) [99, 100].

The connection between innate immunity and a caspase is interesting because a recent publication has shown that the aberrant hyperactivation of innate immune pathways leads to cell death and provides a mechanism behind cell-competition [101]. Myc expressing cells [102] ('winner' cells) express Spz proteins to activate Toll signaling in the neighboring wild-type cells ('loser' cells). This leads to Dorsal turning on the pro-

apoptotic gene *rpr* and inhibition of DIAP1, an inhibitor of apoptosis. In parallel, IMD activation turns on another pro-apoptotic gene *hid*. A slight imbalance in the rate of growth that favors supercompetitor expression at the expense of wild-type cells could drive the growth of premalignant tumors.
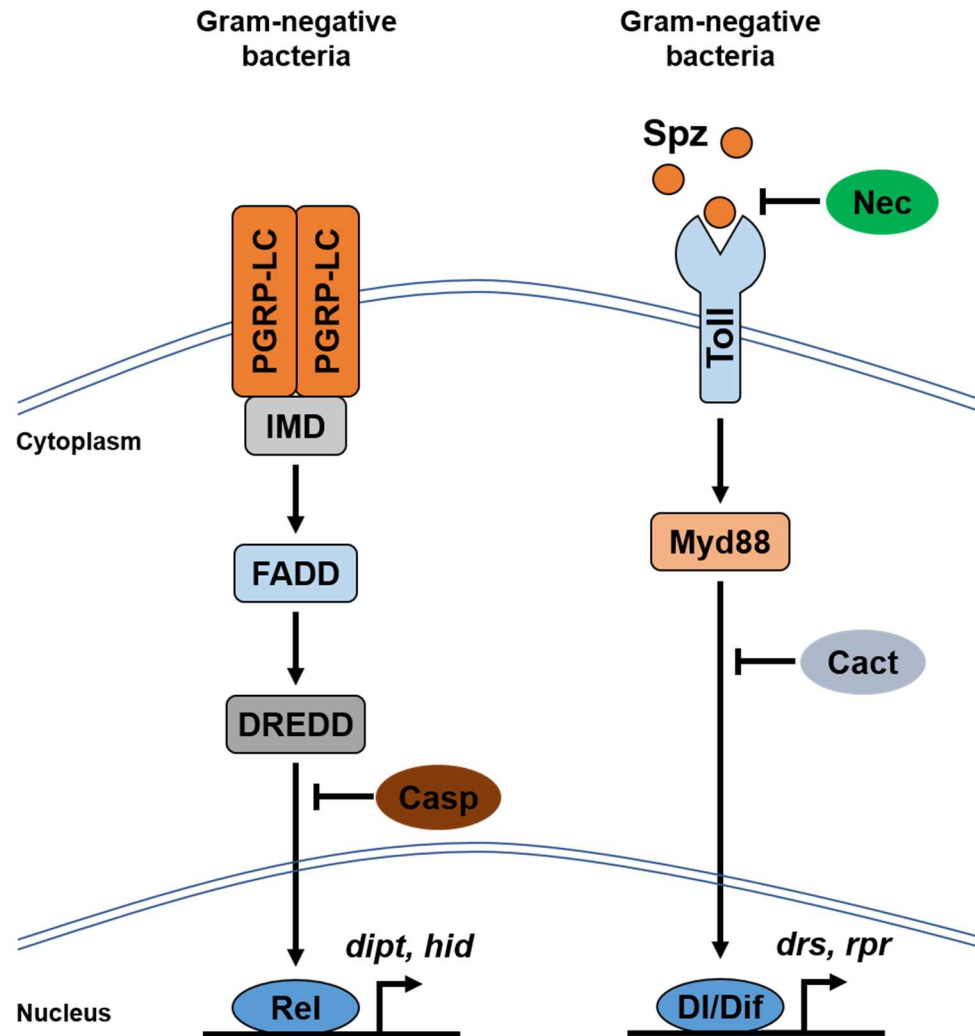
Figure 1.5 The Toll and IMD pathways in *Drosophila*
IMD pathway consists of the receptor PGRP-LC that is activated upon Gram-negative bacterial infection, culminating in the NF-κB homolog Rel relocating into the nucleus to turn on antimicrobial peptide *diptericin (dipt)*. IMD pathway is inhibited by an IκB homolog Casp that prevents DREDD cleaveage of Rel, preventing nuclear localization. A Toll receptor is activated by a cleaved form of Spz protein. Pro-Spz to Spz cleaveage is inhibited by a Serine Protease Inhibitor (SERPIN) Nec. Upon Toll activation, Dl/Dif complex localizes to the nucleus and turns on *drosomycin (drs)*. Another IκB homolog Cact binds to Dl/Dif, preventing nuclear localization. Recent work has shown that pro-apoptotic genes *hid* and *rpr* can be activated by excessive IMD and Toll activation, respectively.

Sterile Inflammation

Innate immunity does not always fight against pathogens or external stimuli. It can be used as a surveillance mechanism for the overall fitness and integrity of tissues [101]. Wounding of a tissue or the abnormal growth of tumorigenic cells elicits a systemic immune response, known as sterile inflammation (**Figure 1.6**) [14]. In such cases, damaged tissue (whether by mechanical trauma, hypoxia, or malignant tumors) cause various intracellular components to become extracellular. These component are collectively known as damage associated molecular patterns (DAMPs) and they include f-actin, double-stranded DNA, ATP, mitochondrial components and reactive oxygen species (ROS) [14]. These DAMPs can signal to hemocytes and the fat body which lead to the production of *Drosophila* TNF-α homolog Eiger. Eiger activates JNK in the cells in the periphery of hemocytes and can promote hemocyte associated tumor invasion rather than tumor regression [96, 103]. This hemocyte driven cell motility is crucial in the context of tissue repair and wound healing [104, 105]. In addition, the importance of steroid hormone signaling and the Hippo pathway in the proper development and activation of innate immunity has been shown in some studies, however more studies are needed to fully understand this connection [60, 106-109].
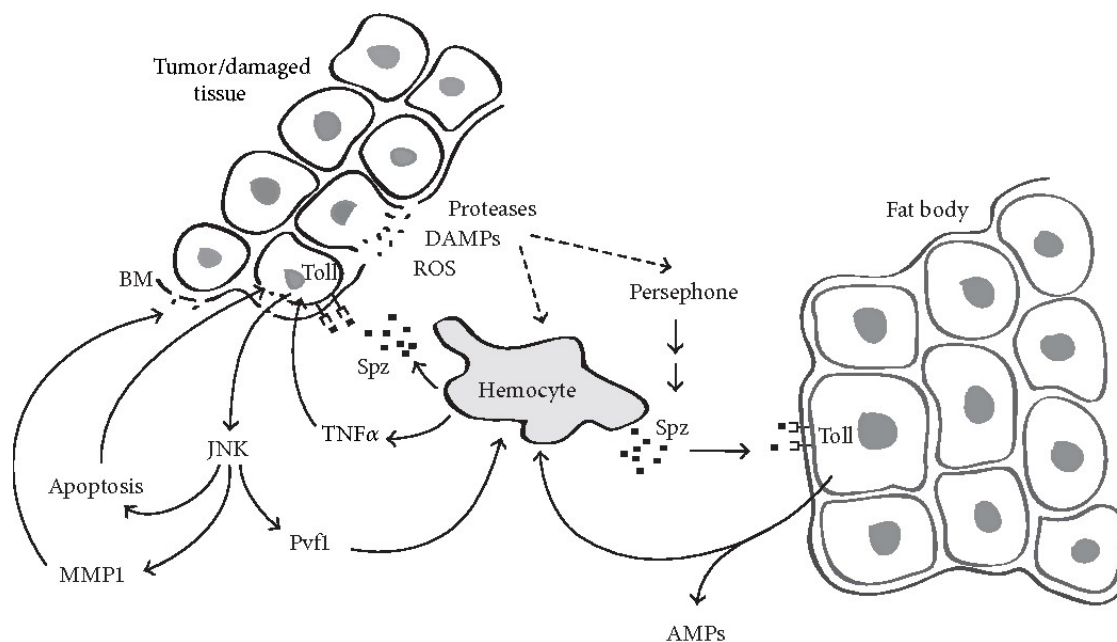
Figure 1.6 Sterile Inflammation
Inflammation in the absence of infection but due to either damaged tissue or a tumor. Various proteases, damage associated molecular patterns (DAMPs), and reactive oxygen species (ROS) trigger an immune response in hemocytes that leads to Spz production and cleavage. Spz expressed by hemocytes activate Toll in the fat body, leading to the production of AMPs that further elicits the immune response in hemocytes. Association of hemocytes with a damaged tissue can result in JNK activation leading to apoptosis and basement membrane degradation by matrix metalloproteinase 1 (MMP1) which breakdown Collagen IV.

Adapted from [14]

Chapter 2

The Taiman transcriptional coactivator engages Toll signals to promote apoptosis

and inter-tissue invasion in *Drosophila*

This chapter was adapted from the following paper in review:

Byun PK, Zhang C, Yao B, Wardwell-Ozgo J, Terry D, Peng J, Moberg KH. *The Taiman transcriptional coactivator engages Toll signals to promote apoptosis and inter-tissue invasion in Drosophila.* Curr Biol. (*in review*)

Introduction

Certain tissues in developing organisms fuse with neighboring structures to generate elements of the mature body plan. These types of developmentally programmed fusion events occur in the mammalian optic cup, palate, heart, neural tube, eyelids and body wall[52]. In invertebrates such as the fruit fly *Drosophila melanogaster*, fusions between the sac-like epithelial primordia of adult structures are required to form anatomical structures such as the thorax[53]. In most of these cases, fused tissues make shared contributions to a single common structure. However, fusion can also involve intercalation of tissues that retain distinct identities. These events can be pathologic, as occurs during the invasion of tumor tissue into adjacent normal tissue during late stage cancer, or physiologic, as occurs during invasive growth of the syncytiotrophoblast into the uterine wall following blastocyst implantation[110, 111].

A number of factors and pathways associated with invasion of one tissue into another have been identified through studies of locally invasive cancers. In breast and prostate cancers, the steroid receptor coactivator protein SRC-3 (steroid receptor coactivator-3), also referred to as Amplified in Breast Cancer-1 (AIB1) or Nuclear Receptor Coactivator-3 (NCOA-3), acts as an oncogene to promote cell proliferation and survival, but is also associated with invasion of transformed cells into surrounding stroma[112-114]. The *Drosophila* protein Taiman (Tai), which is the sole *Drosophila* homolog of SRC-3 and the related proteins SRC-1 and SRC-2, is part of a network of transcription factors that drive epithelial cells transformed by a combination of activated Ras (Ras^{V12}) and *scribble* (*scrib*) loss to invade into adjacent organs (e.g. eye epithelium into brain)[115]. Tai promotes transcription of genes involved in proliferation and

survival through a physical interaction with the Hippo pathway coactivator protein Yorkie (Yki), and cooperates with excessive Yki activity to induce germline stem cell genes in committed wing epithelial cells[49]. Intriguingly Tai is required along with its cognate transcription factor, the ecdysone receptor (EcR), for invasion of a group of posterior follicle cells (border cells; BCs) through the oocyte nurse cells[15]. However, it is not clear whether a common mechanism underlies this developmentally programmed invasion and the pathologic invasion of Ras^{V12}, scrib transformed epithelial cells.

Here we isolate the role of Tai in pathologic intertissue invasion using the *Gal4/UAS* system[116] to overexpress Tai in cells of the developing wing blade. Surprisingly, Tai expression is sufficient to transform the distal portion of the pupal wing into an invasive tissue that breaches the thoracic cuticle and penetrates deeply into underlying tissue in late-stage pupae and adults. Genetic and transcriptomic analysis of this phenomenon reveals links to known Tai-interacting pathways (e.g. EcR and Hippo), but also uncover roles for the Toll innate immune pathway and non-cell autonomous apoptosis as required facilitators of intertissue invasion. Wing:thorax invasion is blocked by alleles of Toll components or by reducing expression of the pro-apoptotic factors Reaper (Rpr), Grim and Head involution defective (Hid). Modeling this phenomenon within the larval wing epithelium confirms that Tai-expressing cells kill neighboring cells via a mechanism that relies on the Toll and immune deficiency (IMD) pathways, and involves induction of *hid* and, to a lesser degree, *rpr* mRNAs. Genetic evidence indicates that Tai-expressing cells evade immune-mediated apoptosis by repression of the IMD pathway, which operates in parallel to Toll and can promote apoptosis of epithelial cells[101, 117-119]. These data provide evidence that immune signals contribute to the

ability of Tai to drive intertissue invasion and killing of non-transformed neighboring cells and indicate that the threshold for IMD activation determines the sensitivity of Tai-expressing cells to apoptotic signals that operate locally at boundaries with normal cells.

Results

Tai expressing wing cells penetrate the thoracic cuticle

Gal4 lines that direct Tai overexpression to multiple tissues and stages (e.g. *engrailed-Gal4*) result in pupal lethality[49]. To bypass this effect and observe the effect of Tai transgenes on a single adult tissue, the wing-specific *MS1096-Gal4* (*Bx-Gal4*) line was used to express Tai in committed wing cells. The *MS1096* line directs Gal4 expression in the dorsal half of the larval pouch and in the full pupal pouch[120, 121]. Approximately 90% of *MS1096>tai* animals die as pharate adults (n=83) with survivors displaying malformed and crumpled wings with distal ends embedded into thoracic cuticle immediately anterior to the haltere (**Figure 2.1A-B**). This "embedded wingtip" phenotype is highly penetrant among eclosed adults (>90% of survivors at 25°C) and accompanied by a slightly raised ring of cuticle around the site of wing:thorax contact (inset in **Figure 2.1B**). Consistent with the temperature sensitivity of the Gal4/UAS system[116], the *MS1096>tai* embedded-wingtip phenotype is absent at 18°C (**Figure 2.1C**).

Physical penetration of adult *Drosophila* wing tissue into the thorax (hereafter termed 'invasion') has not to our knowledge been reported previously. However defects in the developmental process of disc eversion can cause retention of the adult wing inside the thorax[122]. Disc eversion is normally complete by 4-6hrs after puparium formation (APF)[123, 124]. To assess whether the *MS1096>tai* phenotype could result from incomplete eversion, the architecture and positioning of GFP-labeled *tai*-expressing wing discs (*MS1096>tai,GFP*) were assessed by confocal microscopy of 12hr APF pupae, well

鰷　　î　　　　î　　　　î　　　　î　　*鰷*　　儀□ Ĥ晉⌐阁瘡 Ũ瘢Ā

MS1096>tai,GFP wing discs are visible just under the operculum cuticle (dotted line, **Figure 2.2)**, which is consistent with complete wing disc eversion. *MS1096>tai,GFP* discs are larger and extend more posteriorly than *MS1096>GFP* discs, likely due to the pro-proliferative effects of Tai [49, 115, 125]. These findings argue that *MS1096>tai* discs evert after the larval-pupal transition, but subsequently engage in pathologic invasion of the adjacent thorax.

To exclude the possibility that *MS1096>tai* wingtip invasion is due to cryptic Gal4 expression in a tissue other than the wing disc, two additional pouch Gal4 lines, *nubbin-Gal4* (*nub*) and *rotund-Gal4* (*rn*), were combined with the *UAS-tai* transgene. The *nub>tai* and *rn>tai* genotypes each produce an *MS1096>tai*-like phenotype when reared at 25°C (**Figure 2.1D,E**). To assess whether Tai-driven wingtip invasion is an indirect consequence of excessive cell proliferation, *nub-Gal4* was used to overexpress the pro-growth transcription factors Myc or Stat92E[102] [126], or to deplete the growth suppressors Hippo[78] or Pten[127, 128] by RNA-interference (RNAi). Although these genotypes produced enlarged wings (data not shown), they fail to embed into the thorax (**Figure 2.4A**), indicating either that tissue overgrowth is not sufficient to account for the ability of Tai to transform the wing epithelium into an invasive tissue, or that an additional factor (e.g. the pupal pulse of 20E) cooperates with Tai to drive invasion. In this regard, overexpression of the disc-enriched EcR isoform *EcR.A* or knockdown of the EcR-associated Myb/SANT-domain repressor *Smrter* (*Smr*) were each insufficient to drive wing invasion by themselves (**Figure 2.4A**). Thus, Tai seems to be fairly unique in its ability to cause the embedded-wingtip phenotype.

To confirm that Tai-expressing wing cells penetrate the thoracic cuticle, control (*MS1096*) and *MS1096>tai* adults were resin-embedded, sectioned, and visualized by toluidine blue staining (**Figure 2.4B)**. Control *MS1096* sections through the thorax show an unbroken cuticle with underlying layers of cells and flight muscle. By contrast, wing tissue of *MS1096>tai* adult flies penetrate through the cuticle and contacts underlying tissue; these wing tips stain darkly with toluidine blue, perhaps due to a high density of nuclei. Large cells with many vesicles seem to cluster at the breach (red arrowheads in **Figure 2.4B**), possibly indicating a local response to invasion.

The relatively shallow penetration of wing tips in surviving Tai-expressing adults could mask a more severe effect in *MS1096>tai* pupae. To assess pupal invasion and test whether Tai expressing cells survive inside the thorax, a *UAS-green fluorescent protein* (*GFP*) transgene was used as a live-cell marker to track wing-tip invasion in cryosections of 18hr APF pupae (*nub>GFP,tai*). Wing tissue is visible in cryosections of control *nub>GFP* animals as a pair of closely apposed sheets (dorsal and ventral) lying alongside, but not within, the thorax (**Figure 2.1F**). A lateral section ('side view') confirms that *nub>GFP* wing blades develop normally, with highest GFP expression in the distal portion of the blade. Equivalent sections of 18hr APF *nub>GFP,tai* animals show GFP+ Tai-expressing wings penetrating the thorax and projecting deeply toward the midline (**Figure 2.1G**). In a side-view, Tai+/GFP+ cells are seen penetrating into the plane of section at the point of entry. Invaded *MS1096>tai* cells also highly express *diap1-lacZ* (**Figure 2.4C**, arrows), which is a Tai-regulated transcriptional reporter[49, 125]. Collectively, these data demonstrate that Tai-expressing wing cells breach the thoracic

cuticle, remain alive, show evidence of elevated expression of Tai target genes, and penetrate deeply into underlying tissue.

The *nub-Gal4* transgene is active in the wing pouch through larval and pupal development[129]. To define when Tai expression is required to drive wing invasion, a temperature-sensitive *Gal80* transgene was used to restrict *nub-Gal4* activity to specific developmental intervals (*nub>tai,tub>Gal80^{ts}*) (**Figure 2.1H**). Rearing these animals continually at the Gal80 permissive temperature (25°C) completely blocks Tai-driven wing invasion, while rearing at the Gal80 restrictive temperature leads to complete lethality, likely due to elevated Gal4 activity at 29°C. Animals shifted from 25°C→29°C at L2 eclose with approximately 80% invaded wings, while those 25°C→29°C shifted at L3 display roughly 50% invasion. Inverse 29°C→25°C shifts only produce invasion when Tai has been induced through the beginning of L3, indicating that Tai expression in L3 wing discs is sufficient to drive invasion in the subsequent pupal stage. A 25°C→29°C shift at the white prepupal stage (WPP) leads to 5-10% wing invasion. Overall, these temperature-shift data indicate that the minimal developmental window necessary for Tai to transform wing cells into an invasive tissue is from early L3 to early WPP stage.
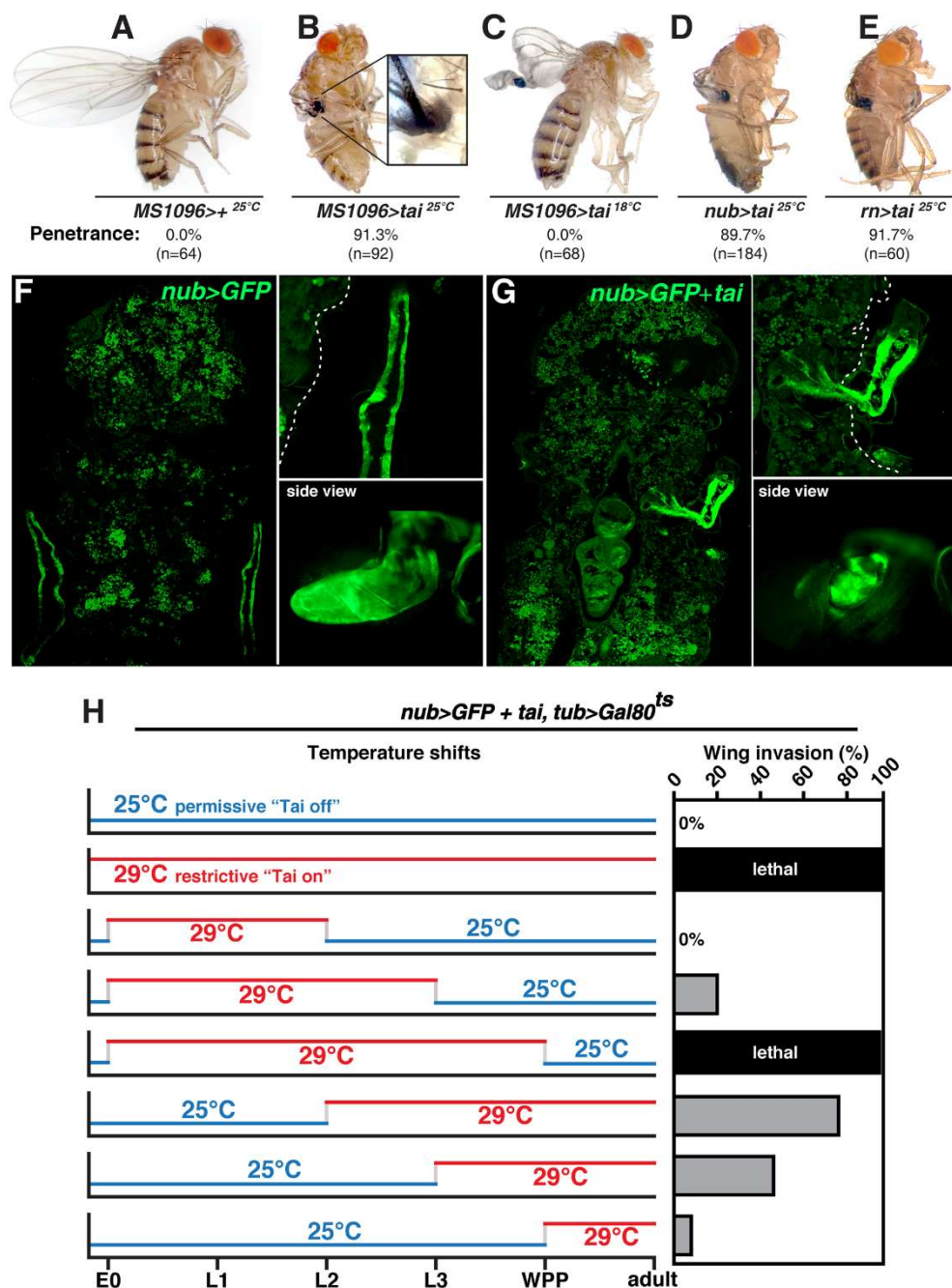
Figure 2.1 Tai expressing wing cells penetrate the thoracic cuticle.
(A-E) Adult flies driving the expression of UAS-tai with three different pan-wing Gal4 lines (*MS1096*, *nubbin*, and *rotund*). Temperature indicates the environmental condition. **(F-G)** Cryosection of 18hrs after puparium formation (APF) control pupae (GFP marks *nub-Gal4*) and *tai* expression. (Upper right) zoomed in view of the wings. (Lower right) side views of the pupae prior to embedding and cryosection. **(H)** Temperature controlled expression of tai at various developmental stages using tubGal80ts and their consequent penetrance of the phenotype (%). Blue line denotes time kept at 25˚C. Red line denotes time kept at 29˚C.
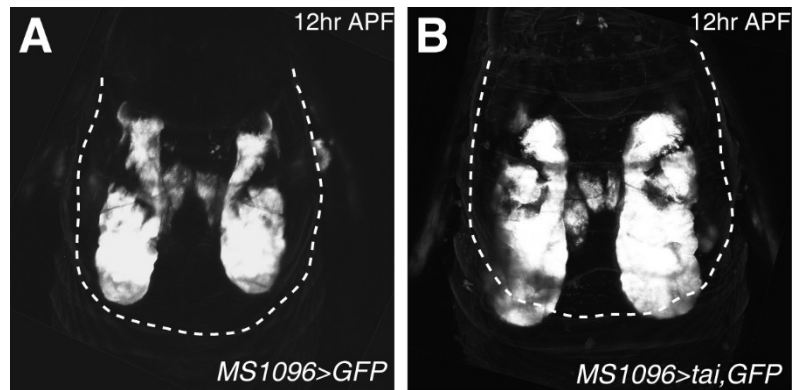
Figure 2.2 *tai* expressing 12hr APF wing discs undergo disc eversion.
12hr APF pupal wing discs imaged through the pupal case of **(A)** wild-type control or **(B)** *MS1096>tai* animals. Dotted line indicates the edge of the operculum.

Tai wing-invasion phenotype is dependent on the Ecdysone and Hippo pathways

The L3-to-WPP period coincides with rising titers of 20-hydroxyecdysone (20E), the bioactive hydroxylated form of ecdysone, and changes in gene expression as wing cells transition from the larval to pupal stage[130, 131]. Because Tai interacts with the 20E receptor (EcR) and co-activates EcR-dependent gene transcription[15, 132], the timing of invasion suggests that 20E may be a required cofactor for Tai-driven wing invasion. Consistent with this hypothesis, *MS1096>tai* wingtip invasion is blocked by RNAi depletion of EcR, which mediates transcriptional effects of 20E in border cells and wing disc cells[15, 49, 125], or expression of a dominant negative *UAS-EcR^{LBD}* transgene encoding a EcR ligand-binding domain fragment that 'sponges' 20E in cells[133, 134] (**Figure 2.3A-B**,**M**). Reciprocally, a *tai^{ΔB}* transgene encoding a version of Tai that cannot be bound and an inhibited by the Abrupt protein[132], enhances invasion at 18°C (**Figure 2.3J,M**). Although RNAi of the EcR-associated repressor *Smr* is alone insufficient for invasion (**Figure 2.4A**), it cooperates with *tai* overexpression to enhance invasion at 18°C (**Figure 2.3H,M**). This result is consistent with the finding that Smr represses expression of EcR and Hippo target genes in wing disc cells[39, 49].

Suppressed *MS1096>tai,EcR^{LBD}* wings are malformed and crumpled (**Figure 2.3B**), suggesting that additional inputs beyond 20E contribute to phenotypes produced by excess Tai. Tai contains a pair of proline:proline:x:tyrosine (PPxY) motifs located in its transactivation domain that are required to bind the Hippo coactivator protein Yorkie (Yki) and stimulate imaginal disc growth[49, 125]. A version of Tai that cannot bind Yki (*UAS-tai^{PPxA}*) has reduced ability to drive wing invasion (**Figure 2.3C,M**), indicating that Yki contributes to *MS0196>tai* invasion. In support of this hypothesis, a small-scale

screen of chromosome 2 (chr2) deficiencies (Dfs) identified the *Df(2L)ED105* and *Df(2R)ED3728* deletions and as dominant enhancers of *MS1096>tai* wing invasion at 18°C (**Table 1**, *see Appendix*). *Df(2L)ED105* uncovers the Hippo pathway component *dachsous* (*ds*), while *Df(2R)ED3728* uncovers the *hippo* (*hpo*) kinase. Individual ds^{33} and hpo^{KS240} alleles significantly enhance Tai-driven wing invasion at 18°C, as does RNAi of the Yki-inhibitor *warts* (*wts*) (**Figure 2.3I,L-M**). A third deletion, *Df(2L)BSC291*, is a strong suppressor of *MS1096>tai* wing invasion at 25°C. Narrowing this interval identified the small deletion *Df(2L)Pvf2-3*, which removes genes encoding the PDGF/VEGF-related ligands Pvf2 and Pvf3[135], as a single-copy suppressor of Tai wing invasion driven by either the *MS1096* or *nub* drivers (**Figure 2.3A,D-F,M**). This interaction parallels a genetic requirement for the third Pvf family member, Pvf1, in Tai-dependent border cell migration[136].

The pattern of genetic interactions between *tai* and Hippo pathway components (e.g. *ds*, *hpo*, and *wts*) implies that transcription of Yki-dependent genes supports Tai driven wing-invasion. To test whether excess Yki can phenocopy Tai and produce wingtip invasion, a weak *yki* transgene (*UAS-yki* on chr2) was expressed from the *MS0196* driver. $MS1096>yki^{chr2}$ wings do not attach to the thorax; however, further elevating Yki activity with a loss-of-function allele of *warts* (wts^{x1})[137], results in an embedded wingtip phenotype ($MS1096>yki^{chr2},wts^{x1/+}$) that resembles *MS1096>tai* (**Figure 2.4A**). Collectively, these genetic data provide evidence that Tai requires elements of the 20E and Hippo pathways, including its binding partner Yki, to drive expression of genes that transform developing L3-WPP wingtip cells into an invasive tissue.
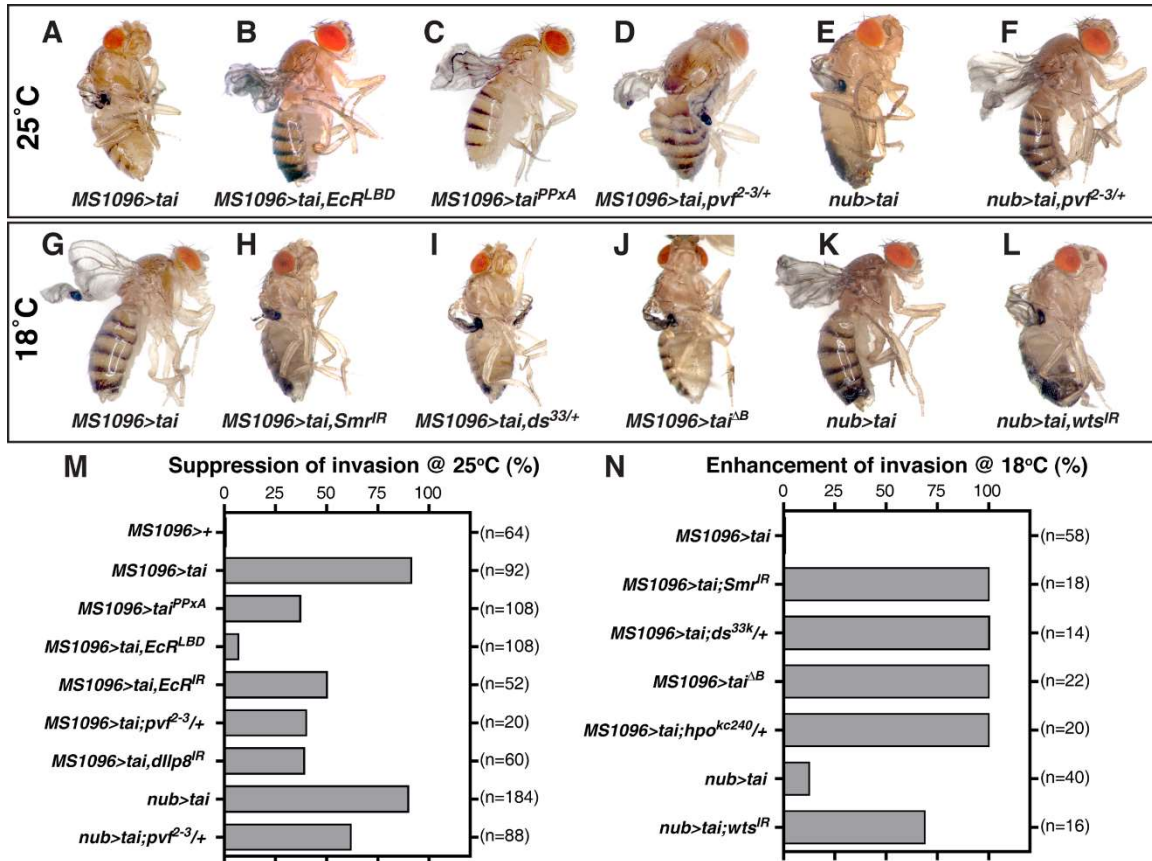
Figure 2.3. Tai wing-invasion phenotype is dependent on the Ecdysone and Hippo pathways.
(A-F) Suppression of Tai driven wing-invasion at 25°C. **(G-L)** Enhancement of Tai drive wing-invasion at 18°C. **(M-N)** Quantitation of suppression and enhancement of the wing-invasion phenotype by various targets and interactors of *tai* measured in penetrance (%). *(See also Figure S2 and Table S1 in Appendix)*
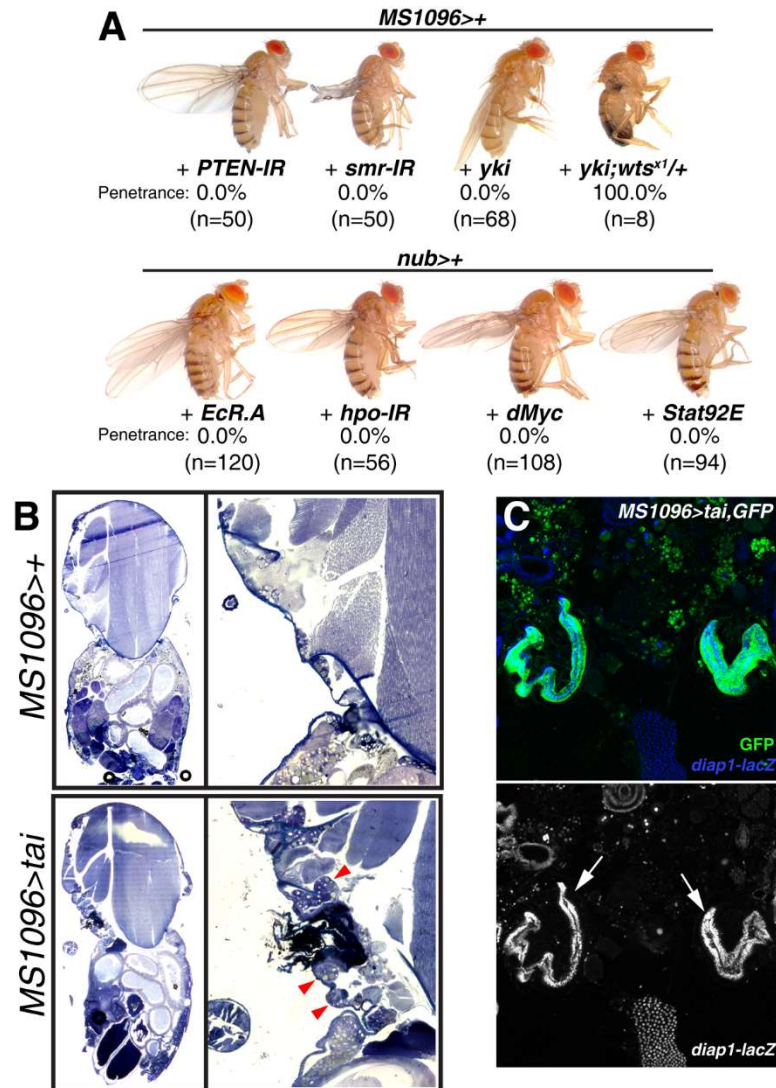
Figure 2.4. Adult wing phenotypes induced by a panel of growth regulators, and wingtip embedding and *diap1-lacZ* expression induced by *tai*. Supporting data for Figure 1 and Figure 2. (A) Overexpression (*dmyc*, *stat92E*, *EcR-A*, *yki*) or RNAi depletion (*hpo*, *Smr*, *Pten*) of candidates using either the *MS1096* or *nubbin* Gal4 drivers. The percentage of embedded wingtips at eclosion and number of wings scored (n) are indicated for each genotype. **(B)** Thin-sections of resin-embedded *MS1096>+* or *MS1096>tai* adult flies stained with toluidine blue. Red arrows indicate large vesicular cells near location of wing entry. (C) Cryosection of 18hr APF *MS1096>tai,GFP* animal stained with anti-ßgal (greyscale) to detect *diap1-lacZ* expression. Arrows denote embedded *MS1096>tai* wing tissue that highly expresses GFP (green) and *diap1-lacZ*.

Identification of Tai-induced transcripts in invasive wing discs

To identify mRNAs induced by Tai in wing disc cells, rRNA-depleted RNA of Tai-expressing wing discs was analyzed by high throughput sequencing (HTS; as in ref.[49]). This HTS analysis used RNA pools harvested from late L3 larval wing discs expressing Tai from the *engrailed-Gal4* driver. *en>tai* discs are enlarged relative to controls (**Figure 2.6**) but show no signs of thorax invasion by late L3 (e.g. see ref. [49]), and therefore provide an opportunity to separate candidate Tai-induced transcripts from those that change as a secondary consequence of invasion. HTS analysis generated informative reads corresponding to 9,525 transcripts (**Table 2**, *see Appendix*). Of these, a group of 995 mRNAs were designated as candidate 'Tai-induced' transcripts based on ≥2-fold increase ($log_2\Delta > 0.8$) in mapped read frequency in experimental (*en>tai*) vs. control (*en>*) samples (**Figure 2.5A**, and **Table 3**, *see Appendix*). This group includes the 20E-regulated genes *Edg78E*, *Eip93F*, *ftz-f1* and *Cyp18a1*, which encodes an enzyme that inactivates 20E in a proposed negative feedback loop[138-143]. It also includes the secreted factor *Drosophila insulin-like peptide-8* (*dIlp8*), a Yki target that is induced following tissue damage and triggers a developmental pause necessary for regrowth of wounded tissue[144-147], the Jak-Stat ligand and Yki-target *unpaired-3* (*upd3*)[147, 148], and the germline stem cell factor *piwi*, a shared Yki-Tai target that reactivates the piRNA pathway in *Ras^{V12}*-transformed *wts*-deficient cells[49, 149]. Induction of *Edg78E*, *ftz-f1*, *dIlp8* and *cpr100A* [150] mRNAs was confirmed by quantitative real-time PCR (qPCR) of RNA harvested from everted, pre-invasion *MS0196>tai* discs at 6hr APF (**Figure 2.5C-D**). Given that a *dIlp8*-induced developmental pause is required for efficient regrowth of wounded tissue[151], elevated expression of *dIlp8* mRNA in *MS1096>tai*

discs could lead to a similar delay that permits invasive growth. Consistent with this hypothesis, depletion of *dIlp8* within *MS1096>tai* discs suppresses wing invasion (**Figure 2.3M**).

In order to focus on secreted factors that could remodel the extracellular environment of Tai-expressing wing discs and facilitate inter-tissue invasion, the 995 candidate Tai-induced wing disc mRNAs were compared to the predicted *Drosophila* secretome[145]. A group of 158 mRNAs were found to be common to both datasets; gene ontology (GO) analysis of this smaller group detected significant enrichment in the categories of *chitin catabolism*, *Toll signaling*, *innate immune response*, and *wound healing* (e.g. *dIlp8*) (**Figure 2.5B**). qPCR on dissected 6hr APF *MS0196>tai* discs wing discs (i.e. pre-invasion) was carried out to confirm induction of selected Toll and immune mRNAs. This analysis detected increases in mRNAs corresponding to the antimicrobial peptide (AMP) *Diptericin-A* (*DptA*), the pattern recognition molecule *Peptidoglycan recognition protein-LD* (*PGRP-LD*), and *chitinase-6* (*cht6*), with more moderate induction of *chitinase-5* (*cht5*), *spätzle* (*spz*) and *spz4*, and the transmembrane receptor *PGRP-LC* (**Figure 2.5D**). Spz and Spz4 belong to a family of secreted proteins that are activated by pro-domain cleavage and act as ligands for Toll receptors[152, 153]. PGRP-LC is the major receptor for the immune deficiency (IMD) pathway and a key transcriptional target of 20E/EcR in immune cells[154-157]. IMD activity results in transcription of secreted AMPs, including *DptA*, by the NF-κB homolog Relish[156, 158]. Although *Drosophila* PGRP-LD is uncharacterized, it's mosquito homolog promotes expression of the mosquito *DptA* homolog[159]. Chitinases comprise a family of secreted enzymes that degrade chitin, a major component of the cuticle exoskeleton[160]. *cht6*

mRNA is normally induced in wing cells during pupation, where it sculpts the layer of apical cuticle on adult wing cells and hairs[161]. Collectively, these data suggest that the microenvironment of *MS1096>tai* discs is characterized by chitinase activity and signaling through the IMD and Toll pathways.

Toll and IMD activation in the absence of a foreign pathogen (termed 'sterile inflammation') has been associated with a number of invasive tumor models in *Drosophila*, primarily as a secondary consequence of tissue damage and basement membrane degradation that acts through secreted PGRPs to stimulate Spz cleavage[162]. However, because the HTS analyses is based on RNA pools harvested from Tai-expressing wing discs before invasion occurs (i.e. L3 *en>tai* and 6hr APF *MS0196>tai*), the enrichment for chitinase and innate immune mRNAs is unlikely to be a consequence of invasion; rather, expression of these factors may precede Tai-driven invasion.
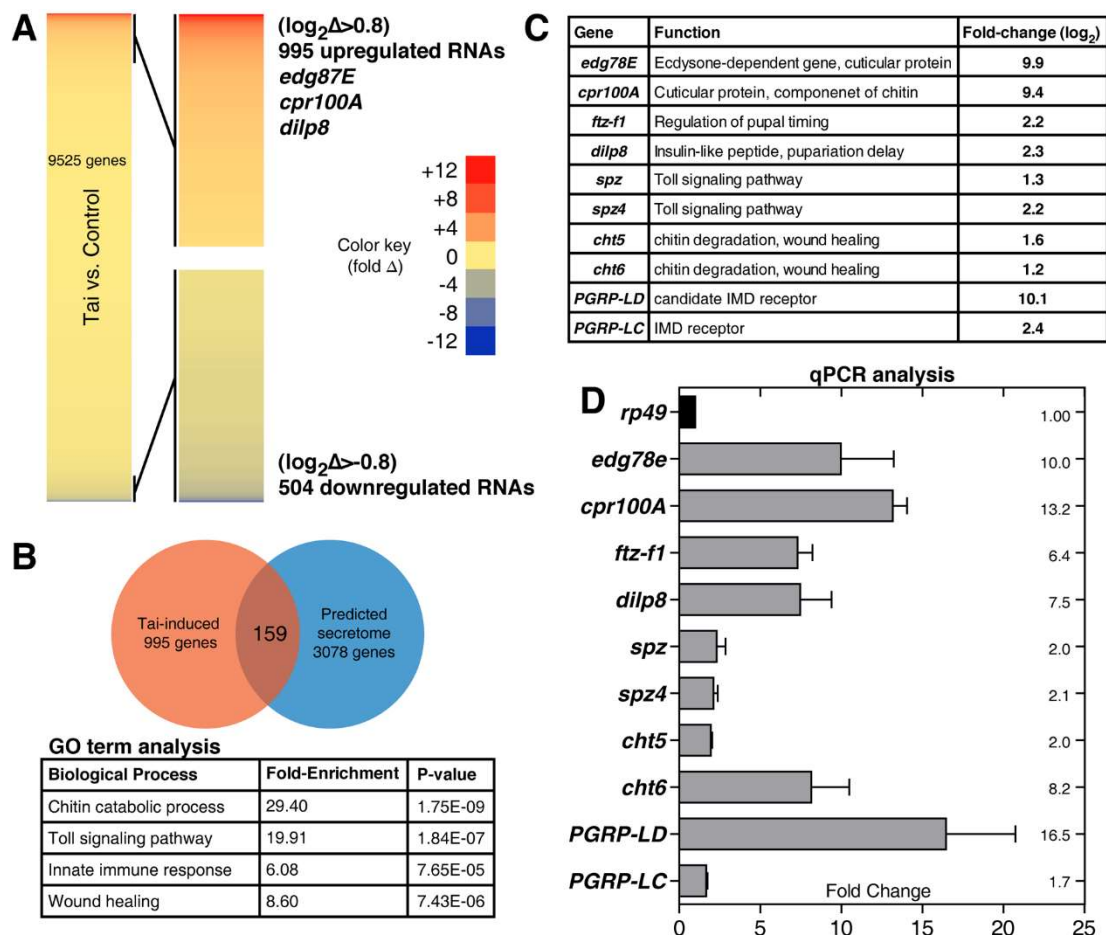
Figure 2.5. Identification of Tai-induced transcripts in invasive wing discs.
(A) Heat-map representation of RNA expression of genes in control versus Tai-expressing (Tai:Ctrl) late L3 wing imaginal discs. The Tai:Ctrl dataset contains 9525 genes of which 995 genes are upregulated using >0.8(log2) as the cutoff and 504 genes are downregulated using <0.8(log2) as the cutoff. **(B)** Go term analysis of 159 upregulated genes that intersect with the predicted secretome of 3078 genes with fold-enrichment and p-values. **(C)** Upregulated genes and their fold-change measured from the RNA-seq. **(D)** validation of RNA-seq targets by quantitative real-time PCR (qPCR) analysis.
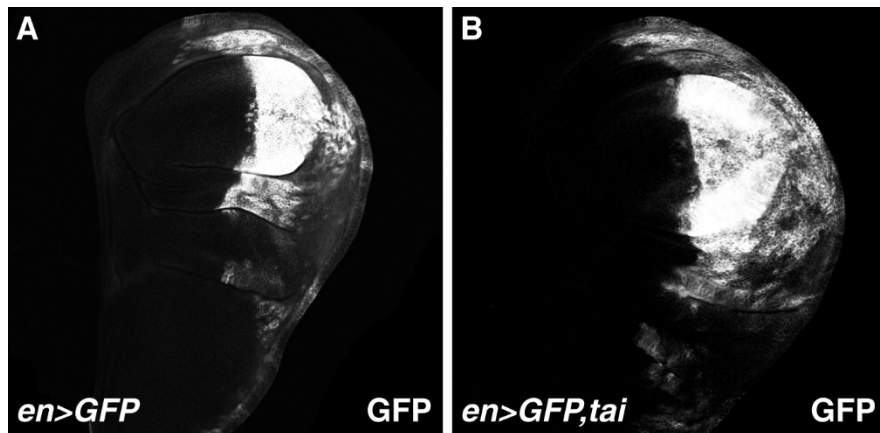
Figure 2.6. Larval *en>tai* wing discs used for RNA-seq analysis are overgrown. Supporting data for Figure 3.
To-scale images of control **(A)** *en>GFP* and **(B)** *en>GFP,tai* larval wing discs showing overgrowth of the posterior (GFP+) domain.

Tai-expressing wing cells elicit an immune response in the surrounding tissue

Drosophila has three types of immune cells, lamellocytes, plasmatocytes, and crystal cells, whose numbers increase in response to immune activation[95, 163]. To test whether immune system of *MS1096>tai* animals is activated prior to wingtip invasion, crystal cell numbers were assessed in L3 larvae by brief heating to 70°C. This treatment activates the prophenoloxidase zymogen in crystal cells and turns them black, making the sessile pool of crystal cells visible through the larval cuticle as dark puncta[164]. Sessile crystal cells concentrate in posterior segments[164] and their numbers are visibly increased in *MS1096>tai* larvae relative to control *MS1096>+* larvae (**Figure 2.7A,B**). Hemolymph smears (Diff-Quik; Electron Microscopy Sciences) also detect an increased concentration of nucleated cells in *MS1096>tai* larvae compared to *MS1096>+* controls (**Figure 2.8**). To complement this analysis of immune cell numbers, the *Drosomycin-GFP* (*Drs-GFP*) transcriptional reporter[165] was used to measure Toll-pathway activity in the larval fat body (FB), which is a key immune organ during sterile inflammation and pathogen-induced immune responses[163]. *Drs-GFP* is a specific target of the Toll pathway and not the parallel immune deficient (IMD) pathway[65]. Relative to control *MS1096>RFP* larvae, *Drs-GFP* expression is strongly elevated in the FB of *MS1096>tai* larvae, which is well before invasion occurs (**Figure 2.7C-D**). Thus, Tai-expressing wing cells trigger a Toll response in FB cells at a stage when the only overt effect on disc morphology is disc overgrowth (see **Figure 2.6**).

Drs-GFP activity was also assessed in cryosections of *MS1096>tai* 14-16hr APF pupae after invasion is underway (**Figure 2.7E-J**). While control *MS1096>RFP* animals show only background *Drs-GFP* fluorescence and RFP-labeled wing blades, *Drs-GFP*

expression is induced in cells located throughout *MS1096>tai,RFP* pupae (**Figure 2.7E-F**). Adult fat body cells in the abdomen express *Drs-GFP* (white arrows, **Figure 2.7F**), as do many smaller cell types distributed throughout the thorax and head capsule. High-magnification views of invaded wings shows that large *Drs-GFP* expressing cells cluster near or envelop Tai-expressing tumors (green in **Figure 2.7G, I**). Other *Drs-GFP* expressing cells located along the axis of penetration of *MS1096>tai* wings are smaller and appear fragmented (**Figure 2.7J**), perhaps indicative of apoptotic cells. Notably, *Drs-GFP* is not expressed in Tai-expressing wing discs themselves. This asymmetry in *Drs-GFP* induction indicates that Toll activation is not autonomous to Tai expressing cells, but rather a paracrine effect associated with entry of Tai-transformed wing cells into the thorax.
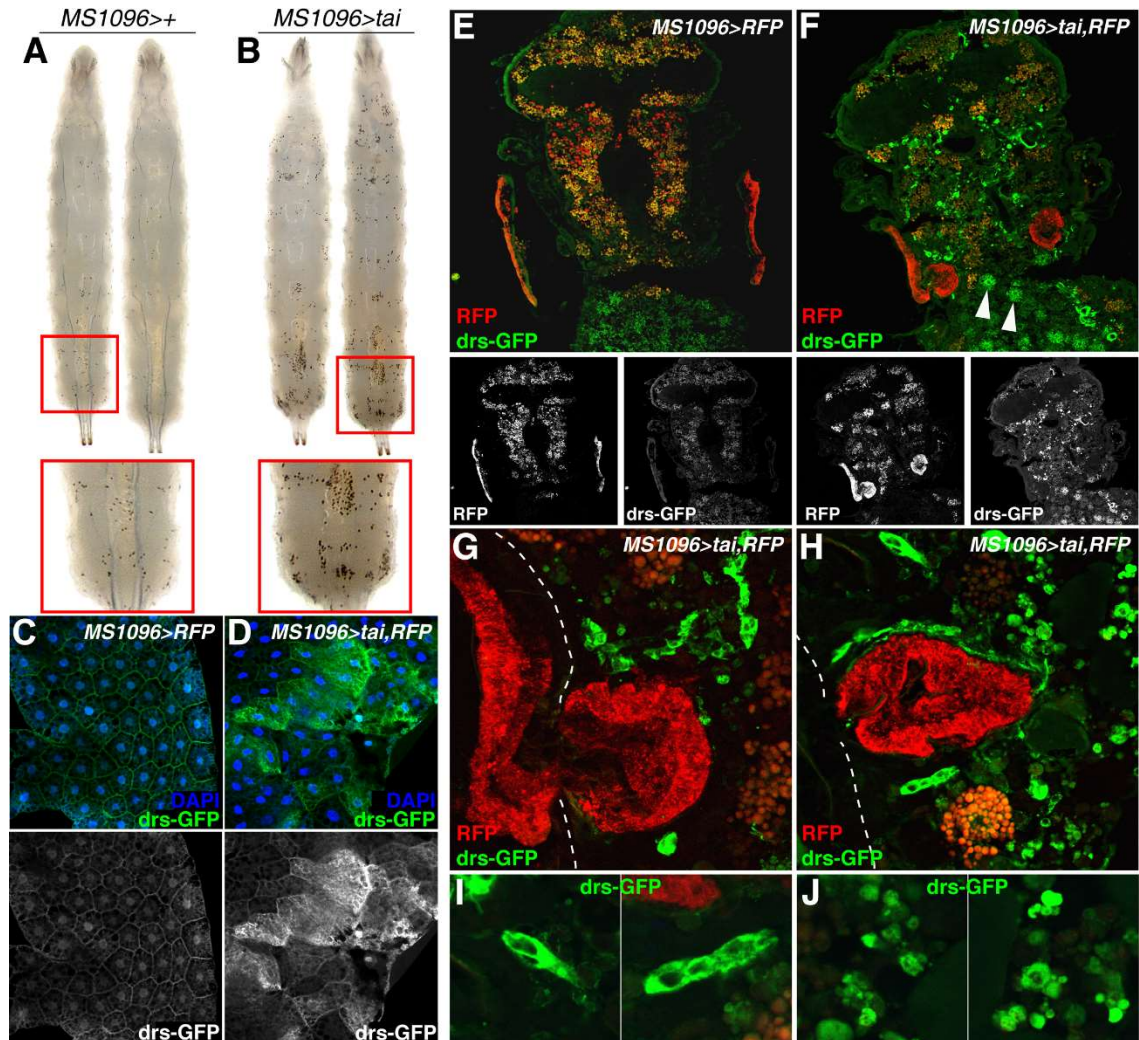
Figure 2.7. Tai expression wing cells elicit an immune in the response surrounding.
(A-B) Crystal cell assay of Tai vs. control larvae. **(C-D)** *Drs-GFP* reporter of Tai vs. control larval fat body indicating the status of an immune response. **(E-F)** Cryosection of 18hrs APF Tai vs. control pupae showing *Drs-GFP* reporter. **(G-H)** Tai expressing wing tissue (RFP) invading into the thorax and Drs-GFP+ cells surrounding the wing tissue. **(I-J)** Closer look at Drs-GFP+ cells in the sections. *(See also Figure S4).*
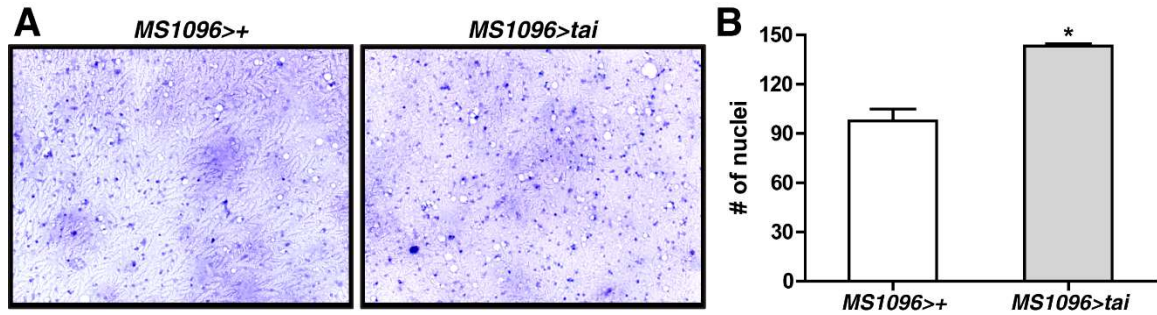
Figure 2.8. *tai* **expression in wing tissue increases hemocyte numbers.**
Diff-quik™ staining (a modified Giemsa stain that highlights nuclei; refer to STAR methods section) of hemocytes from larval bleeds of control *MS1096>+* (left) and *MS1096>tai* (right) animals. (B) Quantification of hemocyte nuclei per field (n=3; * = p<0.05).

Genetic requirement for Toll components in invasion

The correlation between expression of immune-related mRNAs in Tai^{+} cells and induction of Toll activity in thoracic cells raises the possibility that immune signals facilitate Tai-driven invasion. To assess the roles of specific factors in Tai-invasion, alleles of individual Toll and IMD pathway components and other factors of interest, were tested for dominant modification of invasion frequency in *nub>tai* adults raised at 25°C, which have a baseline wing invasion frequency of approximately 90% (**Figure 2.9A,B**). Reducing IMD signaling with loss-of-function alleles of *relish* (*rel^{E20}*), *Fas-associated death domain* (*FADD^{f06954}*), or *death-related ced3/Nedd2-like caspase* (*Dredd^{B118}*) had minimal effects on Tai-invasion frequency. Two alleles of the extracellular protease *gastrulation-defective* (*gd*), which promotes Spz cleavage during dorsoventral axis determination the embryo[153], also had minimal effects on the *nub>tai* wing phenotype. However, alleles of core Toll pathway components produced more significant suppressive effects. Two alleles of the NF-κB homolog *dorsal*, *dl^1* and *dl^4*, led to significant reductions in invasion frequency. A mutant allele of the Toll cytoplasmic adaptor *Myd88* (*Myd88^{KG03447}*) dominantly suppressed to a similar degree as *dl^1*, the stronger suppressor of the two *dl* alleles. Deficiencies that uncover both *Myd88* and *dl* were also recovered as suppressors of invasion (**Table 1**, *see Appendix*). Alleles of Spz ligands produced even more robust suppression. Removal of one copy of *spz4* (*spz^{MI15678}*) or *spz6* (*spz6^{c01763}*) respectively led to 2-fold and 5-fold reductions in frequency of *nub>tai* invasion. Compound heterozygosity for *spz2* and *spz5* (*Df(3L)spz5^{Aw18},NT1^{41}/+*) produced a moderate suppressive effect, suggesting that multiple Spz factors make contributions to the *nub>tai* adult intertissue invasion

phenotype. These genetic data highlight a specific genetic sensitivity to reduced Toll activity, but not reduced IMD activity, in Tai-driven wing invasion and provide additional evidence that this phenotype is mechanistically distinct from disc eversion and Tai-dependent border cell migration[15], neither of which have been linked to alleles of Toll pathway components.

To localize the requirement for Toll components, RNAi lines to the ligands *spz*, *spz4*, *spz6*, and the receptor *Toll* were co-expressed with Tai in wing cells (*nub>tai,RNAi*). Consistent with the link between Tai and *spz* mRNAs in the HTS analysis (**Figure 3.5**), RNAi depletion of *EcR* or *spz* ligands within Tai-expressing wing cells suppressed invasion. *spz-IR* and *spz4-IR* each had moderate effects, while *spz6-IR* had the largest suppressive effect, which mirrored the robust dominant effect of the $spz6^{c01763}$ genomic allele (**Figure 2.9A**). The pattern of elevated *Drs-GFP* reporter activity only in thoracic cells (see **Figure 2.7G,H**), implies that the Toll signaling cascade is not engaged in Tai-expressing cells; consistent with this model, *Toll* depletion within Tai-expressing wing cells did not replicate the dominant suppressive effect of *dl* and *Myd88* alleles. Individual depletion of *cht5* or *cht6* also mildly reduce invasion (**Figure 2.10**), suggesting these enzymes may aid in penetration through the epidermal cuticle. Collectively, these data argue that Toll activity is elevated in thoracic cells in response to Spz ligands produced by Tai-expressing wing cells, and that Toll signaling and chitinases are required for intertissue invasion.
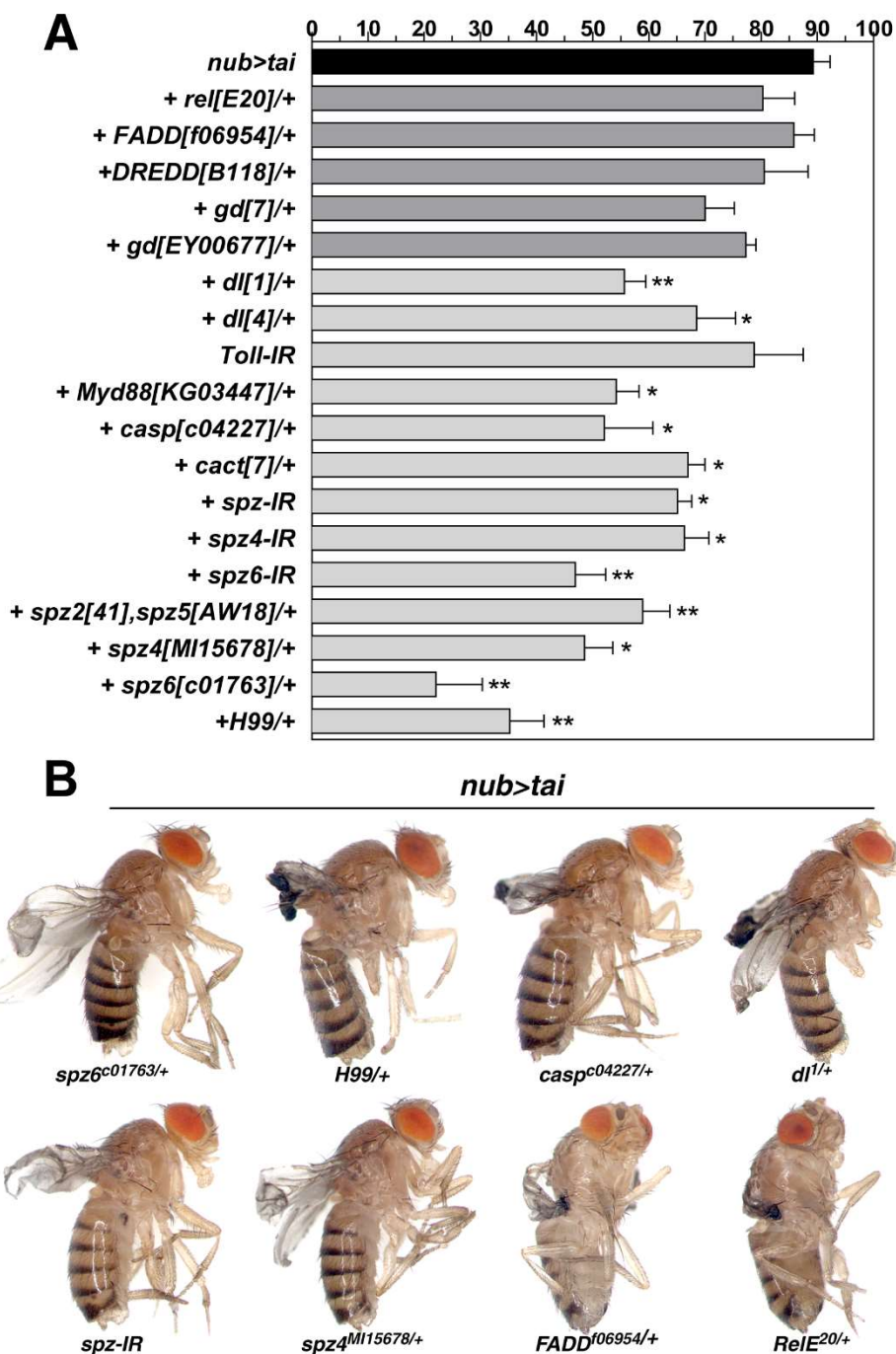
Figure 2.9 Genetic requirement for Toll signaling and chitinases in invasion.
(A) Dominant modification of Tai wing-invasion phenotype by components of the Toll and Imd pathways measured in penetrance (%;*=*p<0.05;**=p<0.01;***=p<0.005)*. **(B)** Resultant adult phenotypes of crossing in alleles of Toll and Imd pathway components. *(See also Table S1 in Appendix).*
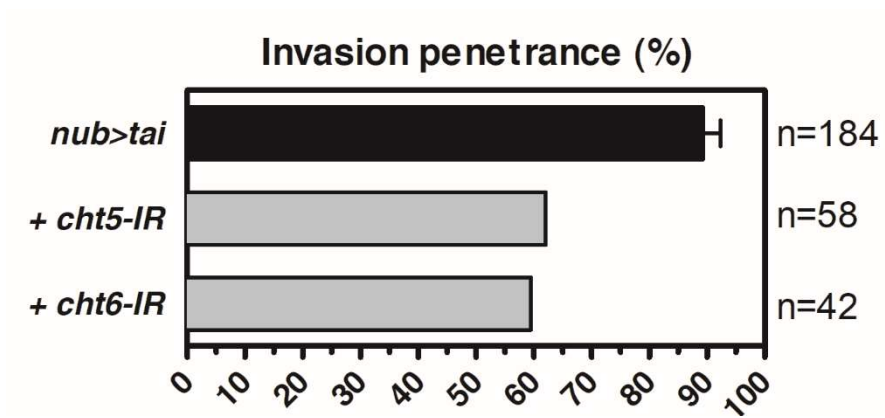
Figure 2.10 Suppression by chitinase RNAi expression in *nub>tai* wing cells.
Penetrance (%) of *nub>tai* wing invasion in the background of *UAS-RNAi* lines to *cht5* or *cht6* (n=1, biological replicate of 40 wings per genotype). Control *nub>tai* is indicated by black fill.
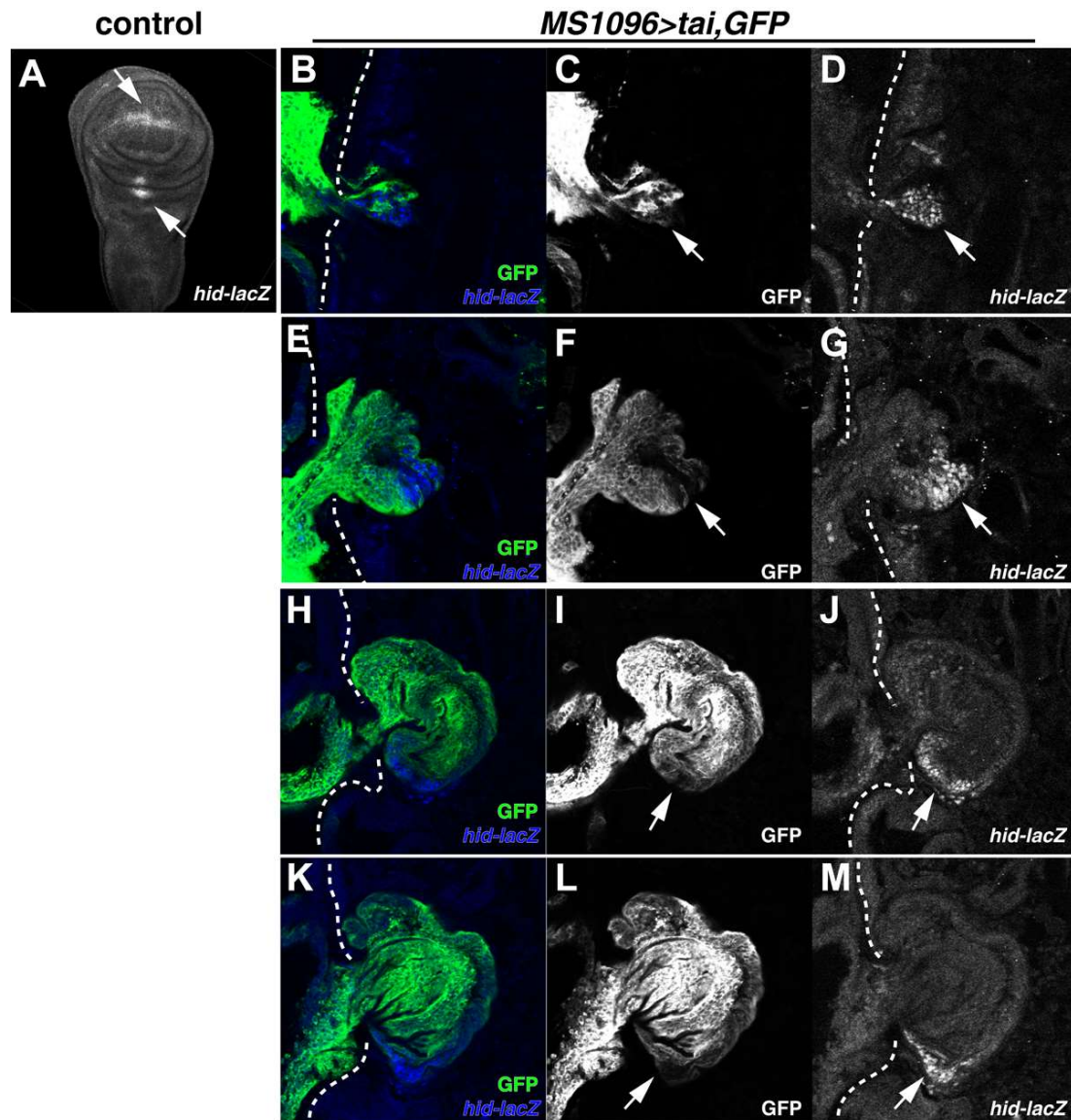
Figure 2.11 *hid-lacZ* marks cells at the tip of invading wing tissue.
(A) Confocal image of a control *MS1096>+* larval wing disc stained with anti-ßgal (greyscale) to detect expression of *hid-lacZ*. Arrows denote *hid-lacZ*-positive cells located along the DV margin in the pouch (top) and in the dorsal hinge (bottom). **(B-M)** Cryosections from *MS1096>tai,GFP+hid-lacZ* animals imaged for GFP fluorescence (green in **B,E,H,K**; greyscale in **C,F,I,L**) and anti-ßgal (blue in **B,E,H,K**; greyscale in **D,G,J,M**) showing position of *hid-lacZ* expressing cells (arrows) during sequential stages of invasion into the thorax. Dotted line indicates the thoracic cuticle.

Invasion of Tai-transformed wing cells requires apoptosis

The phenotypic effects of Toll activation are context dependent. In fat body cells, activation of the Toll pathway induces expression of secreted AMPs (e.g. *Drs*) to combat microbial infection[156]. In larval wing discs, Toll activation autonomously promotes apoptosis of 'loser' cells during dMyc-induced cell competition, a process in which rapidly growing 'winner' cells kill slow growing neighbors[101, 166, 167]. This competitive death requires production of Spz proteins by winners, which in turn activate Toll-dependent transcription of the pro-apoptotic genes *head involution defective* (*hid*) and *reaper* (*rpr*) in losers via the NF-κB factors Dl, Rel and Dif [101]. Notably, the single layer of epidermal cells that secrete the chitin exoskeleton are very sensitive to Toll-induced death caused by mutations in *necrotic* (*nec*), a hemolymphatic Serpin that inhibits Spz processing[92, 168].

To test whether apoptosis contributes to Tai-driven invasion, a genomic deletion (*Df(3L)H99*) removing *hid*, *rpr* and the third RHG (Reaper-Hid-Grim) gene *grim* was placed in the *nub>tai* background at 25°C. Remarkably, a single copy of *Df(3L)H99* suppressed the *nub>tai* adult wing phenotype almost as effectively as the *spz6^{c01763}* allele and *spz6* RNAi (**Figure 2.9A**). To determine whether this genetic requirement for RHG factors correlates with elevated rates of apoptosis, either in invading cells or locally in the thorax, cryosections of 15-18hr APF *MS1096>GFP* control and *MS1096>tai,GFP* pupae were probed for the cleaved, active form of the effector caspase Dcp-1 (aka) (**Figure 2.12A-J**). Expression of Tai leads to a slight increase in the number of Dcp-1-positive (Dcp-1^{+}) cells within the wing epithelium of *MS1096>tai,GFP* pupae, perhaps as a result of EcR-driven transcription of the *dronc* caspase[169]. Dcp-1^{+} cells are quite rare in the

thorax of *MS0196* controls but abundant in *MS1096>tai,GFP* animals in regions surrounding invasive wing tissue (**Figure 2.12B** vs. **E,H**). These apoptotic cells are observed in deeper layers of the thorax (arrowheads, **Figure 2.12E**) and on either side of Tai-expressing tissue as it penetrates the cuticle (arrows, **Figure 2.12E**). In a section through an earlier stage of invasion (**Figure 2.12G-I**), apoptotic cells are evident in the epidermal cell layer that underlies the thoracic cuticle (arrowheads in **Figure 2.12G**; magnified views of boxed regions in **Figure 2.12J**) Quantification of the overall frequency of apoptotic events reveals that the number of Dcp-1$^+$ cells rises from an average of 12.3 cells (±4.7) in control *MS1096>GFP* pupal sections to an average of 54.2 cells (±14.7) in *MS1096>tai.GFP* pupal sections, with a significant majority of these new apoptotic events occurring within the thorax (**Figure 2.11S**). Epidermal cells flanking the point of wing entry also have elevated expression of a second transcriptional marker, the Jun N-terminal kinase (JNK) pathway reporter *puckered-lacZ* (*puc-lacZ*) (arrowheads, **Figure 2.12Q-R**). JNK signaling is activated during inflammation and apoptosis, and JNK-mediated killing requires Toll in some epithelial cell types and occurs in response to Toll and IMD activity in others[117, 170, 171]. These data suggest that cells with elevated JNK activity and cleaved Dcp-1 may surround the epidermal wound made by Tai-transformed wing tissue. Some Dcp-1$^+$ cells located in the thorax also elevate expression of *hid-lacZ* (*hid^{05014}*; circled in **Figure 2.12D-F**), which can be induced by both JNK and Toll activity during apoptosis[101, 172]. The rapid phagocytosis of apoptotic cells *in vivo* suggests that the total number of thoracic cells that die during wing invasion is likely to exceed the number that contain cleaved or express the *hid* and *puc* reporters in single cryosections at fixed time points. Collectively, these observations

confirm that Tai-induced wing invasion correlates with elevated apoptosis among thoracic cells which, based on the robust suppressive effect of the *Df(3L)H99* deletion, is a requirement for invasion.

A small group of invading wing cells expresses *hid-lacZ* but lack cleaved Dcp-1 (**Figure 2.12F,** yellow arrow), suggesting that *hid-lacZ* is not invariably linked to apoptosis in wing disc cells. Indeed, in control larval wing discs *hid-lacZ* is expressed in pouch cells at the dorsoventral (D/V) boundary and a small group of dorsal hinge cells (**Figure 2.11A**). *hid-lacZ* expression in these areas does not correlate with active apoptosis; rather it seems to identify a previously defined group of cells at the DV boundary that have elevated sensitivity to apoptotic stimuli (e.g. irradiation, *dMyc* or *de2f1* overexpression) due in part to a pattern of 'open' chromatin across the *H99* region, which contains the *hid-lacZ* insertion (hid^{05014})[173-176]. In *MS1096>GFP* controls, these *hid-lacZ* expressing cells are often visible at the distal tip of the pupal wing (**Figure 2.12C**, yellow arrow), which is derived from D/V boundary cells in the center of the larval pouch. In *MS1096>tai* 15-18hr APF pupae, these *hid-lacZ*-positive cells are among the first to breach the cuticle and penetrate the thorax (**Figure 2.11B-D**). In sections through stages of the invasive process, these *hid-lacZ* 'leader' cells appear to be followed by *lacZ*-negative wing cells that progressively displace the *hid-lacZ* expressing cells to the side of the invading mass (**Figure 2.11E-M**). This lineage tracing data provide evidence that the Tai-driven invasion is an ordered process, with L3 cells derived from the D/V boundary apparently serving as leader cells in early stages.
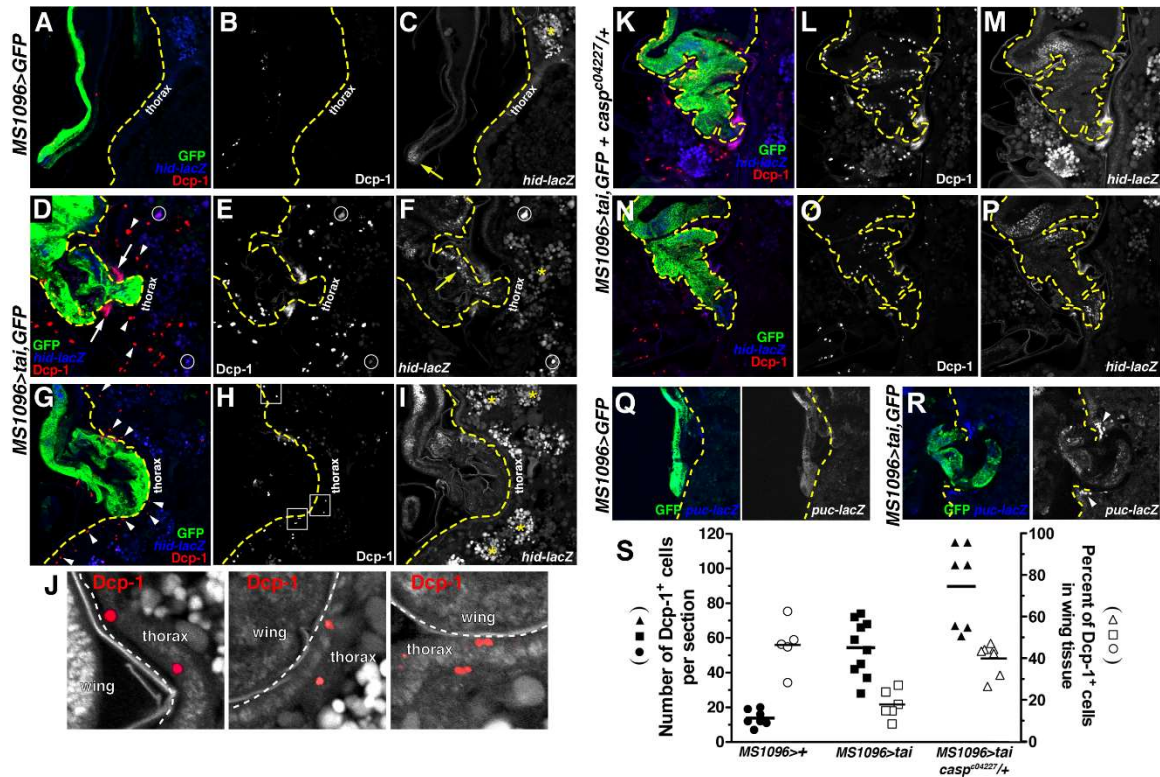
Figure 2.12 Invasion of Tai-transformed wing cells requires apoptosis.
(A-I) Cryosection of 18hr APF control pupae (A-C) vs. Tai wing invasion pupae (D-I) stained with Dcp-1 as an apoptotic marker and *hid-lacZ* reporter. Yellow dotted distinguishes the wing from the thorax. White arrow and arrow heads indicate Dcp-1+ cells. Yellow arrows indicate LacZ+ cells. White circles indicate Dcp-1+ and LacZ+ cells. (J) Zoomed in view from Panel H showing Dcp-1 signal in the thoracic epithelium. (K-P) Cryosection of 18hrs APF pupae expressing Tai in the background of *casp^{c04227}/+*. Yellow dotted line outlines the pupal wing. (Q-R) Cryosection of control pupae and Tai-tissue invasion pupae (18 hrs AFP), stained with LacZ reporting *puckered* transcription. Arrowheads indicate increase in LacZ reporter at the site of tissue invasion. (S) Comparison of total number of Dcp-1+ cells across genotypes per section (left y-axis; closed) and percentage of Dcp-1+ cells in wing tissue across genotypes per section (right y-axis; open).

The IMD-inhibitor Caspar promotes survival of Tai-transformed wing tissue

The enhanced death of thoracic cells in *MS1096>tai* cryosections (see **Figure 2.11**) implies that Tai-transformed wing cells are themselves resistant to the killing mechanism(s) involved in invasion. Neighbor-induced killing is also a key element of Myc-induced cell competition within the wing epithelium[101]. However, in both cases, it is not clear how oncogene-expressing cells are spared the apoptotic fate of their neighbors. It is likely that Tai-driven transcription of *diap-1* and the *bantam* miR, which inhibits Hid translation, contributes in part to this apoptotic resistance[49, 125, 177]. However, in the course of screening Toll and IMD alleles for modification of Tai-driven wing invasion, loss-of-function alleles of the Toll and IMD inhibitors *caspar* ($casp^{c04227}$) and *cactus* ($cact^7$) were identified as dominant suppressors of wing invasion frequency (**Figure 2.9A**). $casp^{c04227}$ is the stronger of the two, suppressing to a similar degree as the Toll pathway alleles $Myd88^{KG03447}$, $spz4^{MI15678}$, and *spz6-IR*. As *casp* and *cact* respectively encode an IMD-inhibitor that blocks DREDD cleavage and a Toll-inhibitor that binds Dl/Dif [100, 178], mutant alleles of these genes would be expected to further elevate IMD/Toll in thoracic cells and consequently enhance, not suppress, invasion. However, the observation that wing cells are killed by elevated Toll/IMD signals following loss of the IMD-inhibitor *PGRP-LF* or *cact* RNAi [118, 119], raises the possibility that *casp* and *cact* alleles may affect the fitness of Tai-expressing cells as well. Increased expression of the IMD receptors *PGRP-LC* and *PGRP-LD* (**Figure 2.5D**) predicts that Tai-expressing pupal wing cells may be primed to respond to IMD ligands. Thus, an alternate possibility is that *casp* alleles, and to a lesser extent *cact* alleles, lower

the threshold for Toll/IMD activation within wing cells, and that resultant apoptosis limits invasion.

To test the hypothesis that lowering the threshold for IMD activity sensitizes Tai-expressing wing cells to apoptosis, the number of Dcp-1$^+$ cells was quantitated in cryosections of 15-18hr APF *MS1096>tai* animals (**Figure 2.12K-P**) in the presence or absence of one copy of *casp^{c04227}*. Addition of the *casp^{c04227}* allele significantly increases overall Dcp-1$^+$ cell number in *MS0196>tai,GFP* cryosections from 54.2±14.7 to 89.1±22 (**Figure 2.11** ■ vs. ⬩). However, the overall fraction of these Dcp-1$^+$ cells located within the thorax decreases from approximately 80% to 50%, indicating that much of this *casp*-induced increase occurs within Tai-positive cells (**Figure 2.11** □ vs. △). In sum, *MS0196>tai* increases the number of apoptotic cells visible in single cryosections yet reduces the percent of apoptosis located in wing tissue. *casp^{c04227}/+* reverses this trend such that additional Tai-induced apoptotic events are now concentrated within Tai-expressing wing tissue. These observations indicate that de-repression of the IMD pathway enhances killing of Tai-expressing wing cells, suggesting that overcoming the threshold to IMD activation sensitizes them to a killing mechanism that operates locally at the site of invasion.

Tai-induced killing within the wing epithelial sheet

To assess whether the pattern of Tai-induced apoptosis in the wing:thorax system also occurs between cells a continuous epithelium, Tai was expressed in a stripe of cells along the anterior-posterior (AP) boundary L3 wing discs with the *ptc-Gal4* driver (*ptc>tai,GFP*; denoted by dotted lines in **Figure 2.13A-F**). Consistent with patterns of Tai-induced apoptosis in *MS1096>tai* pupal sections, qPCR of RNAs harvested from these discs detects strong up-regulation of *hid* and *puc* mRNAs, with more moderate induction of *rpr* and *spz6*, relative to control discs (**Figure 2.13G**). In the absence of Tai expression (*ptc>GFP*), Dcp-1$^+$ cells are relatively infrequent (mean=4 Dcp-1$^+$ cells per disc, n=7) (**Figure 2.13A,H**). Expression of Tai (*ptc>tai*) leads to a significant increase in Dcp-1$^+$ cells (mean=25 Dcp-1$^+$ cells per disc, n=6) with a majority of these apoptotic events located outside the GFP-positive *ptc* domain (approximately 76% in GFP-negative cells) (**Figure 2.13D,H,I**). Consistent with genetic interactions between *tai* and Toll and IMD components during wing invasion, the pattern and extent of *ptc>tai* driven apoptosis in the wing epithelium is sensitive to the IMD inhibitor *casp* and the Toll inhibitor *nec*. Removing one copy of *casp* (*ptc>tai,GFP;casp^{c04227}/+*) further increases the overall rate of death in wing (**Figure 2.13E,H**) and leg discs (**Figure 2.13E'**) relative to *ptc>tai,GFP* alone (mean=40 Dcp-1$^+$ cells per disc, n=10). Importantly, a majority of this new apoptosis occurs within the Tai-expression *ptc* domain (75% within the GFP-positive *ptc* domain) (**Figure 2.13E,I**), which parallels the lethal effect of the *casp^{c04227}* allele on Tai-invasive wing cells (see **Figure 2.11**). Moreover, these additional apoptotic cells that appear in *casp* heterozygous discs are concentrated in the wing pouch (boxed in **Figure 2.13E,E'**), which gives rise to the invasive pool of cells in the wing:thorax model.

Increased death of these Tai-expressing cells is a likely cause of the suppressed invasion observed in *MS1096>tai, casp^{c04227}/+* adults (see **Figure 2.9A,B**).

A mutant allele of the gene *nec* (*ptc>tai,GFP;nec^{10}/+*), which encodes an inhibitor of Spz processing and Toll signaling[92, 168], dominantly enhances the overall level of apoptosis to a very similar degree as *casp* heterozygosity (mean=41 Dcp-1$^+$ cells per disc, n=11) but differs in where this additional apoptosis occurs. In the *nec* heterozygous background, additional apoptotic cells are distributed more evenly between Tai-expressing and non-expressing cells: only 58% of total apoptotic events in *ptc>tai,GFP;nec^{10}/+* discs occur among Tai-expressing cells (**Figure 2.13F,H,I**). These data suggest that uniformly elevating Spz processing and Toll activity across the sheet of *ptc>tai,GFP* epithelial cells with the *nec* allele promotes killing of Tai-expressing cells and their neighbors, while *casp* heterozygosity preferentially kills Tai-transformed cells. The *spz6^{c601763}* allele, which strongly suppresses Tai-driven invasion in the thorax (see **Figure 2.9**), only mildly reduces the ability of Tai-expressing cells to kill neighbors (**Figure 2.13H-I**), suggesting that other Spz family members may play a more significant role in Toll-mediated killing of disc cells. These effects of *casp* and *nec* alleles on Tai-induced autonomous and non-autonomous apoptosis are consistent with a model in which Toll plays a more significant role in Tai-induced killing of neighboring cells during disc development, while a high threshold for IMD activation protects Tai-expressing cells from immune-associated apoptosis associated with Tai driven cell competition (see model, **Figure 2.13J**).
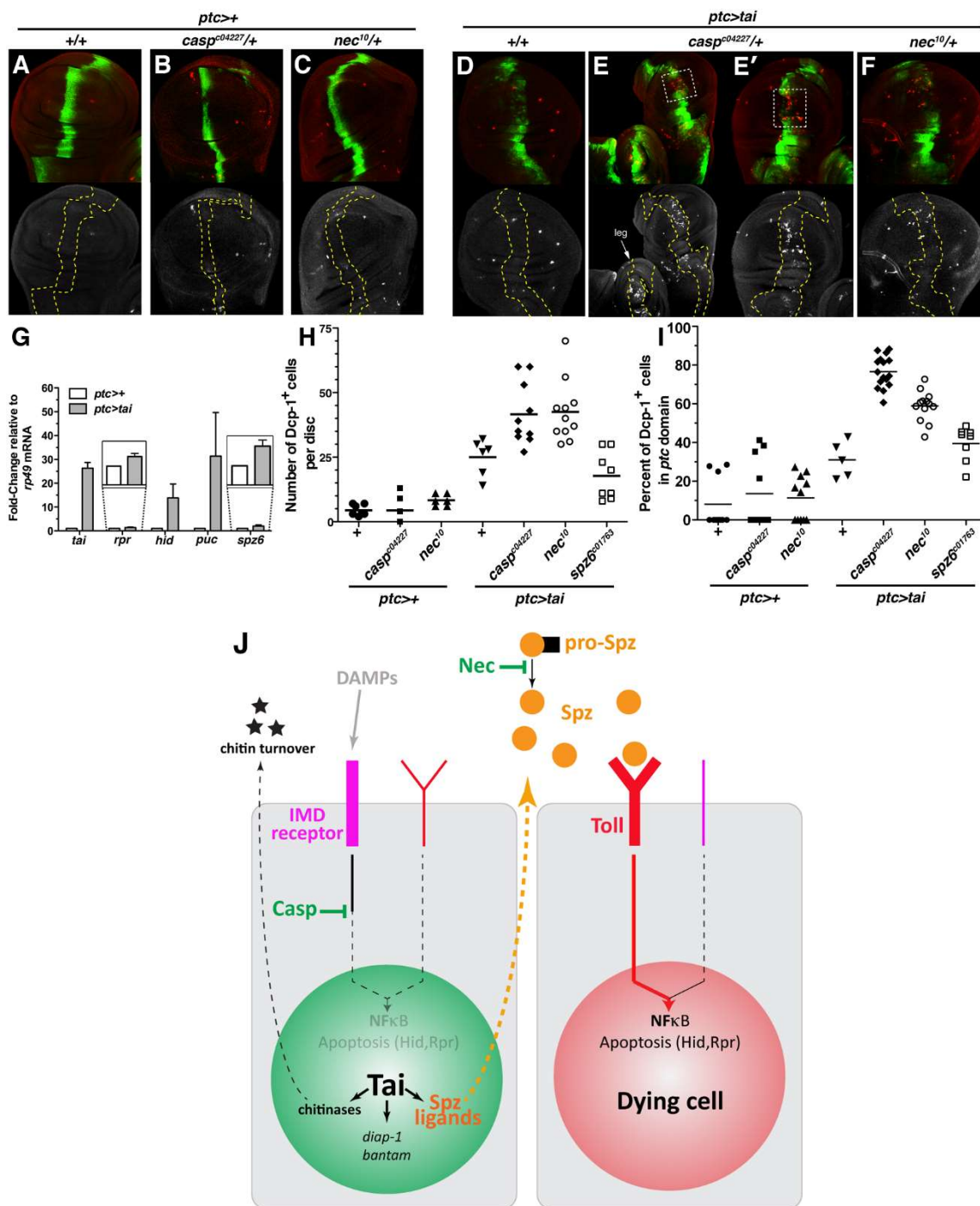
Figure 2.13 Tai-induced apoptosis in the larval wing discs

(A-C) L3 wing discs showing baseline level of Dcp-1+ cells across genotypes with no expression of *tai*. Yellow dotted lines mark *ptc-Gal4* expression domain. (D-F) L3 wing discs showing Dcp-1+ cells across genotypes with *ptc>tai* in the background. (G) qRT-PCR analysis of transcripts fold-change normalized to *rp49*. (H) Quantitation of total numbers of Dcp-1+ cells in wing discs across genotypes. (I) Quantitation of percent of Dcp-1+ cells in *ptc* domain across genotypes.

Discussion

The *Drosophila* Tai protein is a functional and sequence homolog of the steroid-receptor coactivator proteins, SRC-1, 2, and 3, which are overexpressed in a variety of human cancers[15, 179]. Tai has roles in maintenance and proliferation of female germline stem cells, collective motility, intestinal stem cell regeneration, and it promotes epithelial cell proliferation via cooperative effects on transcription with its binding partner Yki[15, 49, 125, 180, 181]. Tai also has a poorly understood role in transforming epithelia into locally invasive tumors[115] that may be shared by its SRC homologs. Here we show that transgenic expression of Tai is sufficient to transform sessile pupal wing cells to an invasive mass that penetrates into the adjacent thorax during a developmental window that coincides with the highest levels of the ecdysteroid 20E (20-hydroxyecdysone)[182]. Candidate-based analysis of this Tai-driven intertissue invasion confirms a reliance on the 20E-response pathway, including the 20E-receptor EcR and its associated repressor Smrter (human NCOR1), and multiple factors within the Hippo pathway, including Yki itself and the shared Yki-Tai target gene *dlp8* [49, 144]. RNA sequencing to identify mechanisms that underlie the invasive process detects enrichment for factors involved in innate immunity, including members of the Spz family of secreted Toll ligands. Spz-bound Toll receptors induce activity of the NF-kB family of transcription factors [156]. Tai expression in larval wing cells induces NF-kB activity in fat body cells prior to invasion, and in thoracic epidermal cells during invasion, raising the possibility that non-cell autonomous induction of the Toll pathway is required for invasion. In support of this hypothesis, alleles of Toll components (e.g. Spz4, Spz6, Myd88 and Dorsal) dominantly suppress Tai-driven intertissue invasion. RNAi depletion localizes the requirement for the

strongest suppressor, Spz6, to Tai-expressing cells, suggesting that an intercellular Spz-Toll circuit facilitates invasion. Excess Toll signaling causes apoptotic cell death in developing epithelia and in the context of Myc-induced cell competition[101, 117, 171]. The suppressive effect of the *H99* deletion, which removes the pro-apoptotic factors Rpr, Grim and Hid, argues that apoptosis is also required for Tai-driven intertissue invasion. Localizing this apoptosis in pupal cryosections reveals increased death of thoracic cells and cuticular epidermal cells adjacent to invading Tai-expressing wing tissue. Modeling these intercellular interactions with domain-specific expression of Tai in larval wing discs (using the *ptc-Gal4* driver) confirms that Tai-expression elevates levels of the *hid* and, to a lesser extent, *rpr* mRNAs and kills neighboring cells, and that this mechanism is enhanced by reducing expression of the *nec* serpin, a Spz-inhibitor. Tai-expressing cells are also killed by *nec* heterozygosity, arguing that these cells can be killed by a Spz/Toll-mediated death signal if its activity is sufficiently increased. Moreover, an allele of the IMD-inhibitor *caspar* selectively elevates death of Tai-expressing cells in the wing disc model and the intertissue invasion system, suggesting that these cells are able to evade local pro-apoptotic immune signals by maintaining repression of IMD signals (see model, **Figure 2.13J**). Overall, these data suggest that Tai-expressing wing cells use a Spz-Toll circuit to selectively kill neighboring cells in the invasion or wing epithelial models, and that differential sensitivity to IMD and Toll regulated apoptosis may underlie these asymmetric fates.

The pro-invasive effect of Tai in wing cells is notably different from its role border cell (BC) invasion through the nurse cell cluster[15]. BC migration does not involve death of nurse cells to make way for the BC cluster, nor is it known to genetically

depend on elements of the IMD or Toll pathways[183]. Rather, the ability of Tai to induce the apoptotic death of neighboring cells is more similar to Toll-mediated killing of 'loser' cells by Myc-overexpressing 'super competitor' cells[101]. Both phenomena are induced by expression of an oncoprotein (Myc or Tai), can occur between cells in an epithelial sheet (e.g. the wing disc), and involve non-cell autonomous apoptosis requiring elements of the Toll and IMD pathways. However, a Tai transgene drives intertissue invasion with multiple Gal4 drivers, while a dMyc transgene does not (**Figure 2.4**). One reason for the enhanced effect of Tai relative to dMyc may relate to the timing of the pupal 20E pulse, which seems likely to amplify the effect of transgenic Tai on immune gene expression via EcR[184]. The pupal 20E pulse also coincides with substantial epithelial remodeling and developmentally programmed interdisc fusion[185]. Alleles of the EcR/Tai-target *broad* (*br*) block some of these disc fusion events, arguing that transcription of EcR target genes can promote physiologic forms of intertissue fusion[49, 186]. Finally, the 20E pupal pulse also coincides with elevated chitin turnover on the apical surface of pupal wing cells[161]. High 20E levels are thus predicted to amplify Tai transcriptional effects at a time when tissue fusion programs and enzymes that remodel chitin are also active. The combination of these effects may enable Tai-expressing wing cells to penetrate the thoracic cuticle and signal to underlying epidermal cells in a way that Myc-expressing super competitors cannot.

How are Tai-expressing cells spared the apoptotic fate of neighboring cells? In some cell competition scenarios, winner vs. loser status is determined by competition for limiting survival factors (e.g. Dpp)[166]. In others, survival is determined by a unidirectional killing signal that acts on neighbors but not source cells[101, 187]. In this

study, the survival of Tai-expressing wing cells is sensitive to the genetic dose of the secreted Spz/Toll inhibitor Nec and the intracellular IMD pathway inhibitor Casp[92, 100]. The IMD pathway operates in parallel to the Spz-Toll pathway to control activity of the Rel domain transcription factors Relish, Dorsal and Dif[156, 158, 188], which induce AMP mRNAs in immune cells (e.g. fat body), but are also able to induce the pro-apoptotic genes *rpr* and *hid* in non-immune cells such as neurons and epithelial cells[101, 117, 171]. The pattern of Tai-induced sensitivity to these pathways appears to reveal elements of the unidirectional mechanism that operates in *ptc>tai,GFP* discs. Lowering Nec enhances killing of Tai-expressing cells and neighbors alike, arguing that enhanced Spz processing renders Tai-expressing cells susceptible to apoptosis (see model in **Figure 3.13J**). This effect could be due to an increase in overall levels of processed Spz ligands, or altered distribution of these ligands within the disc (as in [189]). The apoptotic resistance of Tai-expressing cells may stem in part from elevated expression of the anti-apoptotic factors *diap1* and *bantam*[49, 125], but the genetic sensitivity to *casp* gene dosage indicates that it also requires IMD repression. The basis for this requirement is not clear. However, the up-regulation of the *PGRP-LC* and *PGRP-LD* mRNAs in Tai-expressing cells (**Figure 2.5D**) may sensitize these wing cells to damage-associated molecular patterns (DAMPs), which act as IMD ligands[158]. It is interesting to note that Yki, which we find can also drive wing-into-thorax invasion (**Figure 2.4A**), activates expression of the Toll-inhibitor *cactus* in wing disc cells[108]. Elevated Cact protein levels are predicted to raise the threshold for Toll pathway activation in Yki-active cells relative to adjacent normal cells, which could in turn provide Yki-active epithelial cells with enhanced resistance to local innate immune signals that converge on *rpr* and *hid*.

Although cell competition can serve a tumor suppressive role by eliminating potentially cancerous cells in *Drosophila* and mice[187, 190], emerging evidence from *Drosophila* argues that competition-induced death may also promote aspects of the tumor phenotype, including invasion and metastasis. Clones of cells lacking the *Drosophila* Adenomatous polyposis coli (*Apc*) tumor suppressor homolog require competitive death of neighbors to expand within the gut epithelium[191], and competitive killing of neighboring cells is also required for invasive behavior of clones co-overexpressing the *EGFR* and *miR-8* oncogenes[192]. Stereotypic features of Myc-induced cell competition have also been found among normal cells bordering invasive human cancers, leading to the hypothesis that competition-induced death enables these cancers to colonize new sites[193]. The data presented here suggest that expression of the Tai oncoprotein induces killing of neighbors via a mechanism that resembles Toll-dependent killing by dMyc-transformed super competitors, and that this contributes to the pathologic invasion of Tai-expressing wing cells into the thorax. Repression of the IMD pathway, which operates in parallel to Toll to control the NF-kB family of transcription factors, is necessary for Tai-transformed cells to retain 'winner' status in the developing wing epithelium. Local inflammatory signaling mediated by Toll-like receptors (TLRs) and functional homologs of PGRP is also a common feature of many cancers, including those of the breast and prostate[194-196], where it can have either pro- or anti-tumor effects[196]. Interactions between cancer cells and adjacent stroma are likely to underlie these alternative phenotypic effects of TLR activation. The data presented here suggest that the fate of Tai-expressing cells also depends on local immune signals present at the boundary with other cell types. Evidence indicates that the pro-competitor role of Tai is also based on

exchange of immune signals with neighboring cells, and that shifting this system in favor of IMD signaling can transform Tai cells from winners into losers. In future, this model of Tai function may provide insight into immune-based interactions that contribute to the competitive advantage of human tumors overexpressing Tai homologs.

Material and Methods

Genetics & deficiency stocks

All crosses were maintained at 25°C unless otherwise noted. Alleles used: (BDSC stock numbers indicated) *MS1096-Gal4* (#8860), *nubbin-Gal4* (#42699), *rotund-Gal4* (#7405), *engrailed-Gal4* (#30564), *UAS-tai* (#6378), *UAS-tai^{ΔB}* (#28273), *UAS-tai^{PPxA}*, *UAS-wts-IR* (#34064), *pvf^{2-3}* (gift of R. Read), *ds^{33k}* (#288), *UAS-smr-IR* (#34087), *drs-GFP,dipt-lacZ* (gift of R.Jones), *rel^{E20}* (#9457), *FADD^{f06954}* (#19026), *DREDD^{B118}* (#55712), *gd^{7}* (#3109), *gd^{EY00677}* (#15472), *myd88^{KG03447}* (#14091), *casp^{c04227}* (#11373), *dl^{1}* (#3236), *dl^{4}* (#7096), *UAS-spz-IR* (#28538), *UAS-spz4-IR* (#60044), *UAS-spz6-IR* (#57510), *NT1^{41},spz5^{AW18}* (#64069), *spz4^{MI15678}* (#61127), *spz6^{c01763}* (#10719), *UAS-Pten-IR* (#33643), *hid^{W05014}* (*hid-lacZ*; gift of T.T. Su*)*, *UAS-dMyc*, *UAS-EcR^{LBD}*, *UAS-EcR-IR* (#29374), *UAS-dIlp8-IR* (VDRC: v102604), *hpo^{kc240}* (#25090), *Df(3L)H99* (#1576), *UAS-cht5-IR* (#57512), *UAS-cht6-IR* (#54823), *UAS-Toll-IR* (#31477), *nec^{10}* (#4288), *UAS-stat92E* (#20181), *wts^{x1}* (#44251), *UAS-yki* (D.J. Pan), *UAS-EcR.A* (#6470), *UAS-hpo-IR* (#35176), *th-lacZ* (*diap1-lacZ*, #12093). A subset of deletion lines from the chromosome 2L and 2R deficiency (*Df*) kits (BDSC) were crossed with *MS1096-Gal4,UAS-tai/TM6B,tub>Gal80* in duplicate at 18°C and 25°C. Wings of F1 progeny were scored by visual inspection under light microscopy.

RNA sequencing and analysis

Total RNA extracted from ~80 L3 wing discs per genotype (Trizol™) was subjected to high-throughput sequencing (HTS) as described previously[49]. Briefly, 4 μg of total RNA was rRNA depleted and utilized for library construction with the Illumina TruSeq RNA Sample Preparation Kit v2 following the manufacturer's instructions. Libraries were

sequenced with an Illumina HiScan platform. Cluster generation was performed with Illumina TruSeq cluster kit v2-cBot-HS. Single-read 50 bp sequencing was completed with Illumina TruSeq SBS kit v3-HS. Reads were aligned using Tophat2 v2.0.12, and RPKM expression values from different conditions were extracted and compared by cuffdiff v2.2.1 using Refseq gene models [197].

Adult imaging and pupal cryosections

Adult flies were frozen at -20°C for >2 hours and imaged on a Leica DFC500 CCD camera. Multiple focal planes were merged and processed to generate a final image. White pre-pupae (WPP) were washed in 1x phosphate buffered saline (PBS), aged for 18hr in fresh vials, then detached from the vials and glued onto a glass slide with nail polish. After 20min, the case was removed, and the pupa was transferred to 4% paraformaldehyde in PBS-T 0.1% (Triton-X100) and incubated at 4°C overnight. Pupae were then rinsed in PBS-T 0.1% incubated at 4°C overnight in 15% sucrose/PBS-T 0.1%, and then overnight in 30% sucrose/ PBS-T 0.1% solution. Pupae that have sunk to the bottom were embedded in Optimal Cutting Temperature (OCT) resin and thin-sectioned onto charged slides for immunofluorescence microscopy.

Immunofluorescence microscopy

Immunostaining and confocal microscopy were performed using standard procedures. Primary antibodies used: mouse anti-ß-Gal, 1:1000 (Promega); rabbit anti-GFP, 1:500; rabbit anti-cleaved Dcp-1, 1:400 (Cell Signaling). Secondary antibodies: goat anti-rabbit-FITC, 1:100; goat anti-mouse-Cy3, 1:100 (Jackson Labs); goat anti-mouse-Cy5, 1:100 (Jackson Labs); goat anti-rat Cy3, 1:100 (Jackson Labs); goat anti-rabbit Cy5, 1:100 (Jackson Labs); DAPI, 1:5000. Images were collected on a Zeiss LSM7-10 or Olympus

FV1000 system. Images were viewed and prepared with Fiji[198] and Photoshop software.

Quantitative reverse-transcription PCR (qPCR)

For pupal wing RNAs: WPP were isolated, washed, sex sorted, and transferred to a new vial for aging. After 6 hours, pupal wings are dissected and dissolved in 0.5mL of TRIzol. For L3 wing imaginal disc RNAs: discs from wandering L3 larvae were dissected and dissolved in TRIzol. RNA isolation was done using standard protocol utilizing TRIZOL and Qiagen RNeasy kit. cDNA library preparation was done using SuperScript™-III RT kit from ThermoFisher. cDNAs generated with Superscript III RT and random primers (Invitrogen) were analyzed by qPCR with exon-junction spanning primers with SYBR Green I Master Mix (Roche) on a Roche LightCycler 480 in triplicate. Primers were designed using Primer3Plus [199] and purchased from IDT technologies.

Gene	Primer 1	Primer 2
rp49	CGGATCGATATGCTAAGCTGT	GCGCTTGTTCGATCCGTA
edg78e	GCGGCCAGTCATTGTTATTT	CATCCGCCTGAAATTTGTTT
cpr100A	AAGTTCGGAGCTGCCTATGA	GGCAAGTGATCTCCAGAAGC
ftz-f1	TGATCGACTTCAAGCACCTG	CTCGAGGCACTTCTGGAATC
dilp8	GCTGGTCATCGGAGTCTGTT	TAGCTGCTTCGGCTGATGT
spz	GGAAGCTGGTGTACCCAAAA	GTCCAGTTCGCCATCACTTT
spz4	CACAGTTGGGGCTTCGTAAT	GATGCGGGTGAGTACTTGGT
spz6	TTCAGGCACGCTGTCACTAC	TGCCCTCTTCTGCAGGTACT
cht5	CCAGGTCCTGTTCCAACTGT	ATCTCGTTGGGATCGAACTG
cht6	TCAGCGAAGCTTCAGAGACA	CAATTTTTCAATGCCCTCGT
PGRP-LD	TCGGCACACTGAACTTCTTG	TCTTCCAGCGAAGAAGGAAA
PGRP-LC	GCTCAACGATTCGAAATTGG	GGGCGGTACATTATTTTTCGT
tai	CTCCGTTTGGCTCTAACTCG	TGTTGTTGCAGCGTTCTACC
rpr	ACGGGGAAAACCAATAGTCC	TGGCTCTGTGTCCTTGACTG
hid	CTAAAACGCTTGGCGAACTT	CCCAAAAATCGCATTGATCT
puc	GTTTCTGAAGCCACCTCTGC	GTTTTCGCTTTGTGGTTGGT

Differential Quik (Diff-Quik) hemocyte counts

Wandering L3 larvae were washed, transferred in a glass well in15 µL of 1xPBS, and exsanguinated using tweezers. 5 µL of PBS/hemocytes mix was dropped onto a glass slide and dried completely, then stained with Diff-Quik stain kit™ (EMS #26096-25) and imaged. Blue stained nuclei were counted by light microscopy across multiple fields.

Statistics

Unpaired student t-test (GraphPad Prism™) was used to analyze significance between paired data sets. Unless noted, significance values in text and figures are denoted by asterisks as follows: *=0.01<p<0.05, **=0.001<p<0.01, ***=p<0.001.

Chapter 3

A deficiency screen for uncovering dominant modifiers of Tai-driven wing invasion

Parts of this chapter was adapted from the following paper in review:

Byun PK, Zhang C, Yao B, Wardwell-Ozgo J, Terry D, Peng J, Moberg KH. *The Taiman transcriptional coactivator engages Toll signals to promote apoptosis and inter-tissue invasion in Drosophila.* Curr Biol. (*in review*)

Introduction

Tissue invasion, both in development and in pathology, is a complex biological process carried out in multiple mechanisms and contexts. A well-described pathological example is the metastasis of cancer cells represented by delamination, degradation of the basement membrane, and cytoplasmic extensions [56]. However, neoplastic tumors can invade the surrounding tissue as an intact tissue, maintaining adhesion between cells, termed collective invasion [200]. A similar developmental example of tissue invasion is the border cell migration in the developing egg of *Drosophila*. A *Drosophila* egg is composed of polyploid nurse cells, an egg, and cuboidal epithelial follicle cells that encapsulate them [201]. Upon a developmental cue, pole cells which reside in the anterior most part of the egg chamber recruit neighboring follicle cells (now border cells) to become a ball that delaminates and starts to invade through the nurse cells towards the egg. This process requires the border cell cluster to be fluid enough for filopodial extensions and migrating between nurse cells but also sustain adhesion within the cluster to prevent disassembly [202]. Study into border cell migration has posited a different perspective on defining tissue invasion. A necessary developmental cue for this process is the steroid hormone ecdysone and its signaling pathway executed by the Ecdysone Receptor (EcR) and its co-activator Tai [15]. Border cells mutant for *tai* are either too slow or do not migrate at all. Tai/EcR complex turns on necessary transcriptional program for cell motility.

We have discovered that overexpression of Tai in the developing wing epithelia in *Drosophila* leads to adults eclosing (hatching) from the pupae with wing tips embedded on the side of the thorax, penetrating the thoracic cuticle and epidermis. Taiman is the

sole *Drosophila* homolog of human steroid receptor co-activator family (SRC 1-3) of proteins, most closely resembles SRC-3, also known as Amplified in Breast Cancer 1 (AIB1) [15]. SRCs have been shown to be oncogenic and promotes invasive behavior in cancers [48, 203-206]. However, knowledge about the transcriptional landscape that contributes to the invasiveness of the steroid hormone signaling is limited. With such a visually tractable phenotype, Tai driven wing tissue invasion phenotype presents an opportunity to perform a high throughput genetic screen to identify downstream targets of Tai/EcR assembly that may elucidate the pathogenic effect of hyper steroid hormone signaling in wing epithelia. Here we show the result of a deficiency screen performed on the second chromosome of the *Drosophila* genome to look for dominant modification of the phenotype.

Results

Overexpression of *tai* drives invasion of the *Drosophila* wing into the thorax

To model ectopic expression of Tai and its effect on an epithelium, Tai transgene was expressed using the wing-specific *MS1096-Gal4* (*Bx-Gal4*). The *MS1096* line directs Gal4 expression in the dorsal half of the larval pouch and in the dorsal sheet of the pupal wing [120, 121]. Approximately 90% of *MS1096>tai* animals die as pharate adults (n=83) with survivors displaying malformed and crumpled wings with distal ends embedded into thoracic cuticle immediately anterior to the haltere (**Figure 3.1A-B**). This "embedded wingtip" phenotype is highly penetrant among eclosed adults (>90% of survivors at 25°C) and accompanied by a slightly raised ring of cuticle around the site of wing:thorax contact (inset in **Figure 3.1B**). Consistent with the temperature sensitivity of the Gal4/UAS system[116], the *MS1096>tai* embedded-wingtip phenotype is absent at 18°C (**Figure 3.1C**). This phenotype is repeatable using different pan-wing drives *nubbin-Gal4 (nub)* and *rotund-Gal4 (rn)* (**Figure 3.1D,E**).

To test whether this 'wing invasion' phenotype is specific to Tai biology and function, we modified known physical and genetic interactions between Tai and its interactors. Because Tai interacts with the 20E receptor (EcR) and co-activates EcR-dependent gene transcription[15, 132], it suggests that 20E and EcR/Tai complex stability may be a required Tai-driven wing invasion. Consistent with this hypothesis, *MS1096>tai* wingtip invasion is blocked by RNAi depletion of EcR, which mediates transcriptional effects of 20E in border cells and wing disc cells[15, 49, 125], or expression of a dominant negative *UAS-EcR^{LBD}* transgene encoding a EcR ligand-binding domain fragment that 'sponges' 20E in cells[133, 134] (**Figure 3.1F**). Reciprocally, a

tai$^{\Delta B}$ transgene encoding a version of Tai that cannot be bound and an inhibited by the Abrupt protein[132], enhances invasion at 18ºC (**Figure 3.1G**). Although RNAi of the EcR-associated repressor *Smr* is alone insufficient for invasion (**Figure 2.4A**), it cooperates with *tai* overexpression to enhance invasion at 18ºC (**Figure 3.1G**). This result is consistent with the finding that Smr represses expression of EcR and Hippo target genes in wing disc cells[39, 49].

Consistent with previous described interaction between Yki and Tai, a version of Tai that cannot bind Yki (*UAS-tai*^{PPxA}) has reduced ability to drive wing invasion (**Figure 3.1F**), indicating that Yki contributes to *MS0196>tai* invasion. In addition, RNAi knockdown of *wts* encoding upstream kinase that de-activates Yki protein in the background of Tai expression at 18°C enhances the phenotype (**Figure 3.1G**). The pattern of genetic interactions between *tai* and Hippo pathway components (e.g. PPxA allele and *wts-IR*) implies that transcription of Yki-dependent genes supports Tai driven wing-invasion. To test whether excess Yki can phenocopy Tai and produce wingtip invasion, a weak *yki* transgene (*UAS-yki* on chr2) was expressed from the *MS0196* driver. *MS1096>yki*^{chr2} wings do not attach to the thorax; however, further elevating Yki activity with a loss-of-function allele of *warts* (*wts*^{x1})[137], results in an embedded wingtip phenotype (*MS1096>yki*^{chr2},*wts*$^{x1/+}$) that resembles *MS1096>tai* (**Figure 2.4A**). Collectively, these genetic data provide evidence that Tai requires elements of the 20E and Hippo pathways, including its binding partner Yki, to drive expression of genes that transform developing wingtip cells into an invasive tissue.
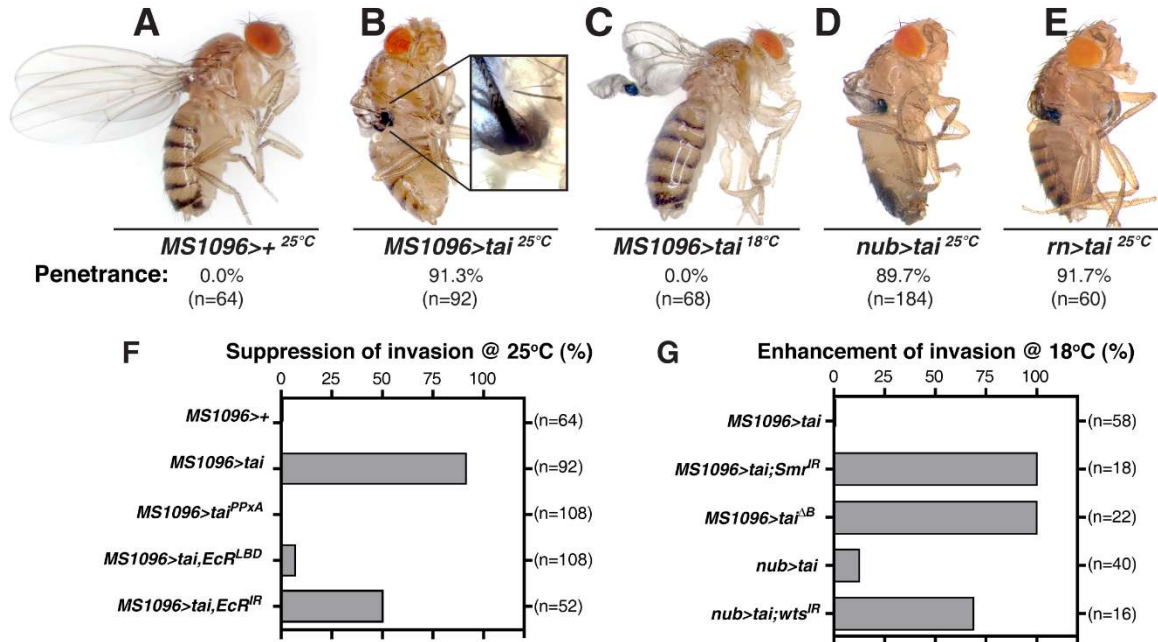
Figure 3.1 Overexpression of *tai* drives invasion of the *Drosophila* wing into the thorax.

(A-E) Adult flies driving the expression of UAS-tai with three different pan-wing Gal4 lines (*MS1096*, *nubbin*, and *rotund*). Temperature indicates the environmental condition. **(F-G)** Alleles of known tai interactors can modify the wing invasion phenotype.

A discovery-based deficiency screen reveals genetic loci that dominantly modify Tai driven wing invasion

To determine downstream pathways that contribute to this phenotype, we performed a dominant modifier screen using the deficiency kit from the Bloomington Stock Center (Bloomington, IN) (**Figure 3.2A**). *MS1096>UAS-tai* stock is highly lethal, and a small percentage of escapers exhibit wing-thorax invasion phenotype (90% lethal, n=83) that maintaining a stable line is untenable. So, we balanced the stock over a balancer chromosome that expressed GAL80 protein constitutively under *tubulin* promoter.

The deficiency kit across 2L and 2R of *Drosophila* genome consists of 185 stocks. The stable line that expresses *UAS-tai* in the wing under the MS1096-GAL4 driver is crossed to each deficiency allele and the F1 progeny was scored based on suppression at 25°C. Due to the temperature sensitive nature of the GAL4-UAS system where in a colder environment, the transgene expression is weaker, *MS1096-GAL4>UAS-tai* flies reared at 18°C do not show the wing-to-thorax invasion phenotype (**Figure 3.2B**). Therefore, we made duplicate crosses at 18°C to look for dominant enhancers of the phenotype. Examples of suppression almost always have deformed and crumpled wings but no invasion through the thorax (**Figure 3.2B**) suggesting that genes within that deletion acts to promote invasion. Of the alleles tested, a total of 32 alleles dominantly suppressed the wing invasion phenotype: 10 alleles suppressed the phenotype strongly (+++), 8 alleles showed mild suppression (++), and 14 alleles showed weak (+) suppression. Strength of suppression was assessed by qualitative measures, and a few candidate genes were tested based on their gene ontology and known relevance to tissue invasion and cell motility. *Df(2L)BSC291* includes two genes *pvf2* and *pvf3* which

encodes ligands for Pvr, a PDGF/VEGF-related receptor which are shown genetically interact with *tai* in border cell migration (**Figure 3.3A&E**) [135]. An allele that deletes both *pvf2* and *pvf3* called *pvf²⁻³* can dominantly suppress the Tai wing invasion phenotype (penetrance 40%, n=20), confirming that the deficiency takes out a crucial component that enables Tai to promote wing epithelium to invade the thorax. This is repeatable using *nub* as the driver (penetrance 61.8%, n=88). Deficiency alleles *Df(2L)BSC278* (**Figure 3.3D**), *Df(2R)BSC280*, and *Df(2L)BSC148* contain genes involved in the Toll innate immune pathway *cactus* (*cact*), *myd88*, and *dorsal* (*dl*), respectively. Null alleles to these genes can dominantly suppress the wing invasion phenotype as well (**Figure 3.3F**), suggesting that the Toll pathway or innate immunity might be involved in tissue invasion.

Enhancement at 18°C brings back the invasion phenotype suggesting the deleted genes normally inhibit wing invasion (**Figure 3.2B**). Of the alleles tested, 9 enhancing deficiencies were identified. Since the penetrance of wing invasion at 18°C is 0%, any increase in penetrance was measured as enhancement. Interestingly, two deficiencies *Df(2R)ED3728* and *Df(2L)ED105* identified as enhancers harbor upstream regulators of Yki activity, *hippo* (*hpo*) and *dachsous* (*ds*), respectively. Hpo protein phosphorylates Wts, which phosphorylates Yki and keep it in the cytoplasm for inactivation [78]. Dachsous is a cadherin-like protein involved in cell-cell adhesion that negatively regulates Yki as loss of adhesion leads to Yki activation [207]. These results support the notion that Hippo pathway, thus Yki, help facilitate the Tai-driven transformation of wing tissue to invade the thorax.
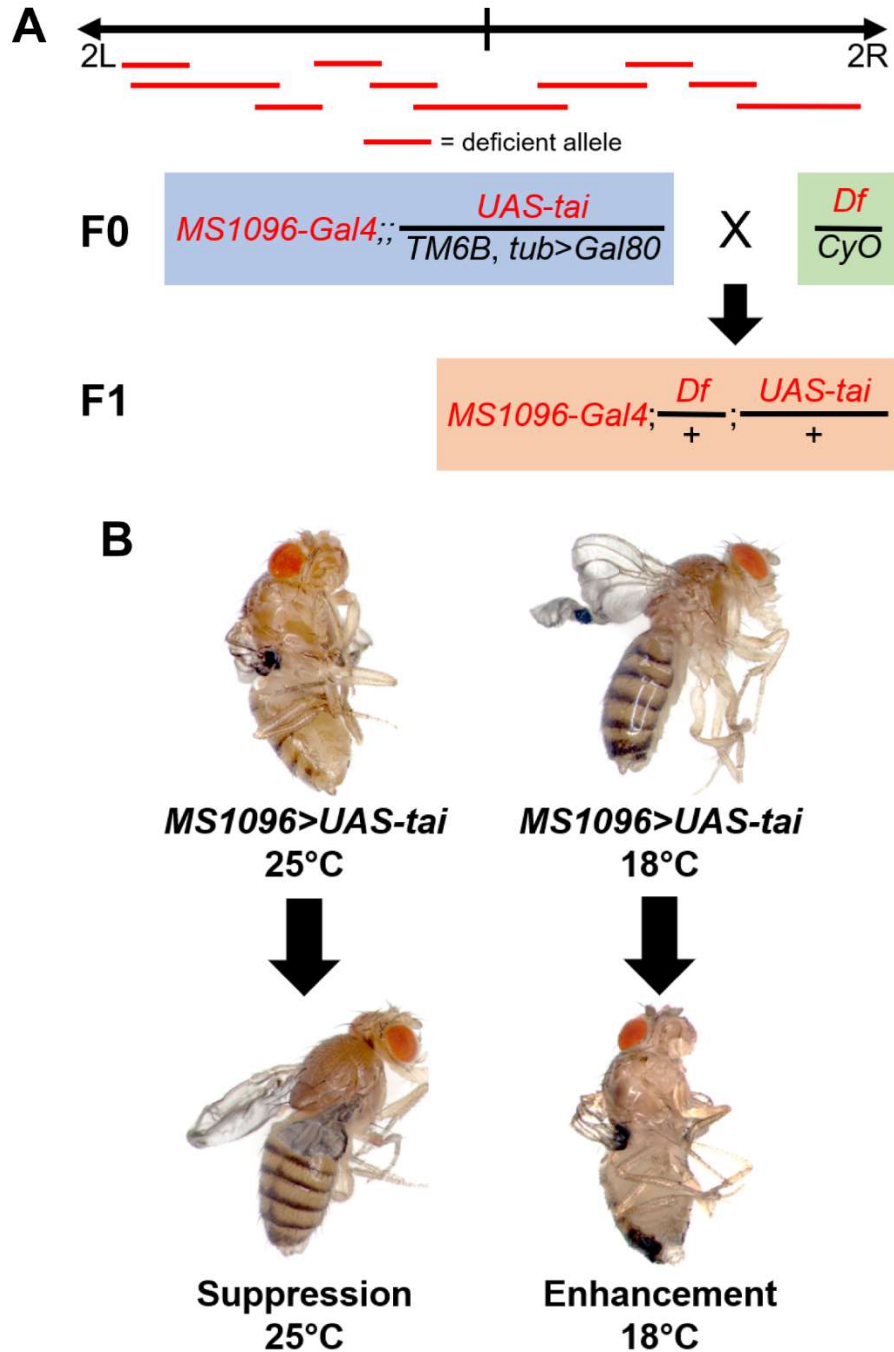
Figure 3.2 Mating Scheme for the Deficiency Screen across 2L and 2R
(**A**) A stable stock expressing *UAS-tai* is made using a balancer stock that constitutively expressed GAL80 protein that binds to GAL4 and prevents transgene expression. In the F0 across, the stable GAL4 line and a deficient allele (Df) is crossed. In the F1 generation, the progeny has the Df in the background *UAS-tai* overexpression in the wing is sorted and recorded for suppression at 25 °C and enhancement at 18 °C. (B) An example of what a suppression and enhancement look like at 25°C and 18°C, respectively.
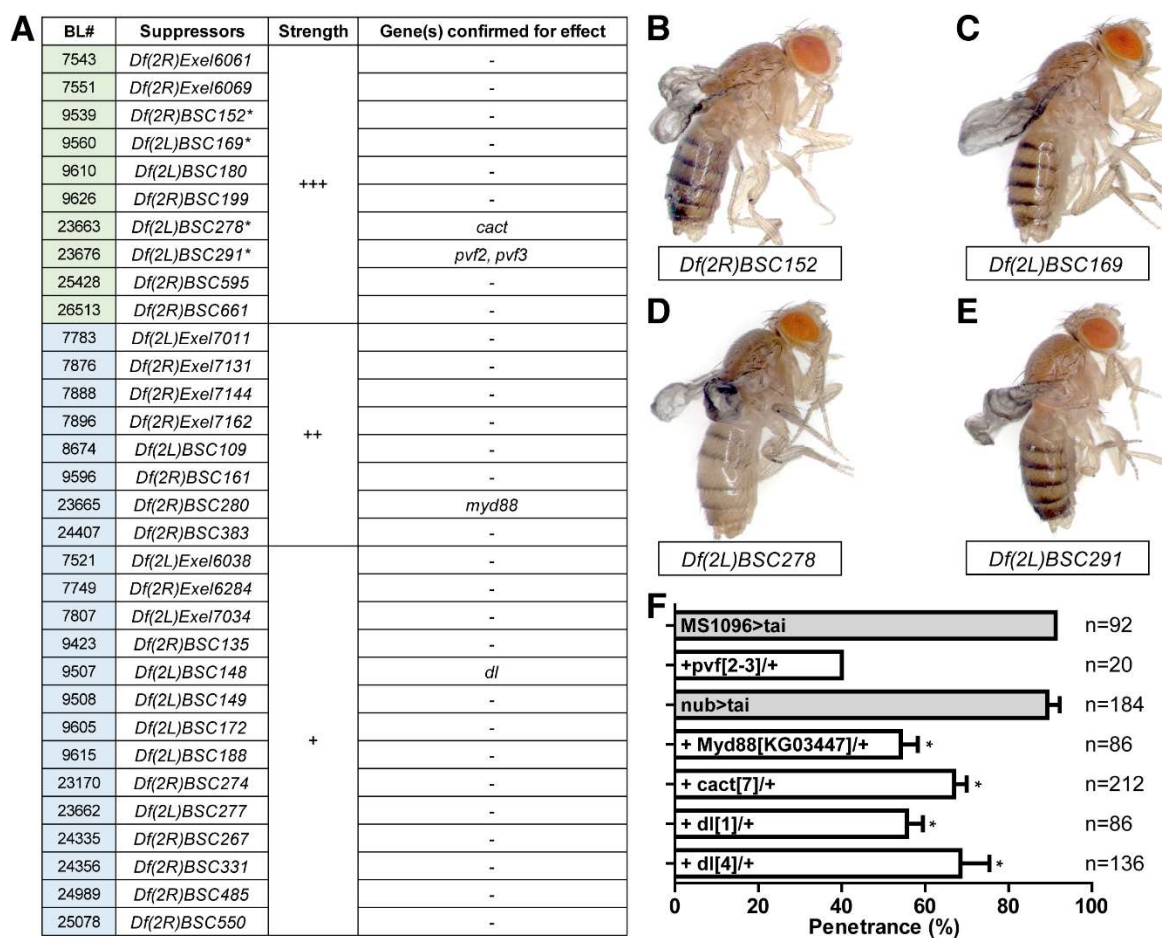
Figure 3.3. Alleles to suppress the invasion phenotype.
(A) A table of alleles that suppress the wing invasion phenotype in varying strength (+ = weak, ++ = mild, +++ = strong). **(B-E)** resultant adult phenotype of alleles marked with asterisks. **(D)** Penetrance of suppressing alleles identified from deficiencies. (*=$p<0.05$)

A

BL#	Enhancers	Strength	Gene(s) confirmed for effect
90	Df(2L)C144		-
2471	Df(2R)M60E		-
6338	Df(2L)BSC6		-
8901	Df(2L)ED19		-
8915	Df(2R)ED2457*	+++	-
8931	Df(2R)ED1715		-
9067	Df(2R)ED3728		hpo
24118	Df(2L)ED105*		ds
25705	Df(2R)BSC630		-

B

Df(2R)ED2457

C

Df(2L)ED105

D

MS1096>tai — n=58

+ds[33k]/+ — n=14

+hpo[kc240]/+ — n=20
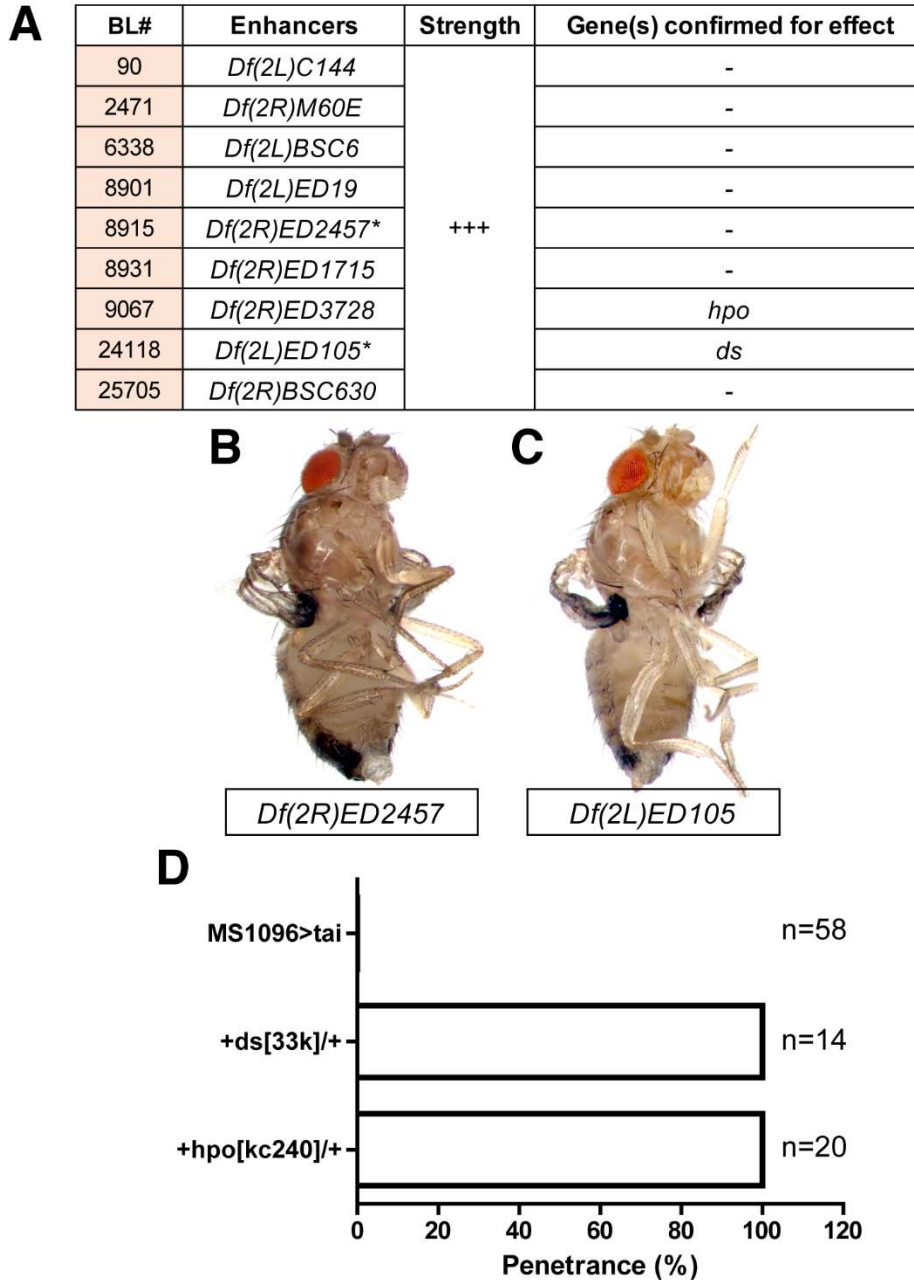
Penetrance (%)

Figure 3.4. Alleles to enhance the invasion phenotype.
(A) A table of alleles that enhace the wing invasion phenotype. **(B-C)** resultant adult phenotype of alleles marked with asterisks. **(D)** Penetrance of enhancing alleles identified from deficiencies.

Discussion

Here we utilize the wing-thorax intertissue invasion driven by EcR co-activator Tai as a model to identify downstream targets of EcR/Tai complex that enables the wing epithelium to transform and invade the neighboring tissue. We find that Tai-driven wing invasion is sensitive to the manipulation of two pathway that cooperate with Tai, namely the Hippo pathway and the Ecdysone Receptor pathway. Knocking down *ecr* gene or overexpressing a version of EcR that binds to 20E but cannot binds DNA (dominant-negative) can suppress the wing invasion phenotype cause by Tai overexpression (**Figure 3.1F**). In addition, expressing a version of Tai transgene that cannot bind Yki does not lead to any tissue invasion, but coupled expression of Tai and *wts-IR* at 18°C does (**Figure 3.1F-G**)

Using discovery-based approach we identified several genes and genetic loci that modify Tai-driven tissue invasion and could potentially define novel pathways can contribute to tissue invasion. The deficiency screen uncovered a few expected genes that are known to genetically interact with Tai or Yki including *pvf2*, *pvf3*, *ds*, and *hpo*. However, uncovering of Toll signaling pathway components was unexpected. The requirement of *dl, cact,* and *myd88* suggests that Toll pathway or its well-known role in innate immunity could be involved in the tissue invasion of Tai expressing cells in to the thorax. Published work by the Johnston lab shows that Toll pathway plays an important role in cell competition and the hyperactivation of the Toll leads to upregulation of pro-apoptotic gene *reaper* [101]. This leads to the hypothesis that Tai expressing wing tissue invades the thorax via upregulating Toll. Further investigation of this hypothesis and its significance will be elaborated in Chapter 3 of this dissertation.

Experimental Procedures

the GAL4-UAS System and GAL80

Adapted from *Saccharomyces cerevisiae*, the GAL4-UAS system is binary expression system where the GAL4 protein is expressed by a desired promoter (often referred to as a 'driver') and can turn on a gene under the control of the UAS (Upstream Activating Sequence). This allows for tissue specific and temporal specific expression of the transgene in the animal whether it'd be a full-length protein or a RNAi cassette for knocking down expression. Transgene expression is achieved by crossing a fly from the GAL4 'driver' line to another fly from the transgene line. The F1 offspring receives the GAL4 driver from one parent and the transgene from the other, culminating in the expression of the transgene in a tissue-specific/time-specific manner.

GAL80 is a protein that binds to GAL4 protein and inhibits transgene transcription. Continuous expression of certain GAL4 induced transgene expression can be lethal or disadvantageous. In such cases, subsequent generations of progeny can cull for weaker activation of transgene expression. Therefore, controlling the expression of the transgene is important for a more precise and accurate genetic analysis.

Deficiency Kit

A deficiency allele contains a deletion in a region of the *Drosophila* genome that can span from a few kilobases to a megabase. As a collection of deletion alleles that overlap, a deficiency kit can cover an entire chromosomal deletion and can be a tool to discover dominant modifiers of a phenotype. Deficiency kits are curated and sold by the Blooming Stock Center (Bloomington, IN)

Chapter 4

The requirement of steroid hormone production in the wing epithelium

for proper growth

Introduction

Cell growth and organ size control receive various inputs such as nutrition, developmental timing, and injury. A developmental input that is conserved from *Drosophila* to humans is the steroid hormone signaling pathway that allows systematic changes to cell growth, cell death, and tissue organization at the organismal level. Aberrant steroid hormone signaling pathways in humans including estrogen, androgen, and progesterone have been linked to multiple diseases, most notably cancer [46, 48, 203, 208]. One of the first strategies clinicians take against steroid hormone related breast and prostate cancers is to prescribe anti-estrogen or anti-androgen drugs [47, 209]. However, the extent of steroid hormone signaling is far reaching in any genomic landscape and inputs into many biological processes that a more precise understanding of how the hormone signaling converges on cell growth pathways is needed.

In *Drosophila*, the most analogous steroid hormone to human sex hormones is ecdysone (E), also known as molting (ecdysis) hormone that controls major developmental changes including larval to pupal transition and metamorphosis [210-212]. Ecdysone binds to its receptor the Ecdysone Receptor (EcR) which forms heterodimeric complex with RXR homolog Ultraspiracle (Usp) to turn on necessary gene transcription. In the presence of Ec, a co-activator Taiman (Smr), analogous to human Steroid Receptor Coactivator (SRC) family, binds to EcR and help facilitate gene expression while in the absence of Ec, a co-repressor Smrter (Smr) binds EcR to repress gene expression [39, 213]. During *Drosophila* development, pulses of ecdysone activates a cascade of gene expression that results in larval molting and metamorphosis (Figure 3.1A). These high peaks of ecdysone titer that marks each developmental stage are linked to cell fate

changes and differentiation [210, 214] and have been well studied. However, low concentrations of ecdysone have been linked to proliferation of germline stem cells and stem cell maintenance in adults [33].

Recent work in our lab has revealed that Tai and the Hippo pathway nuclear co-activator protein Yorkie (Yki) physically bind in the nucleus to turn on germline stem cell genes (*nanos* and *piwi*) [49]. Yki is known to have a role in intestinal stem cell maintenance but the cooperation with EcR/Tai pathway was unknown [76, 215]. Its human homolog YAP1 has also been linked to bone marrow stem cell osteogenesis, and elevated levels of YAP1 promotes cancer stem cell-like characteristics in prostate cancer, leading to castration resistant growth [216, 217]. One possible explanation for castration resistance could be explained by YAP1 binding to androgen receptor (AR) in the nucleus, likely through an SRC mediating the binding where gene transcription occurs in a hormone independent manner [45, 48, 51]. Another possibility is that cancer cells synthesize their own supply of steroid hormone. A study in this area shows an aromatase CYP19A1, a key enzyme that regulates local production of androgens, is highly elevated in metastatic prostate cancer cells, providing an evidence for steroid synthesis as the reason for steroid independence [218].

In *Drosophila,* ecdysone synthesis pathway consists of a group of genes called Halloween genes, responsible for converting the basic substrate cholesterol to ecdysone [36]. All steps of ecdysone synthesis except for the last occur in a ring-like structure adjacent to the brain stem called the prothoracic gland (PG) (Figure 3.1B). Once E is made, it is released from PG and cells in the gut and the fat body convert E to 20E (the active substrate for the EcR/Tai complex) by a cytochrome P450 enzyme Shade (Shd),

Drosophila homolog of CYP24A1 [37, 219]. The conventional understanding of 20E production and reception is that its production is systemically controlled, and its reception is through simple diffusion through the cell membrane since steroids are often diffusible. However, recent studies challenge these notions. First, border cells are shown to produce their own titer of 20E for migration (refer to Chapter 1 for more information) [35]. Although this is a specific developmental example, this posits to a possibility of more examples of local 20E regulation. Second, a 20E specific importer (Ecdysone Importer; EcI) was identified recently and is shown to be required in a cell-autonomous manner to drive ecdysone dependent gene expression [220]. Both discoveries point toward the fact that local production and local regulation of 20E titer is possible and important for biological processes

In this study, we seek to elucidate the role of local production of 20E by knocking down the gene *shd* involved in the last step of the ecdysteroid synthesis pathway converting E to 20E. We show that *shd* knockdown leads to a smaller organ in an autonomous manner and this is due to excess apoptosis. We show that this effect is due to the decreased activity of the Hippo nuclear effector co-activator Yki leading to decreased expression of pro-survival and pro-proliferative genes.
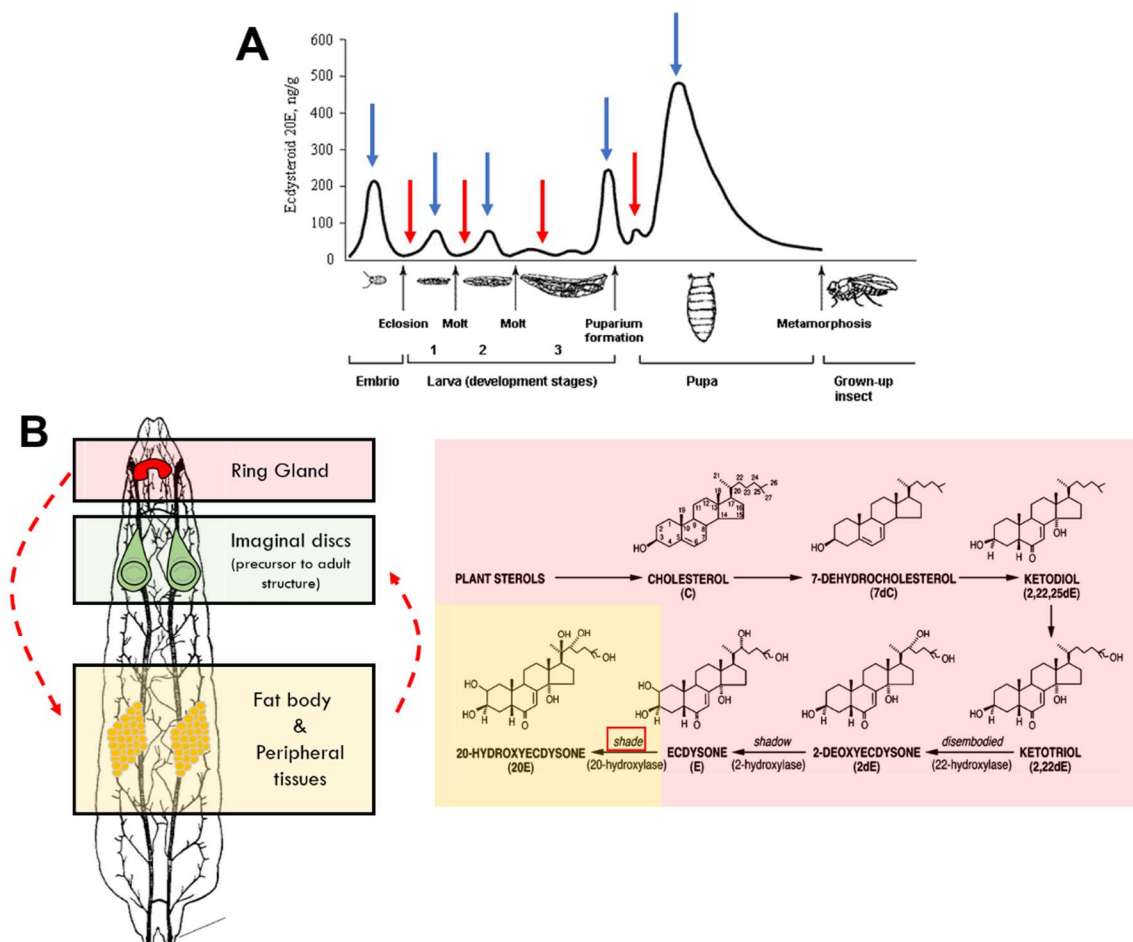
Figure 3.1 Ecdysone titer during *Drosophila* development and ecdysteroid synthesis pathway

(A) Blue arrows indicate peaks of ecdysone titer and red arrow for low titer (not zero). The highest peak of ecdysone occurs soon after pupariation formation. Often, a high titer of ecdysone has a pleiotropic effect depending on the context and the type of cells. (B) Most steps of the ecdysteroid synthesis pathway occur in the ring gland. Ecdysone hormone is converted to its active form 20E in the fat body and taken up by peripheral tissues such as the imaginal discs.

Results

***shd* knockdown affects organ growth**

Knocking down *shd* expression via RNAi using pan-wing drivers *MS1096-Gal4 (Bx-Gal4), nub-Gal4,* and *rn-Gal4* all leads to small wings that often show blistering phenotype (data not shown) (Figure 4.1A-C, E). Knocking down *shd* expression in the eye using *GMR-Gal4* also reduced the eye size by a significant amount compared to control (Figure 4.1D, F). Though area of the eye is the measurement to compare size different in the eye, often the height of the eye measure from the bottom to the top is a good indication of overall eye size. As shown, *shd* knockdown fly has significantly small eyes and head capsule (*GMR-Gal4* expression includes the head capsule). This result is striking considering that *shd* expression is not known to be present in the *Drosophila* wing or that its loss should have any consequence in the growth of the wing or the eye. Shd enzyme carries out the last enzymatic reaction that converts E to the active form 20E [37]. The fact that *shd* knockdown leads to smaller organ size means the systemic titer of ecdysone in the whole animal is not enough or is not the way an epithelial tissue like the wing receives its steroid hormone titer but that the last step in 20E conversion is crucial for the normal growth of the wing.
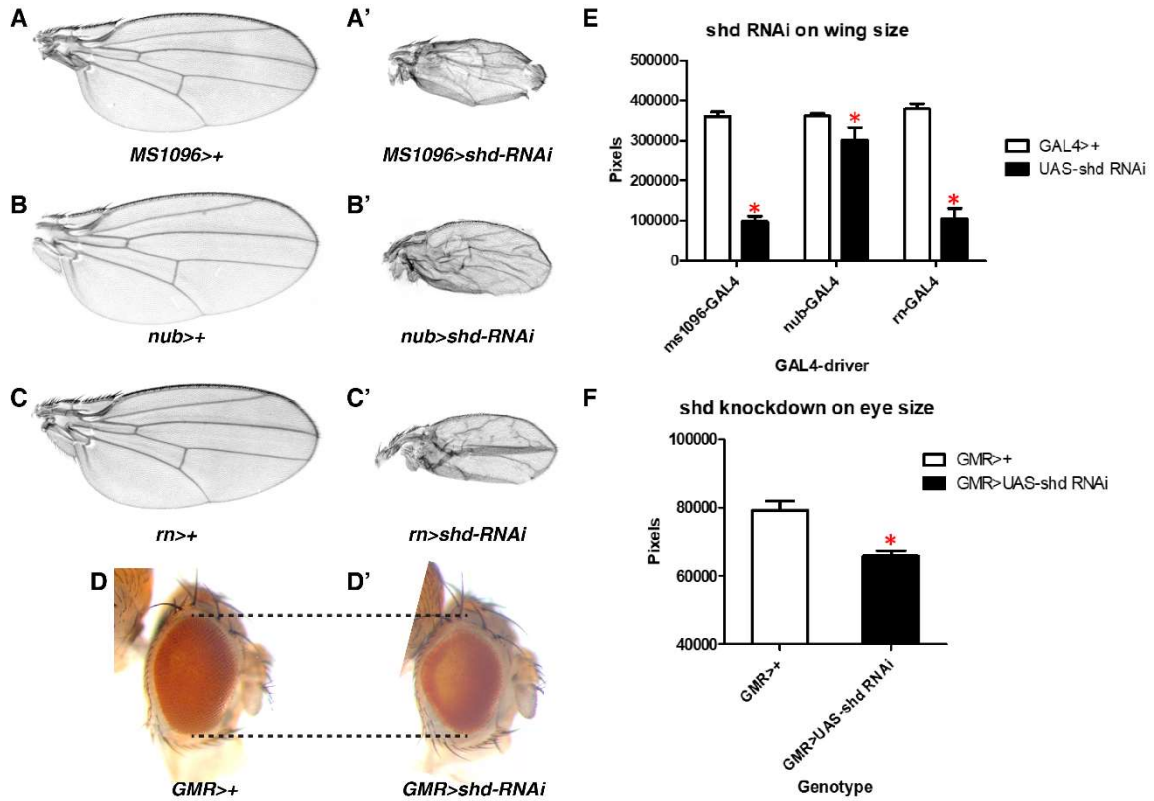
Figure 4.1 *shd* knockdown affects organ growth
(A-A') *shd-RNAi* expression in the developing wing using the wing driver *MS1096-GAL4* compared to control. (B-B') *shd-RNAi* expression using *nub-GAL4* compared to control. (C-C') *shd-RNAi* expression using *rn-GAL4* compared to control. (D) quantification of *shd* knockdown in the wing.

Growth defect of *shd* knockdown does not cross compartment boundaries and is caused by elevated apoptosis.

To test if the growth defect of *shd* knockdown is a cell-autonomous event, we knockdown *shd* only in the posterior compartment of the wing using *en-Gal4*. If the knockdown does not result in a smaller wing, this suggests, though the titer of 20E is modulated locally, its effect is not autonomous and the available titer of 20E surrounding the tissue would be enough to confer proper growth. However, *en-Gal4* expression of *shd-RNAi* led to wings with smaller posterior compartment (Figure 4.2A-B) in a compartment autonomous manner. This can be measured by comparing the ratio of the posterior compartment measured to the entire wing (Figure 4.2C). Conventional knowledge assumes that because 20E is a steroid it can pass through the lipid bi-layer freely and production 20E by a group of cells would non-autonomously affect the neighboring cells. The data shown provides evidence against that notion and further supported by recent publications showing that E and 20E are transported via vesicles, not by diffusion [219]. However, much 20E is made in the cells are kept in the cells and does not cross the compartment boundary.

By what mechanism the reduced level of *shd* leads to growth defect was still unknown and to test it, we stained the wing discs driving *shd* knockdown in the posterior compartment of the L3 wing discs with DCP-1, a cleaved caspase that is present in cells undergoing apoptosis. The posterior compartment with *shd* knockdown showed higher amount of DCP-1 signaling than the anterior compartment (Figure 4.2D-E). Furthermore, the growth defect caused by *shd* knockdown can be rescued by expressing anti-apoptotic protein Diap1 and a caspase suicide substrate P35 (Figure 4.2F-I). Diap1 inhibits the

activation of DCP-1 and other pro-apoptotic proteins such as Dronc [79]. A stronger effect of P35 expression can be explained by the fact that P35 is a potent inhibit of caspase which can block the very last step of caspase cascade by binding to a cleaved caspase as a suicide substrate and leads to its degradation [79]
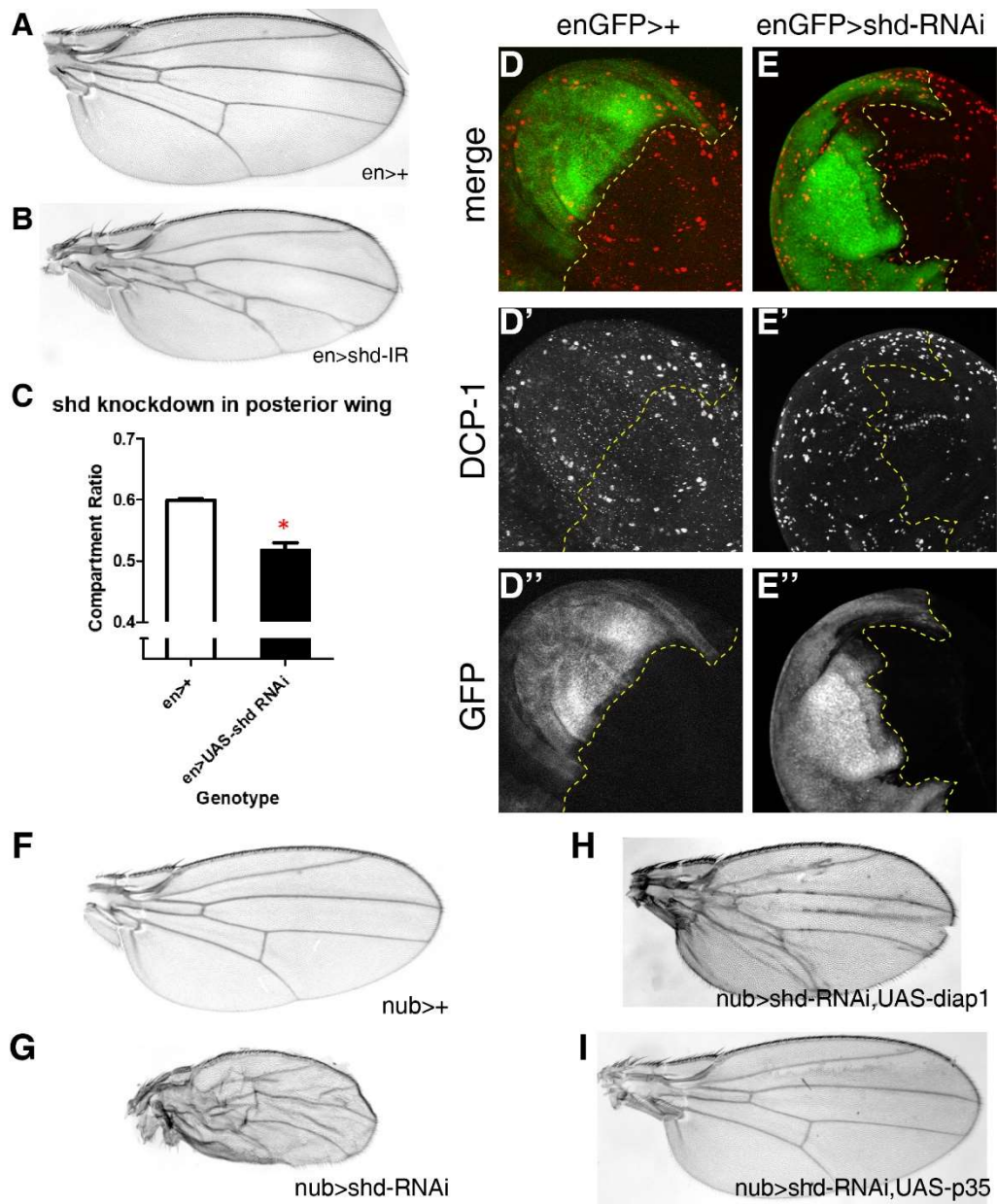
Figure 4.2 Growth defect of *shd* knockdown does not cross compartment boundaries and is caused by elevated apoptosis.
(A-B) *shd-RNAi* expression in the posterior compartment of the wing (*en-Gal4*) compared to control. **(C)** Posterior compartment ratio comparing *en>shd-RNAi* to control. **(D-E)** L3 wing discs stained with DCP-1 antibody. **(F-I)** Adult female wings showing the rescue of *shd* knockdown growth defect by Diap1 and P35.

***Shd* knockdown can suppress *yki* driven overgrowth and reduced the expression of its target *expanded*.**

Previously published article from the lab describes the physical association of Tai/EcR and Yki/Sd complexes in certain targets to drive overgrowth and activation of germline stem cell genes [49]. Since 20E is the hormone that leads to Tai binding of EcR, we sought to test if *shd* knockdown, thus causing local 20E titer to drop in the tissue autonomous matter, can suppress *yki* driven overgrowth in the eye. When the Hippo tumor suppressor pathway is active, Yki protein is normally phosphorylated by Wts kinase and kept in the cytoplasm, leading to its eventual degradation [221]. By mutating the phosphorylation site Serine to an Alanine (S186A), Yki protein localizes to the nucleus to turn on its target genes. Overexpression of a version Yki that cannot be phosphorylated leads to a gross overgrowth phenotype in the *Drosophila* eye compared to control (Figure 4.3A-B). Remarkably, the Yki driven growth in the eye can be suppress by the knockdown of Shd supporting the hypothesis that loss of local 20E titer can modulate Yki activity in the nucleus, most likely due to perturbing the binding to Tai to EcR (Figure 4.3C).

To see if *shd* knockdown can modify the expression of a well-known Yki target *expanded (ex), shd-RNAi* was expressed using *en-Gal4* in the background of the *ex-LacZ* a LacZ element inserted in the *ex* genomic locus to report the transcriptional activity. In the control, *ex-LacZ* pattern shows basal level of expression with reduced expression in the zone of non-proliferating cells (ZNC) that runs along the DV boundary (Figure 4.3D). In the *en>shd* knockdown, *ex-LacZ* signal is reduced, reporting reduced Yki activity in that locus. This is consistent with the model that local 20E titer provided by Shd is

required for proper growth control in the eye and wing, and the reduced level of Shd and the consequent drop in 20E titer is responsible for decreased Yki transcriptional output (Figure 4.4).
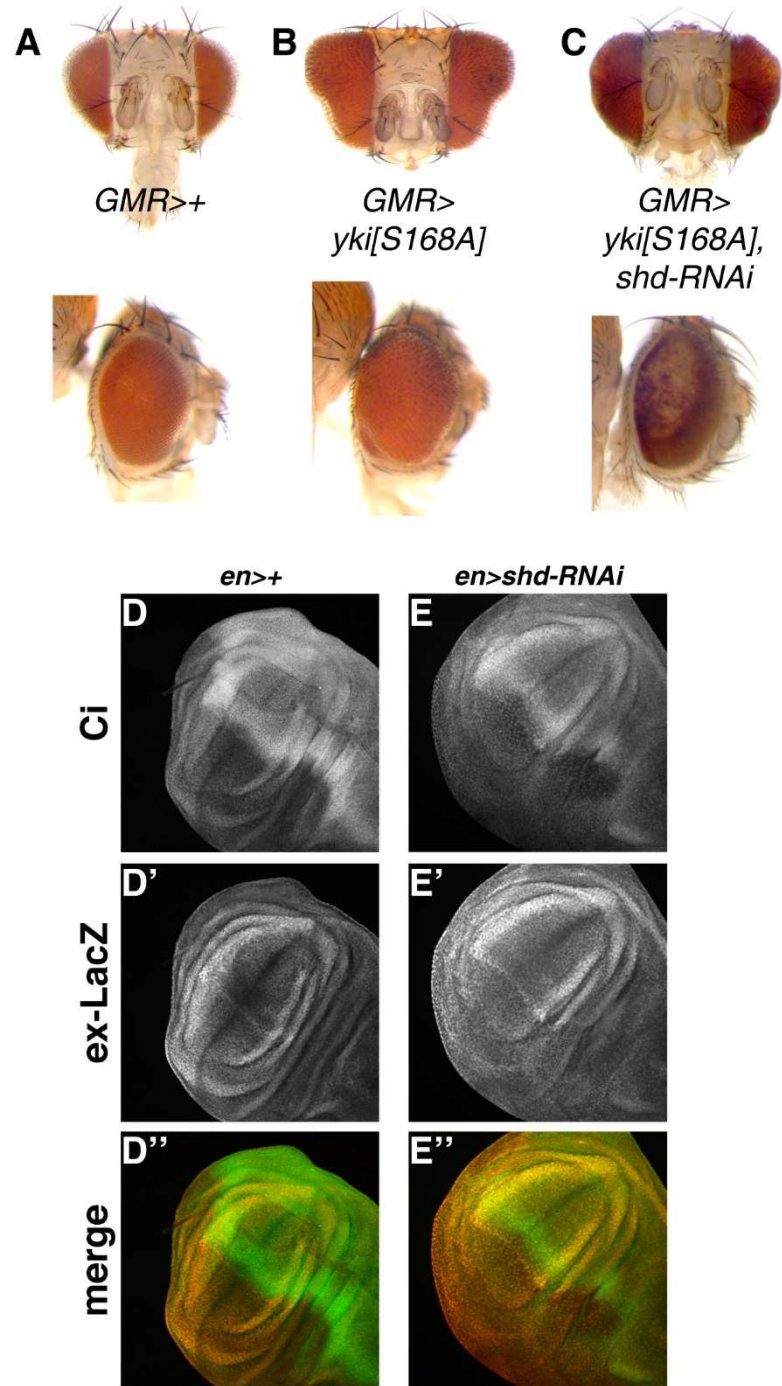
Figure 4.3 *Shd* knockdown can suppress *yki* driven overgrowth and reduced the expression of its target *expanded*.
(A-B) Yki[S186A] driven overgrowth in the eye compared to control. **(C)** *shd-RNAi* suppression of Yki[S186A] driven overgrowth. **(D-E)** decreased *ex-LacZ* expression in the *en* domain of the L3 wing discs compared to control. Ci staining marks the anterior compartment of the wing disc.
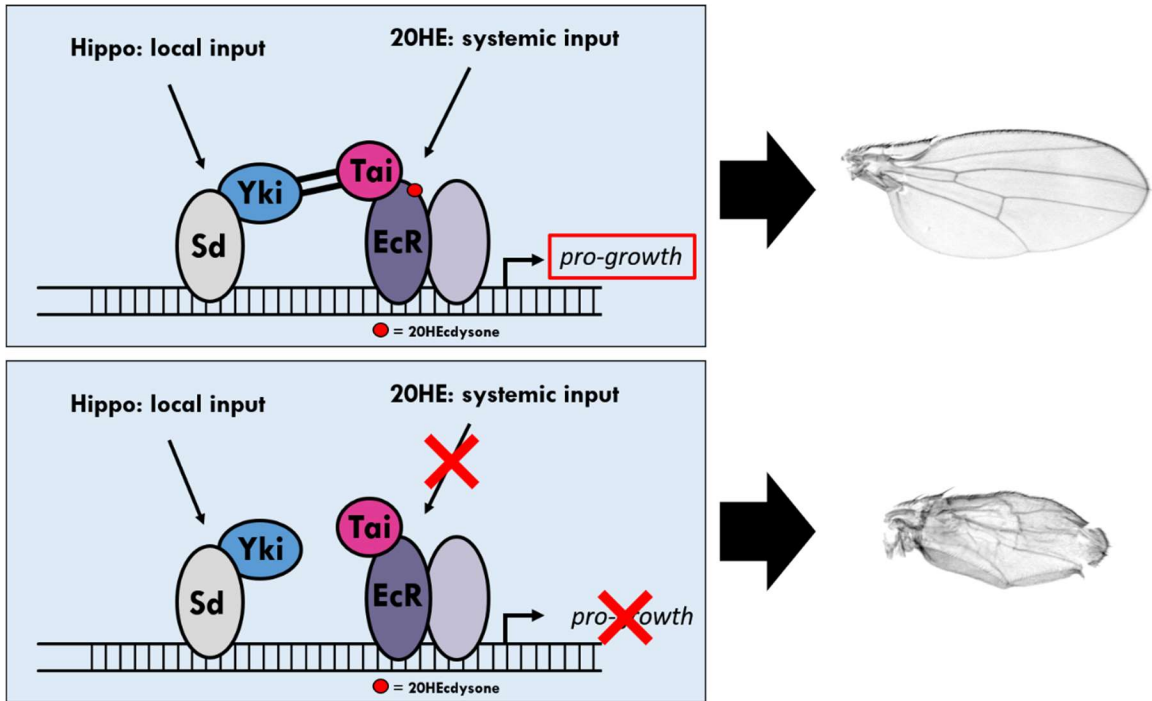
Figure 4.4 Removing local 20E production leads to tissue autonomous growth defect by perturbing the EcR input into Yki target genes.

Discussion

The local production of 20E and its consequence in the proper development of imaginal discs and their adult appendages was never described and thought to be irrelevant since 20E level is systemically controlled by nutrition and developmental timing. Here we show that local production of 20E carried out by a cytochrome P450 enzyme Shd is important for proper organ size control in the *Drosophila* wing and eye, and the knockdown of *shd* affects the Hippo pathway nuclear effector Yki and the transcriptional output of its target gene *ex*. Though it is not tested or shown, *shd* knockdown can likely impact the transcription of other well-known Yki targets such as *thread* which encodes the anti-apoptotic protein Diap1. The fact that decrease amount of 20E titer leads to more apoptotic death supports this notion since Diap1 is ubiquitously expressed in almost all cell types and the loss Diap1 proteins leads to the activation of caspases in eventual cell death.

The requirement of local titer of ecdysone in the proper development of the wing is an important discovery, especially in light of border cells requiring both *shd* and *phantom* expression for migration [35]. Due to its prominent role in development, the systemic titer of ecdysone received much focus while the requirement of the local titer was overlooked. Furthermore, our data suggest that two titers of ecdysone may have different effect. Developmentally, Ecdysone hormone is understood to inhibit growth and to be pro-apoptotic [211]. During the transition from larval to pupal stages, the high pulse of ecdysone is responsible for the cessation of larval feeding and the clearing of old larval tissue (ecdysis) as the larvae pupates [222]. However, during the L3 stage when the wing imaginal disc gains such significant growth in size, the ecdysone titer is already low

(though not zero), that reducing the level was thought to be inconsequential. The presented data proposes a possibility of two distinct functions of ecdysone hormone in low and high titer. Perhaps high and low titer leads to two different chromatin states that some gene loci are not open to be turned on while others are. Pathologically, data further supports the hypothesis in *Zhang et. al. (Dev. Cell* 2015) describing the requirement of both the Tai/EcR and Yki/Sd complexes and the binding of Tai and Yki to turn on specific genes [49, 50]. The parallel mammalian examples of this model that Yki/Sd axis receives input from SRC/hormone receptor axis has begun to be elucidated in multiple models of cancer [51]. Some cancer cells are shown to modulate their own local titer of steroid hormones, and this is linked to hormone-independence. Thus, hormone-independence is not achieved simply by by-passing the requirement of steroid hormone, but cancer cells supply their own titer [179].

Material and Methods

Genetics & deficiency stocks

All crosses were maintained at 25°C unless otherwise noted. Alleles used: (BDSC stock numbers indicated) *MS1096-Gal4* (#8860), *nubbin-Gal4* (#42699), *rotund-Gal4* (#7405), *engrailed-Gal4* (#30564)

UAS-shd-IR, Ex-LacZ, UAS-Yki^{S186A}, GMR-Gal4, UAS-Diap1, UAS-P35, UAS-GFP

Immunofluorescence microscopy

Immunostaining and confocal microscopy were performed using standard procedures. Primary antibodies used: mouse anti-ß-Gal, 1:1000 (Promega); rabbit anti-GFP, 1:500; rabbit anti-cleaved Dcp-1, 1:400 (Cell Signaling). Secondary antibodies: goat anti-rabbit-FITC, 1:100; goat anti-mouse-Cy3, 1:100 (Jackson Labs); goat anti-mouse-Cy5, 1:100 (Jackson Labs); goat anti-rat Cy3, 1:100 (Jackson Labs); goat anti-rabbit Cy5, 1:100 (Jackson Labs); DAPI, 1:5000. Images were collected on a Zeiss LSM7-10 or Olympus FV1000 system. Images were viewed and prepared with Fiji[198] and Photoshop software.

Statistics

Unpaired student t-test (GraphPad Prism™) was used to analyze significance between paired data sets. Unless noted, significance values in text and figures are denoted by asterisks as follows: *=$0.01<p<0.05$, **=$0.001<p<0.01$, ***=$p<0.001$.

Chapter 5

Future directions & concluding remarks

Additional deficiency screens

The discovery of downstream targets and upstream regulators of Tai/EcR complex transcriptional output are of importance considering its developmental role in flies as well as its pathological role represented in this dissertation and analogous pathological roles NCoAs/SRCs play in human cancer. Developmentally, the most well-known tissue for Tai activity is the border cells. Indeed, one group isolated Tai expressing border cells from hundreds of embryos and performed RNA-seq from isolated mRNAs [34]. However, this method is extremely laborious and difficult to replicate its results. Our pathological model of *MS1096>tai* presents an opportunity to perform modifier screens in a high-throughput fashion and has been used to perform both an unbiased deficiency screen and a candidate-based screen. Since deficiency kits exist for every chromosome in the fly genome, available to order from Bloomington stock center, additional screens along the X, 3L and 3R would be helpful in validating existing candidates and discovering new genes and pathways that either promote or perturb Tai driven tissue invasion.

Moving forward, the additional screens will be carried out using *nubbin-Gal4* instead of *MS1096-Gal4*. Since *MS1096* is on the X chromosome, and genes on the X chromosome are expressed twice as much in males as opposed to females, *UAS-tai* transgene expression is doubled in males and leads to lethality. This reduces the number of potential offspring appropriate for analysis by half. To improve upon this issue, *nubbin-Gal4* is used for subsequent candidate screens involving Toll and IMD alleles since *nubbin-Gal4* on the 2nd chromosome. Of course, the crosses will be duplicated in 18°C to screen for enhancers.

The power of Tai-invasion model is that the phenotype is visible apparent that there is so sophisticated analysis to be done on these flies. Once the first pass of deficiency screen is completed, each 'hit' of modifying alleles will need to be narrowed down using smaller or overlapping deficiencies. After that, a list of genes contained in each modifying allele will need to be compiled. If staying truly unbiased in the approach, every gene represented on each deficiency will need to be tested against the phenotype for suppression of enhancement. Because of the screen being so high-throughput, screening RNAi's or alleles through all the genes in the list would be a tenable experiment, though it may require an exceptional organization skill. However, first filtering through the list of genes for their biological relevance to tissue invasion, tumor growth, Toll/IMD, apoptosis, and cell-competition would be an appropriate approach before performing the secondary screen. Discovering additional players in Tai-driven wing invasion could illuminate more pathways and mechanisms through which Tai expressing tissue gains invasiveness and how these pathways interact with each other.

Reactive oxygen species

In this thesis, a substantial effort was focused on understanding the role of Toll/IMD pathways and how the mechanism of cell-competition plays out in Tai-driven wing invasion through the thorax. One of the ways that the fly immune system gets activated is through reactive oxygen species (ROS). Hemocytes can recognize ROS since it is a DAMP (damage associated molecular pattern) and is a by-product of necrosis or injury [14]. In fact, a wound healing model in flies show that hemocyte recruitment to the wound is necessary for regeneration and the biomarker that recruits hemocytes to the wound is ROS [223, 224]. Under tissue damage, continual ROS signaling is important for JNK-pathway mediated regenerative growth [223]. This mechanism was also shown in pathological tissue invasion model $scrib^{-/-} + RAS^{V12}$ where hemocytes recruited by ROS signaling leads to continual activation of JNK pathway, increasing ROS level even more and eventual neoplastic growth/invasion [96]. Such growth and tissue invasion are inhibited by knockdown *duox* (increase ROS) or by overexpressing *catalase* and *sod2* (decreases ROS). The parallel can be observed in human cancers where neoplastic growth of cancer cells is coupled with necrotic death of surrounding wild-type cells [225]. Necrotic cell death releases DAMPs and factors that has tumor promoting functions coupled with recruitment of immune cells to the tumor which provides angiogenesis and invasiveness [226].

Interestingly, our preliminary data show that co-expression of Catalase (penetrance 12.5%, n=40) or knocking down *duox* by RNAi (penetrance 11.1%, n=18) can suppress Tai-driven tissue invasion. Anti-oxidative genes in *Drosophila* include *superoxide dismutase 1* (*sod1*), *superoxide dismutase 2* (*sod2*), and *catalase* (*cat*). Genes

duox and *nox* encodes NADPH dual oxidase and NADPH oxidase, respectively, and generate ROS. Whether the reduction of ROS affects cell death directly or indirectly through the immune cells is unclear. In chapter 2, we have shown that hyperactive Toll signaling leads to non-autonomous cell death in the thorax cells neighboring Tai-expressing wing tissue. ROS is considered a damage-associated molecule and activate hemocytes (immune cells), leading to more local Toll signaling since hemocytes can produce more Spz proteins and secrete them for Toll activation. An easy way to answer that would be to test if *catalase* expression or *duox* knockdown can modify Toll activation and cell death using pupal cryosection of *MS1096>Tai* invasion flies or in L3 wing imaginal disc using *ptc>Gal4* system.

ROS and innate immunity lead naturally to *puckered-LacZ* staining saw in cryosections of Tai-invasion pupae, which is a transcriptional reporter for JNK activity, indicative of AP-1 transcription factor activity in the nucleus (Figure 3.12R). JNK is shown to be activated by the IMD pathway via Tak1/Tab complex that phosphorylates JNK which phosphorylates AP-1 for activation [227]. Excessive JNK activity is linked with invasiveness in tumors and shown to be required in *Drosophila* model of neoplastic tumors to invade the neighboring tissue, from eye to brain (*scrib$^{-/-}$, Ras^{V12}*) [96, 115]. However, co-expressing a dominant-negative version of *Drosophila* JNK *basket* did not suppress Tai-driven invasion. Perhaps JNK activity is a secondary effect of ROS and hyperactive IMD signaling but may not contribute directly to wing tissue invasion. More comprehensive test of alleles and RNAi's need to be done to properly answer the exact role of ROS and JNK in tissue invasion.

Autonomous vs. Non-autonomous

An example of tissue invasion seen in border cell migration require clearly defined intrinsic and extrinsic factors. Intrinsically, Ecdysone hormone and subsequent Tai/EcR signaling is needed. In addition, JAK/STAT signaling turns on *slbo* which turns on numerous downstream targets which includes *Drosophila* E-Cadherin *shotgun*. Extrinsically, *Drosophila* PDGF/VEGF related factors (Pvfs) serve as directional cues that attracts border cell cluster to invade toward the oocyte. In Tai wing invasion model, however, it is unclear if extrinsic factors, non-autonomous signaling exists that allows Tai expressing cells to invade the thorax. As pointed out, the site of tissue invasion is remarkably consistent across the genotype and multiple *Gal4* lines (Figure 3.1). Developmentally, the wing tissue resides adjacent to the thorax and the proximity could be a simple explanation for this occurrence. On the other hand, the possibility is that thoracic tissue may produce factors that attracts or transforms Tai expressing wing tissue to invade. To tease apart the intrinsic and extrinsic factors in answering this problem would require a complicated transgenic system that is technically untenable. *LexA*/*LexAop* or *QF/QUAS* binary expression systems can be used in cooperation with *Gal4/UAS* system. They are other forms of binary transgenic expression system that functions like *Gal4/UAS* but do not interact with each other. QF transcription factor will not bind to *UAS* and Gal4 protein will not bind *QUAS*, vice versa. However, while some tissue specific promoters have been cloned with *LexA* or *QF*, almost all RNAi lines are made with *UAS*. To gain the ability to knockdown a specific gene only in the thorax would require thorax specific *QF* or *LexA* with *QUAS/LexAop* regulated RNAi lines which do not exist.

Additional binding partners of Tai in the nucleus

In the course of completing this dissertation, many RNAi lines and alleles have been tested against *MS1096>tai* or *nubbin>tai* invasion flies. Yet, no allele or RNAi was able to completely revert Tai overexpressing wing tissue to resemble a wild-type wing, demonstrating that Tai transcriptional landscape maybe bigger than with the known binding partners such as Yki or EcR. A simple explanation is that Yki and EcR input equally into Tai activity and its downstream targets that knocking down or dominant modification of one axis do not give complete suppression of the phenotype, and if both Yki and EcR were to be knocked down, Tai will have minimal effect. While this can be tested, knocking down Yki in the wing disc will not results in a wing that is measurable since it will be too small. However, we know that knocking down *scalloped*, the transcription factor that binds Yki, does not suppress Tai driven wing invasion, suggesting Yki activity through Sd is not required for the phenotype. This leads to a hypothesis that Tai can act independently of EcR and may not always require EcR or Yki for some unknown targets. Certainly, for classical Yki targets such has *expanded* and *thread* do require EcR for Tai to turn them on [49]. From the proteomic analysis, we know that Tai binds to a myriad of proteins in the nucleus. How do we, as geneticist, figure out which hits from the proteomic analysis is real? RNAi against each target is an efficient way to test them. But, which transcriptional reporters should be used as a readout of its effect? We can use a combination of reporters: one Yki reporter such as *ex-lacZ*, one Tai dependent Yki reporter such as *dilp8-GFP*, and one EcR dependent reporter such as *ftz-f1* or *edg78e*. However, testing against these reporters will not yield a novel binding partner of Tai that functions outside the realm of Yki/Sd and Tai/EcR. Such

discovery is crucial in understanding the complete picture of Tai biology, not only its pathological function in tissue invasion, but also in development where Tai is required. Therefore, finding the correct set of genes that are Tai sufficient but Yki/Sd and EcR independent would be an ideal place to start. This can be done by performing RNA-seq analysis on the following samples: Tai, Tai+EcR-IR, Tai+Yki-IR. At the intersection of highly expressed genes in these samples would be a list of genes that are Tai sufficient but EcR and Yki independent. "Tai sufficient" is a bit misleading since it is likely that Tai is working through a different binding partner.

Role of *shd* and local steroid level in wound regeneration

The requirement of *shd* expression in the proper growth of the wing is an important discovery because it challenged the conventional understanding of ecdysone synthesis, ecdysone dispersal, and the regulation of local titer. The assumption in the field was that the systemic titer is the local titer of ecdysone and that the entire animal receives the same level of ecdysone. Our data suggests that the local production of the active version of ecdysone (20E) via enzyme Shd is important for proper growth of the wing. In the event of an injury, *dilp8* production by the injured tissue results in decreased production of ecdysone [71, 144, 228]. The physiological effect of this is to slow down the developmental clock for the injury to heal before proceeding to the next phase. The result is decreased expression of all Halloween genes, responsible for synthesizing ecdysone, except for *shd* [229]. A possible explanation for this is that a systemic response to injury is to stop producing ecdysone but locally, steroid hormone titer is needed for regeneration and wound healing. Considering that the Hippo pathway interacts with EcR/Tai complex to confer cell growth and Yki is required in tissue regeneration [76], the necessity of *shd* expression and local 20E production during wound healing is a definite possibility.

Whether *shd* knockdown and 20E loss effect Yki output similar Tai loss is not yet shown. Many reporters of Yki activity, EcR activity, and Tai-dependent Yki activity exists. In our recent publication, we describe *dilp8* being a Tai-dependent Yki target where the expression of *dilp8* is increased by Yki in a Tai-dependent manner. EcR activity can be measure by using GFP reporter coupled with EcR responsive element which is taken from *hsp70* promoter that contains EcR binding sequence. Classic Yki reporters such as *ex-lacZ* or *thread-lacZ* can be used to read out Yki activity. Use of these

reporters in the background of *shd* knockdown or Yki+*shd* RNAi would be able to corroborate whether the growth defect or wound healing defect by *shd* knockdown is through Yki-Tai axis.

Concluding remarks

Our Tai invasion model describes the adaptation of cell competition mechanism in the context of inter-tissue invasion. This is achieved by hyperactive Toll signaling in a non-autonomous manner which leads to cell death in the nearby thoracic epithelia. Interestingly, we show that the loss of inhibition of IMD pathway in the wing cells leads to suppression of the phenotype due to excessive cell death that occurs in the Tai expressing cells. This provides an enormous insight into the mechanism of cell competition and perhaps has a therapeutic relevance. In many cell competition models put forth by the community suggests that processed Spz recognized by Toll leads to Toll activation and subsequent cell death. Yet, they do not provide the answer to why Spz can kill other cells but do not kill the source; why is Spz activity non-autonomous when Spz is a soluble, extracellular molecular that can bind to Toll receptors on 'winner' cells? A possible explanation supported by our data is that 'winner' cells have higher threshold for death by Spz signaling and when this threshold is lowered by the loss of the inhibiting mechanism, 'winner' cells start to die. A simple way to test this in human cancer cells is to use cancer cell line and hyperactive Toll-like receptor (TLR) pathway by knocking down IκB (*casp* homolog). Therefore, further studies into the cell competition mechanism may reveal ways to sensitize tumor cells to be more susceptible to chemotherapy or other therapeutic interventions.

References

1. Wallingford, J.B., S.E. Fraser, and R.M. Harland, *Convergent extension: the molecular control of polarized cell movement during embryonic development.* Dev Cell, 2002. **2**(6): p. 695-706.
2. Sanders, E.J. and S. Prasad, *Invasion of a basement membrane matrix by chick embryo primitive streak cells in vitro.* J Cell Sci, 1989. **92 (Pt 3)**: p. 497-504.
3. Sanders, E.J., *Embryonic cell invasiveness: an in vitro study of chick gastrulation.* J Cell Sci, 1991. **98 (Pt 3)**: p. 403-7.
4. Pocha, S.M. and D.J. Montell, *Cellular and Molecular Mechanisms of Single and Collective Cell Migrations in Drosophila: Themes and Variations.* Annual review of genetics, 2014. **48**(1): p. 295-318.
5. Vacquier, V.D., *The connection of blastomeres of sea urchin embryos by filopodia.* Exp Cell Res, 1968. **52**(2): p. 571-81.
6. Montell, D.J., P. Rorth, and A.C. Spradling, *slow border cells, a locus required for a developmentally regulated cell migration during oogenesis, encodes Drosophila C/EBP.* Cell, 1992. **71**(1): p. 51-62.
7. Scarpa, E. and R. Mayor, *Collective cell migration in development.* J Cell Biol, 2016. **212**(2): p. 143-55.
8. Weber, G.F., M.A. Bjerke, and D.W. DeSimone, *A mechanoresponsive cadherin-keratin complex directs polarized protrusive behavior and collective cell migration.* Dev Cell, 2012. **22**(1): p. 104-15.
9. VanderVorst, K., et al., *Cellular and molecular mechanisms underlying planar cell polarity pathway contributions to cancer malignancy.* Semin Cell Dev Biol, 2018. **81**: p. 78-87.
10. Kuphal, S., et al., *Snail-regulated genes in malignant melanoma.* Melanoma Res, 2005. **15**(4): p. 305-13.
11. Friedl, P. and D. Gilmour, *Collective cell migration in morphogenesis, regeneration and cancer.* Nat Rev Mol Cell Biol, 2009. **10**(7): p. 445-57.
12. Choi, J., et al., *The role of tumor-associated macrophage in breast cancer biology.* Histol Histopathol, 2018. **33**(2): p. 133-145.
13. Singh, S., et al., *Initiative action of tumor-associated macrophage during tumor metastasis.* Biochim Open, 2017. **4**: p. 8-18.
14. how tShaukat, Z., D. Liu, and S. Gregory, *Sterile inflammation in Drosophila.* Mediators Inflamm, 2015. **2015**: p. 369286.
15. Bai, J., Y. Uehara, and D.J. Montell, *Regulation of invasive cell behavior by taiman, a Drosophila protein related to AIB1, a steroid receptor coactivator amplified in breast cancer.* Cell, 2000. **103**(7): p. 1047-58.
16. Wang, X., et al., *Analysis of Cell Migration Using Whole-Genome Expression Profiling of Migratory Cells in the Drosophila Ovary.* Developmental Cell, 2005. **10**(4): p. 483-95.
17. Montell, D.J., *Developmental regulation of cell migration. Insight from a genetic approach in Drosophila.* Cell biochemistry and biophysics, 1998. **31**(3): p. 219-29.
18. Cai, D., et al., *Mechanical Feedback through E-Cadherin Promotes Direction Sensing during Collective Cell Migration.* Cell, 2014. **157**(5): p. 1146-1159.

19. Montell, D.J., *Command and control: regulatory pathways controlling invasive behavior of the border cells.* Mechanisms of development, 2001. **105**(1-2): p. 19-25.

20. Geisbrecht, E.R. and D.J. Montell, *Myosin VI is required for E-cadherin-mediated border cell migration.* Nature Cell Biology, 2002. **4**(8): p. 616-620.

21. Olson, H.M. and A.V. Nechiporuk, *Using Zebrafish to Study Collective Cell Migration in Development and Disease.* Front Cell Dev Biol, 2018. **6**: p. 83.

22. Peterson, S.J. and M.A. Krasnow, *Subcellular Trafficking of FGF Controls Tracheal Invasion of Drosophila Flight Muscle.* Cell, 2015. **160**(1-2): p. 313-23.

23. Murphy, A.M., et al., *The breathless FGF receptor homolog, a downstream target of Drosophila C/EBP in the developmental control of cell migration.* Development (Cambridge, England), 1995. **121**(8): p. 2255-63.

24. Wang, X., J.C. Adam, and D. Montell, *Spatially localized Kuzbanian required for specific activation of Notch during border cell migration.* Developmental Biology, 2006. **301**(2): p. 532-40.

25. Prasad, M. and D.J. Montell, *Cellular and molecular mechanisms of border cell migration analyzed using time-lapse live-cell imaging.* Developmental cell, 2007. **12**(6): p. 997-1005.

26. Murphy, A.M. and D.J. Montell, *Cell type-specific roles for Cdc42, Rac, and RhoL in Drosophila oogenesis.* The Journal of cell biology, 1996. **133**(3): p. 617-30.

27. Silver, D.L. and D.J. Montell, *Paracrine signaling through the JAK/STAT pathway activates invasive behavior of ovarian epithelial cells in Drosophila.* Cell, 2001. **107**(7): p. 831-41.

28. McDonald, J.A., E.M. Pinheiro, and D.J. Montell, *PVF1, a PDGF/VEGF homolog, is sufficient to guide border cells and interacts genetically with Taiman.* Development (Cambridge, England), 2003. **130**(15): p. 3469-78.

29. Geisbrecht, E.R. and D.J. Montell, *A role for Drosophila IAP1-mediated caspase inhibition in Rac-dependent cell migration.* Cell, 2004. **118**(1): p. 111-25.

30. Wong, G.S. and A.K. Rustgi, *Matricellular proteins: priming the tumour microenvironment for cancer development and metastasis.* British journal of cancer, 2013. **108**(4): p. 755-61.

31. Enomoto, M. and T. Igaki, *Src controls tumorigenesis via JNK-dependent regulation of the Hippo pathway in Drosophila.* EMBO reports, 2013. **14**(1): p. 65-72.

32. Jang, A., et al., *Border-cell migration requires integration of spatial and temporal signals by the BTB protein Abrupt.* Nature Cell Biology, 2009. **11**(5): p. 569-579.

33. Belles, X. and M.D. Piulachs, *Ecdysone signalling and ovarian development in insects: from stem cells to ovarian follicle formation.* Biochim Biophys Acta, 2015. **1849**(2): p. 181-6.

34. Manning, L., et al., *A hormonal cue promotes timely follicle cell migration by modulating transcription profiles.* Mech Dev, 2017. **148**: p. 56-68.

35. Domanitskaya, E., L. Anllo, and T. Schüpbach, *Phantom, a cytochrome P450 enzyme essential for ecdysone biosynthesis, plays a critical role in the control of border cell migration in Drosophila.* Developmental biology, 2014. **386**(2): p. 408-18.

36.   Warren, J.T., et al., *Molecular and biochemical characterization of two P450 enzymes in the ecdysteroidogenic pathway of Drosophila melanogaster.* Proceedings of the National Academy of Sciences of the United States of America, 2002. **99**(17): p. 11043-8.

37.   Petryk, A., et al., *Shade is the Drosophila P450 enzyme that mediates the hydroxylation of ecdysone to the steroid insect molting hormone 20-hydroxyecdysone.* Proceedings of the National Academy of Sciences of the United States of America, 2003. **100**(24): p. 13773-8.

38.   Yao, T.P., et al., *Drosophila ultraspiracle modulates ecdysone receptor function via heterodimer formation.* Cell, 1992. **71**(1): p. 63-72.

39.   Tsai, C.C., et al., *SMRTER, a Drosophila nuclear receptor coregulator, reveals that EcR-mediated repression is critical for development.* Mol Cell, 1999. **4**(2): p. 175-86.

40.   York, B. and B.W. O'Malley, *Steroid Receptor Coactivator (SRC) Family: Masters of Systems Biology.* Journal of Biological Chemistry, 2010. **285**(50): p. 38743-50.

41.   Dasgupta, S., D.M. Lonard, and B.W. O'Malley, *Nuclear receptor coactivators: master regulators of human health and disease.* Annu Rev Med, 2014. **65**: p. 279-92.

42.   Antoon, J.W., et al., *Inhibition of p38-MAPK alters SRC coactivation and estrogen receptor phosphorylation.* Cancer biology & therapy, 2012. **13**(11): p. 1026-33.

43.   Long, W., et al., *ERK3 signals through SRC-3 coactivator to promote human lung cancer cell invasion.* Journal of Clinical Investigation, 2012. **122**(5): p. 1869-80.

44.   Jordan, V.C., et al., *Structural derivatives of tamoxifen and oestradiol 3-methyl ether as potential alkylating antioestrogens.* Eur J Cancer, 1981. **17**(2): p. 193-200.

45.   Karmakar, S., et al., *Distinctive functions of p160 steroid receptor coactivators in proliferation of an estrogen-independent, tamoxifen-resistant breast cancer cell line.* Endocr Relat Cancer, 2011. **18**(1): p. 113-27.

46.   Moi, L.L., et al., *Steroid receptor coactivators, HER-2 and HER-3 expression is stimulated by tamoxifen treatment in DMBA-induced breast cancer.* BMC Cancer, 2012. **12**(1): p. 1-12.

47.   Alkner, S., et al., *The role of AIB1 and PAX2 in primary breast cancer: validation of AIB1 as a negative prognostic factor.* Annals of oncology : official journal of the European Society for Medical Oncology / ESMO, 2013. **24**(5): p. 1244-52.

48.   Larsen, S.L., et al., *SRC drives growth of antiestrogen resistant breast cancer cell lines and is a marker for reduced benefit of tamoxifen treatment.* PLoS One, 2015. **10**(2): p. e0118346.

49.   Zhang, C., et al., *The ecdysone receptor coactivator Taiman links Yorkie to transcriptional control of germline stem cell factors in somatic tissue.* Dev Cell, 2015. **34**(2): p. 168-80.

50.   Wang, C., et al., *Taiman acts as a coactivator of Yorkie in the Hippo pathway to promote tissue growth and intestinal regeneration.* Cell Discov, 2016. **2**: p. 16006.

51. Kuser-Abali, G., et al., *YAP1 and AR interactions contribute to the switch from androgen-dependent to castration-resistant growth in prostate cancer.* Nat Commun, 2015. **6**: p. 8126.

52. Ray, H.J. and L. Niswander, *Mechanisms of tissue fusion during development.* Development, 2012. **139**(10): p. 1701-11.

53. Usui, K. and P. Simpson, *Cellular basis of the dynamic behavior of the imaginal thoracic discs during Drosophila metamorphosis.* Dev Biol, 2000. **225**(1): p. 13-25.

54. Beaton, A.H., et al., *Interaction of the Stubble-stubbloid locus and the Broad-complex of Drosophila melanogaster.* Genetics, 1988. **120**(2): p. 453-64.

55. Schock, F. and N. Perrimon, *Molecular mechanisms of epithelial morphogenesis.* Annual review of cell and developmental biology, 2002. **18**: p. 463-93.

56. Seyfried, T.N. and L.C. Huysentruyt, *On the origin of cancer metastasis.* Crit Rev Oncog, 2013. **18**(1-2): p. 43-73.

57. Hariharan, I.K., *Growth regulation: a beginning for the hippo pathway.* Curr Biol, 2006. **16**(24): p. R1037-9.

58. He, J., et al., *The role of Hippo/yes-associated protein signalling in vascular remodelling associated with cardiovascular disease.* Br J Pharmacol, 2018. **175**(8): p. 1354-1361.

59. Park, J.A. and Y.G. Kwon, *Hippo-YAP/TAZ signaling in angiogenesis.* BMB Rep, 2018. **51**(3): p. 157-162.

60. Taha, Z., H.J. Janse van Rensburg, and X. Yang, *The Hippo Pathway: Immunity and Cancer.* Cancers (Basel), 2018. **10**(4).

61. Pan, D., *The hippo signaling pathway in development and cancer.* Developmental cell, 2010. **19**(4): p. 491-505.

62. Robinson, B.S., et al., *Crumbs regulates Salvador/Warts/Hippo signaling in Drosophila via the FERM-domain protein Expanded.* Current biology : CB, 2010. **20**(7): p. 582-90.

63. Robinson, B.S. and K.H. Moberg, *Cell-cell junctions: α-catenin and E-cadherin help fence in Yap1.* Current biology : CB, 2011. **21**(21): p. R890-2.

64. Gilbert, M.M., et al., *A screen for conditional growth suppressor genes identifies the Drosophila homolog of HD-PTP as a regulator of the oncoprotein Yorkie.* Developmental cell, 2011. **20**(5): p. 700-12.

65. Oh, H. and K.D. Irvine, *In vivo regulation of Yorkie phosphorylation and localization.* Development (Cambridge, England), 2008. **135**(6): p. 1081-8.

66. Oh, H. and K.D. Irvine, *In vivo analysis of Yorkie phosphorylation sites.* Oncogene, 2009. **28**(17): p. 1916-27.

67. Goulev, Y., et al., *SCALLOPED interacts with YORKIE, the nuclear effector of the hippo tumor-suppressor pathway in Drosophila.* Curr Biol, 2008. **18**(6): p. 435-41.

68. Peng, H.W., M. Slattery, and R.S. Mann, *Transcription factor choice in the Hippo signaling pathway: homothorax and yorkie regulation of the microRNA bantam in the progenitor domain of the Drosophila eye imaginal disc.* Genes Dev, 2009. **23**(19): p. 2307-19.

69. Sturm, A., et al., *The Piwi-piRNA pathway: road to immortality.* Aging Cell, 2017. **16**(5): p. 906-911.

70.   Bhat, K.M., *The posterior determinant gene nanos is required for the maintenance of the adult germline stem cells during Drosophila oogenesis.* Genetics, 1999. **151**(4): p. 1479-92.

71.   Hariharan, I.K., *How growth abnormalities delay "puberty" in Drosophila.* Science signaling, 2012. **5**(229): p. pe27.

72.   Colombani, J., D.S. Andersen, and P. Léopold, *Secreted peptide Dilp8 coordinates Drosophila tissue growth with developmental timing.* Science (New York, N.Y.), 2012. **336**(6081): p. 582-5.

73.   Colombani, J., et al., *Drosophila Lgr3 Couples Organ Growth with Maturation and Ensures Developmental Stability.* Current biology : CB, 2015. **25**(20): p. 2723-9.

74.   Lucas, E.P., et al., *The Hippo pathway polarizes the actin cytoskeleton during collective migration of Drosophila border cells.* J Cell Biol, 2013. **201**(6): p. 875-85.

75.   Lin, T.H., et al., *The Hippo pathway controls border cell migration through distinct mechanisms in outer border cells and polar cells of the Drosophila ovary.* Genetics, 2014. **198**(3): p. 1087-99.

76.   Zhao, B., K. Tumaneng, and K.L. Guan, *The Hippo pathway in organ size control, tissue regeneration and stem cell self-renewal.* Nat Cell Biol, 2011. **13**(8): p. 877-83.

77.   Rivlin, N., et al., *Mutations in the p53 Tumor Suppressor Gene: Important Milestones at the Various Steps of Tumorigenesis.* Genes Cancer, 2011. **2**(4): p. 466-74.

78.   Harvey, K.F., C.M. Pfleger, and I.K. Hariharan, *The Drosophila Mst ortholog, hippo, restricts growth and cell proliferation and promotes apoptosis.* Cell, 2003. **114**(4): p. 457-67.

79.   Quinn, L.M., et al., *An essential role for the caspase dronc in developmentally programmed cell death in Drosophila.* J Biol Chem, 2000. **275**(51): p. 40416-24.

80.   Salvesen, G.S. and C.S. Duckett, *IAP proteins: blocking the road to death's door.* Nat Rev Mol Cell Biol, 2002. **3**(6): p. 401-10.

81.   White, K., et al., *Genetic control of programmed cell death in Drosophila.* Science, 1994. **264**(5159): p. 677-83.

82.   Lin, N., et al., *By design or by chance: cell death during Drosophila embryogenesis.* Apoptosis, 2009. **14**(8): p. 935-42.

83.   Nakajima, Y.I. and E. Kuranaga, *Caspase-dependent non-apoptotic processes in development.* Cell Death Differ, 2017. **24**(8): p. 1422-1430.

84.   Govind, S., *Control of development and immunity by rel transcription factors in Drosophila.* Oncogene, 1999. **18**(49): p. 6875-87.

85.   Hultmark, D., *Drosophila immunity: paths and patterns.* Curr Opin Immunol, 2003. **15**(1): p. 12-9.

86.   Hetru, C., L. Troxler, and J.A. Hoffmann, *Drosophila melanogaster antimicrobial defense.* J Infect Dis, 2003. **187 Suppl 2**: p. S327-34.

87.   Govind, S., *Innate immunity in Drosophila: Pathogens and pathways.* Insect Sci, 2008. **15**(1): p. 29-43.

88.   Konrad, K.D., T.J. Goralski, and A.P. Mahowald, *Developmental analysis of fs(1)gastrulation defective, a dorsal-group gene of Drosophila melanogaster.* Roux's Archives of Developmental Biology, 1988. **197**(2): p. 75-91.

89.   Cho, Y., et al., *A Ventrally Localized Protease in the Drosophila Egg Controls Embryo Dorsoventral Polarity.* Current Biology, 2012. **22**(11).

90.   Belvin, M.P. and K.V. Anderson, *A conserved signaling pathway: the Drosophila toll-dorsal pathway.* Annu Rev Cell Dev Biol, 1996. **12**: p. 393-416.

91.   Manfruelli, P., et al., *A mosaic analysis in Drosophila fat body cells of the control of antimicrobial peptide genes by the Rel proteins Dorsal and DIF.* EMBO J, 1999. **18**(12): p. 3380-91.

92.   Green, C., et al., *The necrotic gene in Drosophila corresponds to one of a cluster of three serpin transcripts mapping at 43A1.2.* Genetics, 2000. **156**(3): p. 1117-27.

93.   Rutschmann, S., et al., *Role of Drosophila IKK gamma in a toll-independent antibacterial immune response.* Nat Immunol, 2000. **1**(4): p. 342-7.

94.   Rutschmann, S., et al., *The Rel protein DIF mediates the antifungal but not the antibacterial host defense in Drosophila.* Immunity, 2000. **12**(5): p. 569-80.

95.   Parsons, B. and E. Foley, *Cellular immune defenses of Drosophila melanogaster.* Dev Comp Immunol, 2016. **58**: p. 95-101.

96.   Perez, E., J.L. Lindblad, and A. Bergmann, *Tumor-promoting function of apoptotic caspases by an amplification loop involving ROS, macrophages and JNK in Drosophila.* Elife, 2017. **6**.

97.   Mukherjee, T., et al., *Interaction between Notch and Hif-alpha in development and survival of Drosophila blood cells.* Science (New York, N.Y.), 2011. **332**(6034): p. 1210-3.

98.   Martinelli, C. and J.M. Reichhart, *Evolution and integration of innate immune systems from fruit flies to man: lessons and questions.* J Endotoxin Res, 2005. **11**(4): p. 243-8.

99.   Stoven, S., et al., *Caspase-mediated processing of the Drosophila NF-kappaB factor Relish.* Proc Natl Acad Sci U S A, 2003. **100**(10): p. 5991-6.

100.   Kim, M., et al., *Caspar, a suppressor of antibacterial immunity in Drosophila.* Proc Natl Acad Sci U S A, 2006. **103**(44): p. 16358-63.

101.   Meyer, S.N., et al., *An ancient defense system eliminates unfit cells from developing tissues during cell competition.* Science, 2014. **346**(6214): p. 1258236.

102.   Johnston, L.A., et al., *Drosophila myc regulates cellular growth during development.* Cell, 1999. **98**(6): p. 779-90.

103.   Ratheesh, A., V. Belyaeva, and D.E. Siekhaus, *Drosophila immune cell migration and adhesion during embryonic development and larval immune responses.* Curr Opin Cell Biol, 2015. **36**: p. 71-9.

104.   Wood, W., C. Faria, and A. Jacinto, *Distinct mechanisms regulate hemocyte chemotaxis during development and wound healing in Drosophila melanogaster.* J Cell Biol, 2006. **173**(3): p. 405-16.

105.   Sanchez-Sanchez, B.J., et al., *Drosophila Embryonic Hemocytes Produce Laminins to Strengthen Migratory Response.* Cell Rep, 2017. **21**(6): p. 1461-1470.

106.   Regan, J.C., et al., *Steroid hormone signaling is essential to regulate innate immune cells and fight bacterial infection in Drosophila.* PLoS Pathog, 2013. **9**(10): p. e1003720.

107. Tan, K.L., I. Vlisidou, and W. Wood, *Ecdysone mediates the development of immunity in the Drosophila embryo.* Curr Biol, 2014. **24**(10): p. 1145-52.

108. Liu, B., et al., *Toll Receptor-Mediated Hippo Signaling Controls Innate Immunity in Drosophila.* Cell, 2016. **164**(3): p. 406-419.

109. Zhang, Y., H. Zhang, and B. Zhao, *Hippo Signaling in the Immune System.* Trends Biochem Sci, 2018. **43**(2): p. 77-80.

110. Kohan-Ghadr, H.R., et al., *Potential role of epigenetic mechanisms in regulation of trophoblast differentiation, migration, and invasion in the human placenta.* Cell Adh Migr, 2016. **10**(1-2): p. 126-35.

111. Lala, P.K. and P. Nandi, *Mechanisms of trophoblast migration, endometrial angiogenesis in preeclampsia: The role of decorin.* Cell Adh Migr, 2016. **10**(1-2): p. 111-25.

112. Ory, V., et al., *The nuclear coactivator amplified in breast cancer 1 maintains tumor-initiating cells during development of ductal carcinoma in situ.* Oncogene, 2014. **33**(23): p. 3033-42.

113. Long, W., et al., *ERK3 signals through SRC-3 coactivator to promote human lung cancer cell invasion.* The Journal of clinical investigation, 2012. **122**(5): p. 1869-1880.

114. Blattner, M., et al., *SPOP Mutation Drives Prostate Tumorigenesis In Vivo through Coordinate Regulation of PI3K/mTOR and AR Signaling.* Cancer cell, 2017. **31**(3): p. 436-451.

115. Atkins, M., et al., *An Ectopic Network of Transcription Factors Regulated by Hippo Signaling Drives Growth and Invasion of a Malignant Tumor Model.* Curr Biol, 2016. **26**(16): p. 2101-13.

116. Brand, A.H. and N. Perrimon, *Targeted gene expression as a means of altering cell fates and generating dominant phenotypes.* Development, 1993. **118**(2): p. 401-15.

117. Foldi, I., et al., *Three-tier regulation of cell number plasticity by neurotrophins and Tolls in Drosophila.* The Journal of cell biology, 2017.

118. Maillet, F., et al., *The Drosophila peptidoglycan recognition protein PGRP-LF blocks PGRP-LC and IMD/JNK pathway activation.* Cell host & microbe, 2008. **3**(5): p. 293-303.

119. Friedman, A.A., et al., *Proteomic and functional genomic landscape of receptor tyrosine kinase and ras to extracellular signal-regulated kinase signaling.* Sci Signal, 2011. **4**(196): p. rs10.

120. Neumann, C.J. and S.M. Cohen, *Distinct mitogenic and cell fate specification functions of wingless in different regions of the wing.* Development, 1996. **122**(6): p. 1781-9.

121. Capdevila, J. and I. Guerrero, *Targeted expression of the signaling molecule decapentaplegic induces pattern duplications and growth alterations in Drosophila wings.* EMBO J, 1994. **13**(19): p. 4459-68.

122. Srivastava, A., et al., *Basement membrane remodeling is essential for Drosophila disc eversion and tumor invasion.* Proc Natl Acad Sci U S A, 2007. **104**(8): p. 2721-6.

123. Pastor-Pareja, J.C., et al., *Invasive cell behavior during Drosophila imaginal disc eversion is mediated by the JNK signaling cascade.* Dev Cell, 2004. **7**(3): p. 387-99.

124. Diaz de la Loza, M.C. and B.J. Thompson, *Forces shaping the Drosophila wing.* Mech Dev, 2017. **144**(Pt A): p. 23-32.

125. Wang, C., et al., *Taiman acts as a coactivator of Yorkie in the Hippo pathway to promote tissue growth and intestinal regeneration.* Cell Discovery, 2016. **2**: p. 16006.

126. Bach, E.A., et al., *A sensitized genetic screen to identify novel regulators and components of the Drosophila janus kinase/signal transducer and activator of transcription pathway.* Genetics, 2003. **165**(3): p. 1149-66.

127. Goberdhan, D.C., et al., *Drosophila tumor suppressor PTEN controls cell size and number by antagonizing the Chico/PI3-kinase signaling pathway.* Genes Dev, 1999. **13**(24): p. 3244-58.

128. Huang, H., et al., *PTEN affects cell size, cell proliferation and apoptosis during Drosophila eye development.* Development, 1999. **126**(23): p. 5365-72.

129. Calleja, M., et al., *Generation of medial and lateral dorsal body domains by the pannier gene of Drosophila.* Development, 2000. **127**(18): p. 3971-80.

130. Lavrynenko, O., et al., *The ecdysteroidome of Drosophila: influence of diet and development.* Development, 2015. **142**(21): p. 3758-68.

131. Ren, N., et al., *Gene expression during Drosophila wing morphogenesis and differentiation.* Genetics, 2005. **171**(2): p. 625-38.

132. Jang, A.C., et al., *Border-cell migration requires integration of spatial and temporal signals by the BTB protein Abrupt.* Nat Cell Biol, 2009. **11**(5): p. 569-79.

133. Kozlova, T. and C.S. Thummel, *Spatial patterns of ecdysteroid receptor activation during the onset of Drosophila metamorphosis.* Development, 2002. **129**(7): p. 1739-50.

134. Kozlova, T. and C.S. Thummel, *Methods to characterize Drosophila nuclear receptor activation and function in vivo.* Methods Enzymol, 2003. **364**: p. 475-90.

135. Parsons, B. and E. Foley, *The Drosophila platelet-derived growth factor and vascular endothelial growth factor-receptor related (Pvr) protein ligands Pvf2 and Pvf3 control hemocyte viability and invasive migration.* J Biol Chem, 2013. **288**(28): p. 20173-83.

136. McDonald, J.A., E.M. Pinheiro, and D.J. Montell, *PVF1, a PDGF/VEGF homolog, is sufficient to guide border cells and interacts genetically with Taiman.* Development, 2003. **130**(15): p. 3469-78.

137. Xu, T., et al., *Identifying tumor suppressors in genetic mosaics: the Drosophila lats gene encodes a putative protein kinase.* Development, 1995. **121**(4): p. 1053-63.

138. Kawasaki, H., S. Hirose, and H. Ueda, *BetaFTZ-F1 dependent and independent activation of Edg78E, a pupal cuticle gene, during the early metamorphic period in Drosophila melanogaster.* Dev Growth Differ, 2002. **44**(5): p. 419-25.

139. Huet, F., C. Ruiz, and G. Richards, *Sequential gene activation by ecdysone in Drosophila melanogaster: the hierarchical equivalence of early and early late genes.* Development, 1995. **121**(4): p. 1195-204.

140. Woodard, C.T., E.H. Baehrecke, and C.S. Thummel, *A molecular mechanism for the stage specificity of the Drosophila prepupal genetic response to ecdysone.* Cell, 1994. **79**(4): p. 607-15.

141. Lavorgna, G., et al., *Potential role for a FTZ-F1 steroid receptor superfamily member in the control of Drosophila metamorphosis.* Proc Natl Acad Sci U S A, 1993. **90**(7): p. 3004-8.

142. Mou, X., et al., *Control of target gene specificity during metamorphosis by the steroid response gene E93.* Proc Natl Acad Sci U S A, 2012. **109**(8): p. 2949-54.

143. Guittard, E., et al., *CYP18A1, a key enzyme of Drosophila steroid hormone inactivation, is essential for metamorphosis.* Developmental biology, 2011. **349**(1): p. 35-45.

144. Boone, E., et al., *The Hippo signalling pathway coordinates organ growth and limits developmental variability by controlling dilp8 expression.* Nature communications, 2016. **7**: p. 13505.

145. Colombani, J., D.S. Andersen, and P. Leopold, *Secreted peptide Dilp8 coordinates Drosophila tissue growth with developmental timing.* Science, 2012. **336**(6081): p. 582-5.

146. Garelli, A., et al., *Imaginal discs secrete insulin-like peptide 8 to mediate plasticity of growth and maturation.* Science, 2012. **336**(6081): p. 579-82.

147. Bunker, B.D., et al., *The transcriptional response to tumorigenic polarity loss in Drosophila.* Elife, 2015. **4**.

148. Li, Q., et al., *The conserved misshapen-warts-yorkie pathway acts in enteroblasts to regulate intestinal stem cells in Drosophila.* Dev Cell, 2014. **31**(3): p. 291-304.

149. Fagegaltier, D., et al., *Oncogenic transformation of Drosophila somatic cells induces a functional piRNA pathway.* Genes Dev, 2016. **30**(14): p. 1623-35.

150. Karouzou, M.V., et al., *Drosophila cuticular proteins with the R&R Consensus: annotation and classification with a new tool for discriminating RR-1 and RR-2 sequences.* Insect Biochem Mol Biol, 2007. **37**(8): p. 754-60.

151. Skinner, A., S.J. Khan, and R.K. Smith-Bolton, *Trithorax regulates systemic signaling during Drosophila imaginal disc regeneration.* Development, 2015. **142**(20): p. 3500-11.

152. Parker, J.S., K. Mizuguchi, and N.J. Gay, *A family of proteins related to Spatzle, the toll receptor ligand, are encoded in the Drosophila genome.* Proteins, 2001. **45**(1): p. 71-80.

153. Morisato, D. and K.V. Anderson, *The spatzle gene encodes a component of the extracellular signaling pathway establishing the dorsal-ventral pattern of the Drosophila embryo.* Cell, 1994. **76**(4): p. 677-88.

154. Rämet, M., et al., *Functional genomic analysis of phagocytosis and identification of a Drosophila receptor for E. coli.* Nature, 2002. **416**(6881): p. 644-648.

155. Gottar, M., et al., *The Drosophila immune response against Gram-negative bacteria is mediated by a peptidoglycan recognition protein.* Nature, 2002. **416**(6881): p. 640-644.

156. Lindsay, S.A. and S.A. Wasserman, *Conventional and non-conventional Drosophila Toll signaling.* Developmental and comparative immunology, 2014. **42**(1): p. 16-24.

157. Rus, F., et al., *Ecdysone triggered PGRP-LC expression controls Drosophila innate immunity.* The EMBO journal, 2013. **32**(11): p. 1626-1638.

158. Kleino, A. and N. Silverman, *The Drosophila IMD pathway in the activation of the humoral immune response.* Developmental and comparative immunology, 2014. **42**(1): p. 25-35.

159. Wang, S. and B.T. Beerntsen, *Identification and functional analysis of the peptidoglycan recognition protein LD gene in the mosquito, Armigeres subalbatus.* Developmental and comparative immunology, 2014. **42**(2): p. 148-158.

160. Moussian, B., *The apical plasma membrane of chitin-synthesising epithelia.* Insect science, 2012.

161. Adler, P.N., et al., *dusky-like is required to maintain the integrity and planar cell polarity of hairs during the development of the Drosophila wing.* Developmental biology, 2013. **379**(1): p. 76-91.

162. Shaukat, Z., D. Liu, and S. Gregory, *Sterile inflammation in Drosophila.* Mediators of inflammation, 2015. **2015**: p. 369286.

163. Lemaitre, B. and J. Hoffmann, *The host defense of Drosophila melanogaster.* Annual review of immunology, 2007. **25**: p. 697-743.

164. Rizki, T.M., R.M. Rizki, and E.H. Grell, *A mutant affecting the crystal cells inDrosophila melanogaster.* Wilhelm Roux's archives of developmental biology, 1980. **188**(2): p. 91-99.

165. Ferrandon, D., et al., *A drosomycin-GFP reporter transgene reveals a local immune response in Drosophila that is not dependent on the Toll pathway.* EMBO J, 1998. **17**(5): p. 1217-27.

166. Moreno, E. and K. Basler, *dMyc transforms cells into super-competitors.* Cell, 2004. **117**(1): p. 117-29.

167. de la Cova, C., et al., *Drosophila myc regulates organ size by inducing cell competition.* Cell, 2004. **117**(1): p. 107-16.

168. Levashina, E.A., et al., *Constitutive activation of toll-mediated antifungal defense in serpin-deficient Drosophila.* Science, 1999. **285**(5435): p. 1917-9.

169. Cakouros, D., T.J. Daish, and S. Kumar, *Ecdysone receptor directly binds the promoter of the Drosophila caspase dronc, regulating its expression in specific tissues.* The Journal of cell biology, 2004. **165**(5): p. 631-640.

170. Katsukawa, M., et al., *Serpin Facilitates Tumor-Suppressive Cell Competition by Blocking Toll-Mediated Yki Activation in Drosophila.* Current biology : CB, 2018. **28**(11): p. 1756-1767000000.

171. Wu, C., et al., *Toll pathway modulates TNF-induced JNK-dependent cell death in Drosophila.* Open biology, 2015. **5**(7): p. 140171.

172. Moreno, E., M. Yan, and K. Basler, *Evolution of TNF signaling mechanisms: JNK-dependent apoptosis triggered by Eiger, the Drosophila homolog of the TNF superfamily.* Curr Biol, 2002. **12**(14): p. 1263-8.

173. Zhang, C., et al., *An intergenic regulatory region mediates Drosophila Myc-induced apoptosis and blocks tissue hyperplasia.* Oncogene, 2015. **34**(18): p. 2385-97.

174. Moon, N.S., et al., *E2F and p53 induce apoptosis independently during Drosophila development but intersect in the context of DNA damage.* PLoS Genet, 2008. **4**(8): p. e1000153.

175. Moon, N.S., L. Di Stefano, and N. Dyson, *A gradient of epidermal growth factor receptor signaling determines the sensitivity of rbf1 mutant cells to E2F-dependent apoptosis.* Mol Cell Biol, 2006. **26**(20): p. 7601-15.

176. Moon, N.S., et al., *Drosophila E2F1 has context-specific pro- and antiapoptotic properties during development.* Dev Cell, 2005. **9**(4): p. 463-75.

177. Brennecke, J., et al., *bantam Encodes a Developmentally Regulated microRNA that Controls Cell Proliferation and Regulates the Proapoptotic Gene hid in Drosophila.* Cell, 2003. **113**(1): p. 25-36.

178. Geisler, R., et al., *cactus, a gene involved in dorsoventral pattern formation of Drosophila, is related to the I kappa B gene family of vertebrates.* Cell, 1992. **71**(4): p. 613-21.

179. Wang, L., D.M. Lonard, and B.W. O'Malley, *The Role of Steroid Receptor Coactivators in Hormone Dependent Cancers and Their Potential as Therapeutic Targets.* Horm Cancer, 2016. **7**(4): p. 229-35.

180. Konig, A., et al., *Ecdysteroids affect Drosophila ovarian stem cell niche formation and early germline differentiation.* Embo J, 2011. **30**(8): p. 1549-62.

181. Ameku, T. and R. Niwa, *Mating-Induced Increase in Germline Stem Cells via the Neuroendocrine System in Female Drosophila.* PLoS genetics, 2016. **12**(6).

182. Riddiford, L.M., P. Cherbas, and J.W. Truman, *Ecdysone receptors and their biological actions.* Vitam Horm, 2000. **60**: p. 1-73.

183. Starz-Gaiano, M. and D.J. Montell, *Genes that drive invasion and migration in Drosophila.* Curr Opin Genet Dev, 2004. **14**(1): p. 86-91.

184. Regan, J.C., et al., *Steroid Hormone Signaling Is Essential to Regulate Innate Immune Cells and Fight Bacterial Infection in Drosophila.* PLoS Pathogens, 2013. **9**(10).

185. Bate, M.a.A., A.M., *The Development of Drosophila melanogaster*, ed. M.a.A. Bate, A.M. Vol. I and II. 1993, Cold Spring Harbor, NY: CSHL Press. 1558.

186. Sampedro, J., J. Galceran, and M. Izquierdo, *Mutation mapping of the 2B5 ecdysone locus in Drosophila melanogaster reveals a long-distance controlling element.* Molecular and cellular biology, 1989. **9**(8): p. 3588-3591.

187. Yamamoto, M., et al., *The ligand Sas and its receptor PTP10D drive tumour-suppressive cell competition.* Nature, 2017. **542**(7640): p. 246-250.

188. Kurata, S., *Peptidoglycan recognition proteins in Drosophila immunity.* Developmental and comparative immunology, 2014. **42**(1): p. 36-41.

189. Alpar, L., C. Bergantinos, and L.A. Johnston, *Spatially Restricted Regulation of Spatzle/Toll Signaling during Cell Competition.* Dev Cell, 2018.

190. Martins, V.C., et al., *Cell competition is a tumour suppressor mechanism in the thymus.* Nature, 2014. **509**(7501): p. 465-470.

191. Suijkerbuijk, S.J., et al., *Cell Competition Drives the Growth of Intestinal Adenomas in Drosophila.* Current biology : CB, 2016. **26**(4): p. 428-438.

192. Eichenlaub, T., S.M. Cohen, and H. Herranz, *Cell Competition Drives the Formation of Metastatic Tumors in a Drosophila Model of Epithelial Tumor Formation.* Current biology : CB, 2016. **26**(4): p. 419-427.

193. Di Giacomo, S., et al., *Human Cancer Cells Signal Their Competitive Fitness Through MYC Activity.* Scientific reports, 2017. **7**(1): p. 12568.

194. Zhao, S., et al., *Toll-like receptors and prostate cancer.* Front Immunol, 2014. **5**: p. 352.

195. Gambara, G., et al., *Toll-like receptors in prostate infection and cancer between bench and bedside.* J Cell Mol Med, 2013. **17**(6): p. 713-22.

196. Rakoff-Nahoum, S. and R. Medzhitov, *Toll-like receptors and cancer.* Nat Rev Cancer, 2009. **9**(1): p. 57-63.

197. Trapnell, C., et al., *Differential gene and transcript expression analysis of RNA-seq experiments with TopHat and Cufflinks.* Nat Protoc, 2012. **7**(3): p. 562-78.

198. Schindelin, J., et al., *Fiji: an open-source platform for biological-image analysis.* Nat Methods, 2012. **9**(7): p. 676-82.

199. Untergasser, A., et al., *Primer3Plus, an enhanced web interface to Primer3.* Nucleic Acids Res, 2007. **35**(Web Server issue): p. W71-4.

200. Kawauchi, T., *Cell adhesion and its endocytic regulation in cell migration during neural development and cancer metastasis.* Int J Mol Sci, 2012. **13**(4): p. 4564-90.

201. He, L., X. Wang, and D.J. Montell, *Shining light on Drosophila oogenesis: live imaging of egg development.* Current Opinion in Genetics & Development, 2011. **21**(5): p. 612-619.

202. Montell, D.J., *The social lives of migrating cells in Drosophila.* Curr Opin Genet Dev, 2006. **16**(4): p. 374-83.

203. Ma, G., et al., *SRC-3 has a role in cancer other than as a nuclear receptor coactivator.* International journal of biological sciences, 2010. **7**(5): p. 664-72.

204. Yi, P., et al., *SRC-3 coactivator regulates cell resistance to cytotoxic stress via TRAF4-mediated p53 destabilization.* Genes & development, 2013. **27**(3): p. 274-87.

205. Wang, Y., et al., *Small molecule inhibition of the steroid receptor coactivators, SRC-3 and SRC-1.* Molecular endocrinology (Baltimore, Md.), 2011. **25**(12): p. 2041-53.

206. Wu, H., *The role of AIB1 in breast cancer (Review).* Oncology Letters, 2012. **4**(4): p. 588-594.

207. Cho, E. and K.D. Irvine, *Action of fat, four-jointed, dachsous and dachs in distal-to-proximal wing signaling.* Development (Cambridge, England), 2004. **131**(18): p. 4489-500.

208. Yoshida, H., et al., *Steroid receptor coactivator-3, a homolog of Taiman that controls cell migration in the Drosophila ovary, regulates migration of human ovarian cancer cells.* Mol Cell Endocrinol, 2005. **245**(1-2): p. 77-85.

209. Narayanan, R., S. Ponnusamy, and D.D. Miller, *Destroying the androgen receptor (AR)-potential strategy to treat advanced prostate cancer.* Oncoscience, 2017. **4**(11-12): p. 175-177.

210. D'Avino, P.P. and C.S. Thummel, *The ecdysone regulatory pathway controls wing morphogenesis and integrin expression during Drosophila metamorphosis.* Dev Biol, 2000. **220**(2): p. 211-24.

211. Mirth, C.K., J.W. Truman, and L.M. Riddiford, *The ecdysone receptor controls the post-critical weight switch to nutrition-independent differentiation in Drosophila wing imaginal discs.* Development, 2009. **136**(14): p. 2345-53.

212. Delanoue, R., M. Slaidina, and P. Léopold, *The steroid hormone ecdysone controls systemic growth by repressing dMyc function in Drosophila fat cells.* Developmental cell, 2010. **18**(6): p. 1012-21.

213. Johnston, D.M., et al., *Ecdysone- and NO-Mediated Gene Regulation by Competing EcR/Usp and E75A Nuclear Receptors during Drosophila Development.* Molecular Cell, 2011. **44**(1): p. 51-61.

214. D'Avino, P.P. and C.S. Thummel, *crooked legs encodes a family of zinc finger proteins required for leg morphogenesis and ecdysone-regulated gene expression during Drosophila metamorphosis.* Development (Cambridge, England), 1998. **125**(9): p. 1733-45.

215. Karpowicz, P., J. Perez, and N. Perrimon, *The Hippo tumor suppressor pathway regulates intestinal stem cell regeneration.* Development (Cambridge, England), 2010. **137**(24): p. 4135-45.

216. Chang, B., C. Ma, and X. Liu, *Nanofibers Regulate Single Bone Marrow Stem Cell Osteogenesis via FAK/RhoA/YAP1 Pathway.* ACS Appl Mater Interfaces, 2018. **10**(39): p. 33022-33031.

217. Jiang, N., et al., *YAP1 regulates prostate cancer stem cell-like characteristics to promote castration resistant growth.* Oncotarget, 2017. **8**(70): p. 115054-115067.

218. Miftakhova, R., et al., *Cyclin A1 and P450 Aromatase Promote Metastatic Homing and Growth of Stem-like Prostate Cancer Cells in the Bone Marrow.* Cancer Res, 2016. **76**(8): p. 2453-64.

219. Yamanaka, N., G. Marqués, and M.B. O'Connor, *Vesicle-Mediated Steroid Hormone Secretion in Drosophila melanogaster.* Cell, 2015. **163**(4): p. 907-19.

220. Okamoto, N., et al., *A Membrane Transporter Is Required for Steroid Hormone Uptake in Drosophila.* Dev Cell, 2018.

221. Huang, J., et al., *The Hippo signaling pathway coordinately regulates cell proliferation and apoptosis by inactivating Yorkie, the Drosophila Homolog of YAP.* Cell, 2005. **122**(3): p. 421-34.

222. Jiang, C., E.H. Baehrecke, and C.S. Thummel, *Steroid regulated programmed cell death during Drosophila metamorphosis.* Development (Cambridge, England), 1997. **124**(22): p. 4673-83.

223. Khan, S.J., et al., *The Drosophila Duox maturation factor is a key component of a positive feedback loop that sustains regeneration signaling.* PLoS Genet, 2017. **13**(7): p. e1006937.

224. Agaisse, H., et al., *Signaling role of hemocytes in Drosophila JAK/STAT-dependent response to septic injury.* Developmental cell, 2003. **5**(3): p. 441-50.

225. Lotfi, R., et al., *Until Death Do Us Part: Necrosis and Oxidation Promote the Tumor Microenvironment.* Transfus Med Hemother, 2016. **43**(2): p. 120-32.

226. Lee, S.Y., et al., *Regulation of Tumor Progression by Programmed Necrosis.* Oxid Med Cell Longev, 2018. **2018**: p. 3537471.

227. Valanne, S., J.H. Wang, and M. Ramet, *The Drosophila Toll signaling pathway.* J Immunol, 2011. **186**(2): p. 649-56.

228. Katsuyama, T., et al., *During Drosophila disc regeneration, JAK/STAT coordinates cell proliferation with Dilp8-mediated developmental delay.* Proceedings of the National Academy of Sciences of the United States of America, 2015. **112**(18): p. E2327-36.

229.   Hackney, J.F., O. Zolali-Meybodi, and P. Cherbas, *Tissue damage disrupts developmental progression and ecdysteroid biosynthesis in Drosophila.* PLoS One, 2012. **7**(11): p. e49105.

Appendix

Table 1. Deficiencies that dominantly modify *tai*-driven wing invasion (supporting Figs. 2,3,5). Table of BDSC or Exelixis deficiency (Df) stocks that dominantly modify the *MS1096>tai* phenotype. Strength of modification: +++ strong, ++ moderate, +mild. Where noted in column 3, suppressive effects were mapped to specific genes using available alleles.

Suppressors	Strength	Gene(s) confirmed for effect
Df(2R)Exel6061	+++	-
Df(2R)Exel6069		-
Df(2R)BSC152		-
Df(2L)BSC169		-
Df(2L)BSC180		-
Df(2R)BSC199		-
Df(2L)BSC278		*cact*
Df(2L)BSC291		*pvf2, pvf3*
Df(2R)BSC595		-
Df(2R)BSC661		-
Df(2L)Exel7011	++	-
Df(2R)Exel7131		-
Df(2R)Exel7144		-
Df(2R)Exel7162		-
Df(2L)BSC109		-
Df(2R)BSC161		-
Df(2R)BSC280		*myd88*
Df(2R)BSC383		-
Df(2L)Exel6038	+	-
Df(2R)Exel6284		-
Df(2L)Exel7034		-
Df(2R)BSC135		-
Df(2L)BSC148		*dl*
Df(2L)BSC149		-
Df(2L)BSC172		-
Df(2L)BSC188		-
Df(2R)BSC274		-
Df(2L)BSC277		-
Df(2R)BSC267		-
Df(2R)BSC331		-
Df(2R)BSC485		-
Df(2R)BSC550		-
Enhancers	**Strength**	**Gene(s) confirmed for effect**
Df(2L)C144	+++	-
Df(2R)M60E		-
Df(2L)BSC6		-
Df(2L)ED19		-
Df(2R)ED2457		-
Df(2R)ED1715		-
Df(2R)ED3728		*hpo*
Df(2L)ED105		*ds*
Df(2R)BSC630		-

Table 2. Mapped reads from HTS RNA-seq analysis of *en>GFP* and *en>tai,GFP* larval wing discs (supporting Fig. 3). Alphabetical gene list with corresponding read frequency (FPKM; fragments per kilobase mapped) for *en>GFP* (Sample/value 1) and *en>tai,GFP* (Sample/value 2) RNA samples. Fold change in FPKM (*GFP* vs. *tai,GFP*) is presented in log base 2 (log[2]Δ).

See Attached PDF File "Table 2"

Table 3. Candidate Tai induced mRNAs (supporting Fig. 3). Alphabetical gene list of mRNAs with FPKM log[2]Δ>0.8 between *en>GFP* and *en>tai,GFP* samples.

Flybase ID	Gene	Sample 1	Sample 2	value 1 (FPKM)	value 2 (FPKM)	Log2(Δ)
FBgn0023129	*aay*	enGFP	enGFP+Tai	1.74866	29.5134	4.07705
FBgn0036752	*Adgf-A*	enGFP	enGFP+Tai	0.67538	2.46474	1.86766
FBgn0038173	*Adgf-C*	enGFP	enGFP+Tai	0.0807451	0.308985	1.93609
FBgn0000055	*Adh*	enGFP	enGFP+Tai	0.719537	2.82377	1.97248
FBgn0015569	*alpha-Est10*	enGFP	enGFP+Tai	3.30501	8.13388	1.29929
FBgn0015576	*alpha-Est8*	enGFP	enGFP+Tai	0.050646	0.116283	1.19912
FBgn0052865	*αγ-element:CR32865*	enGFP	enGFP+Tai	1.29292	3.79315	1.55276
FBgn0034005	*alphaPS4*	enGFP	enGFP+Tai	0.0786319	0.300775	1.9355
FBgn0000075	*amd*	enGFP	enGFP+Tai	9.38171	33.9926	1.8573
FBgn0086782	*amn*	enGFP	enGFP+Tai	0.0987785	0.327594	1.72964
FBgn0032535	*Ance-2*	enGFP	enGFP+Tai	0.15183	0.464801	1.61416
FBgn0033366	*Ance-4*	enGFP	enGFP+Tai	0.141449	0.324766	1.19912
FBgn0023535	*arg*	enGFP	enGFP+Tai	0.116735	0.536103	2.19927
FBgn0065032	*Arpc3B*	enGFP	enGFP+Tai	0.53697	2.26031	2.07361
FBgn0000121	*Arr2*	enGFP	enGFP+Tai	1.11357	2.69881	1.27713
FBgn0015905	*Ast*	enGFP	enGFP+Tai	0.0999566	1.071	3.42152
FBgn0024897	*b6*	enGFP	enGFP+Tai	0.192096	2.05817	3.42146
FBgn0033578	*BBS4*	enGFP	enGFP+Tai	0.197507	0.604637	1.61416
FBgn0038498	*beat-IIa*	enGFP	enGFP+Tai	0.221992	0.951431	2.09959
FBgn0038494	*beat-IIb*	enGFP	enGFP+Tai	0.834953	2.39009	1.5173
FBgn0003890	*betaTub97EF*	enGFP	enGFP+Tai	2.42925	5.89812	1.27974
FBgn0036449	*bmm*	enGFP	enGFP+Tai	1.52638	3.52038	1.20561
FBgn0015905	*bru-3*	enGFP	enGFP+Tai	0.0531095	3.3488	5.97853
FBgn0028525	*c(2)M*	enGFP	enGFP+Tai	0.419813	1.23929	1.56169
FBgn0038247	*Cad88C*	enGFP	enGFP+Tai	0.191189	0.487746	1.35113
FBgn0027844	*CAH1*	enGFP	enGFP+Tai	0.692944	3.40929	2.29866
FBgn0004878	*cas*	enGFP	enGFP+Tai	0.106591	0.32631	1.61416
FBgn0004783	*Ccp84Aa*	enGFP	enGFP+Tai	0.445613	15.3469	5.10602
FBgn0004782	*Ccp84Ab*	enGFP	enGFP+Tai	0.396776	3.94766	3.3146
FBgn0004780	*Ccp84Ad*	enGFP	enGFP+Tai	0.241138	25.4681	6.72269
FBgn0051973	*Cda5*	enGFP	enGFP+Tai	1.5626	16.5565	3.40537
FBgn0034197	*Cda9*	enGFP	enGFP+Tai	0.115098	0.264265	1.19912
FBgn0032785	*CG10026*	enGFP	enGFP+Tai	2.1007	17.8542	3.08732
FBgn0037498	*CG10029*	enGFP	enGFP+Tai	0.105617	0.727492	2.78409
FBgn0039084	*CG10175*	enGFP	enGFP+Tai	0.228633	10.8351	5.56653
FBgn0039094	*CG10184*	enGFP	enGFP+Tai	0.111148	0.680526	2.61416
FBgn0032685	*CG10211*	enGFP	enGFP+Tai	9.19055	43.5232	2.24356
FBgn0039109	*CG10365*	enGFP	enGFP+Tai	1.7243	5.25582	1.6079
FBgn0034638	*CG10433*	enGFP	enGFP+Tai	2.45838	5.01521	1.0286
FBgn0037060	*CG10508*	enGFP	enGFP+Tai	0.108998	1.19117	3.45
FBgn0037044	*CG10585*	enGFP	enGFP+Tai	10.3522	29.5929	1.51531
FBgn0037036	*CG10586*	enGFP	enGFP+Tai	0.368285	1.40931	1.93609
FBgn0037037	*CG10588*	enGFP	enGFP+Tai	0.122178	0.249353	1.0292
FBgn0035612	*CG10625*	enGFP	enGFP+Tai	57.1462	255.93	2.16302
FBgn0035608	*CG10630*	enGFP	enGFP+Tai	0.701075	1.52024	1.11666
FBgn0046302	*CG10650*	enGFP	enGFP+Tai	0.376298	1.00798	1.42152
FBgn0036294	*CG10654*	enGFP	enGFP+Tai	0.124656	0.477016	1.93609
FBgn0036289	*CG10657*	enGFP	enGFP+Tai	15.571	49.2667	1.66175
FBgn0036288	*CG10660*	enGFP	enGFP+Tai	0.0815475	0.312056	1.93609
FBgn0036287	*CG10663*	enGFP	enGFP+Tai	1.72048	5.02009	1.5449
FBgn0029663	*CG10804*	enGFP	enGFP+Tai	0.0678084	0.216584	1.67539
FBgn0037228	*CG1092*	enGFP	enGFP+Tai	0.50388	1.61966	1.68454
FBgn0032857	*CG10947*	enGFP	enGFP+Tai	0.108232	0.207091	0.936141
FBgn0030073	*CG10962*	enGFP	enGFP+Tai	4.10871	9.51243	1.21113
FBgn0034464	*CG11018*	enGFP	enGFP+Tai	0.118877	0.272942	1.19912
FBgn0267033	*CG11071*	enGFP	enGFP+Tai	1.4241	2.92373	1.03776
FBgn0031734	*CG11147*	enGFP	enGFP+Tai	0.963361	5.52102	2.51879
FBgn0264502	*CG11203*	enGFP	enGFP+Tai	0.0341502	0.127071	1.89567
FBgn0037290	*CG1124*	enGFP	enGFP+Tai	0.13402	4.5131	5.07359
FBgn0037280	*CG1126*	enGFP	enGFP+Tai	0.123406	0.28334	1.19912
FBgn0034897	*CG11299*	enGFP	enGFP+Tai	1.12829	8.54232	2.9205

FBgn0039798	*CG11313*	enGFP	enGFP+Tai	0.103486	0.237604	1.19912
FBgn0035557	*CG11353*	enGFP	enGFP+Tai	2.24773	4.90113	1.12464
FBgn0031214	*CG11374*	enGFP	enGFP+Tai	0.502695	1.82747	1.86209
FBgn0040359	*CG11380*	enGFP	enGFP+Tai	1.87442	7.89006	2.07359
FBgn0040367	*CG11382*	enGFP	enGFP+Tai	0.438846	14.8452	5.08014
FBgn0035300	*CG1139*	enGFP	enGFP+Tai	2.38933	9.56516	2.00119
FBgn0034200	*CG11395*	enGFP	enGFP+Tai	0.0946531	0.362206	1.93609
FBgn0035359	*CG1143*	enGFP	enGFP+Tai	0.580994	1.2228	1.07359
FBgn0039749	*CG11498*	enGFP	enGFP+Tai	1.34295	16.4449	3.61416
FBgn0039864	*CG11550*	enGFP	enGFP+Tai	31.1968	54.5208	0.805412
FBgn0036836	*CG11619*	enGFP	enGFP+Tai	1.7627	3.09784	0.813471
FBgn0036196	*CG11658*	enGFP	enGFP+Tai	0.836219	2.71986	1.70158
FBgn0039297	*CG11852*	enGFP	enGFP+Tai	1.95275	67.7126	5.11585
FBgn0039299	*CG11854*	enGFP	enGFP+Tai	0.772745	4.02158	2.3797
FBgn0036678	*CG11905*	enGFP	enGFP+Tai	32.5735	147.049	2.17453
FBgn0037645	*CG11966*	enGFP	enGFP+Tai	1.23326	41.8051	5.08313
FBgn0037646	*CG11967*	enGFP	enGFP+Tai	0.732291	1.90552	1.3797
FBgn0035429	*CG12017*	enGFP	enGFP+Tai	1.25803	4.10241	1.70531
FBgn0262624	*CG12026*	enGFP	enGFP+Tai	29.6881	79.1913	1.41546
FBgn0039808	*CG12071*	enGFP	enGFP+Tai	0.0543488	0.1664	1.61434
FBgn0035241	*CG12105*	enGFP	enGFP+Tai	0.0648603	0.132373	1.0292
FBgn0030041	*CG12116*	enGFP	enGFP+Tai	0.273446	0.488315	0.836554
FBgn0033158	*CG12164*	enGFP	enGFP+Tai	0.31256	506.733	10.6629
FBgn0039131	*CG12268*	enGFP	enGFP+Tai	22.4501	84.9703	1.92023
FBgn0030596	*CG12398*	enGFP	enGFP+Tai	0.0729457	0.167528	1.19951
FBgn0030542	*CG12481*	enGFP	enGFP+Tai	7.56045	43.7744	2.53354
FBgn0263109	*CG12551*	enGFP	enGFP+Tai	3.57902	21.0001	2.55276
FBgn0046294	*CG12699*	enGFP	enGFP+Tai	0.22321	0.512492	1.19912
FBgn0033252	*CG12769*	enGFP	enGFP+Tai	0.314188	5.02985	4.00081
FBgn0033221	*CG12825*	enGFP	enGFP+Tai	1.68867	4.91112	1.54016
FBgn0263934	*CG12835*	enGFP	enGFP+Tai	2.23091	5.61001	1.33037
FBgn0035086	*CG12851*	enGFP	enGFP+Tai	0.171049	0.299222	0.806807
FBgn0033461	*CG12923*	enGFP	enGFP+Tai	0.120743	0.277226	1.19912
FBgn0034022	*CG12964*	enGFP	enGFP+Tai	9.63622	30.1101	1.64371
FBgn0037078	*CG12971*	enGFP	enGFP+Tai	0.213161	0.652556	1.61416
FBgn0037065	*CG12974*	enGFP	enGFP+Tai	0.308873	1.10323	1.83665
FBgn0036677	*CG13023*	enGFP	enGFP+Tai	23.5657	61.5721	1.38559
FBgn0036665	*CG13024*	enGFP	enGFP+Tai	2.93615	5.39313	0.877196
FBgn0036670	*CG13029*	enGFP	enGFP+Tai	0.443547	1.24479	1.48875
FBgn0036605	*CG13041*	enGFP	enGFP+Tai	3.775	18.6189	2.30222
FBgn0040796	*CG13064*	enGFP	enGFP+Tai	16.5035	34.7344	1.07359
FBgn0036577	*CG13073*	enGFP	enGFP+Tai	0.0957576	0.21986	1.19912
FBgn0032804	*CG13081*	enGFP	enGFP+Tai	1.54123	4.12845	1.42152
FBgn0032803	*CG13082*	enGFP	enGFP+Tai	23.5024	74.476	1.66397
FBgn0032084	*CG13101*	enGFP	enGFP+Tai	1.95469	3.76456	0.945544
FBgn0032211	*CG13138*	enGFP	enGFP+Tai	0.210689	0.459407	1.12466
FBgn0033736	*CG13154*	enGFP	enGFP+Tai	0.524942	3.21405	2.61416
FBgn0033732	*CG13157*	enGFP	enGFP+Tai	0.103486	0.237604	1.19912
FBgn0033667	*CG13183*	enGFP	enGFP+Tai	0.370676	3.6407	3.29599
FBgn0033668	*CG13188*	enGFP	enGFP+Tai	1.94246	16.1606	3.05653
FBgn0045827	*CG13245*	enGFP	enGFP+Tai	0.201969	0.46372	1.19912
FBgn0037014	*CG13251*	enGFP	enGFP+Tai	0.0403259	0.0925883	1.19912
FBgn0032582	*CG13258*	enGFP	enGFP+Tai	0.614748	20.4662	5.05711
FBgn0032612	*CG13282*	enGFP	enGFP+Tai	0.251816	0.57817	1.19912
FBgn0032614	*CG13284*	enGFP	enGFP+Tai	1.23158	14.0915	3.51624
FBgn0035921	*CG13305*	enGFP	enGFP+Tai	0.266586	0.611774	1.1984
FBgn0033787	*CG13321*	enGFP	enGFP+Tai	0.14611	1.00641	2.78409
FBgn0033789	*CG13324*	enGFP	enGFP+Tai	0.468984	24.0483	5.68025
FBgn0033868	*CG13340*	enGFP	enGFP+Tai	0.0645323	0.148166	1.19912
FBgn0030544	*CG13403*	enGFP	enGFP+Tai	0.915265	1.86796	1.0292
FBgn0034532	*CG13436*	enGFP	enGFP+Tai	1.59066	3.09881	0.962085
FBgn0036503	*CG13454*	enGFP	enGFP+Tai	0.805933	3.08404	1.93609
FBgn0036443	*CG13471*	enGFP	enGFP+Tai	0.17229	0.395571	1.19909
FBgn0036421	*CG13481*	enGFP	enGFP+Tai	0.245466	0.563591	1.19912
FBgn0034758	*CG13510*	enGFP	enGFP+Tai	0.275089	2.52642	3.19912
FBgn0034788	*CG13532*	enGFP	enGFP+Tai	0.0765759	0.644668	3.07359

FBgn0039203	*CG13618*	enGFP	enGFP+Tai	0.763163	5.84075	2.93609
FBgn0039217	*CG13627*	enGFP	enGFP+Tai	2.29885	7.65128	1.73479
FBgn0040600	*CG13631*	enGFP	enGFP+Tai	1.35898	17.8546	3.7157
FBgn0040601	*CG13643*	enGFP	enGFP+Tai	0.102472	0.745044	2.86209
FBgn0030539	*CG1368*	enGFP	enGFP+Tai	7.77009	125.051	4.00844
FBgn0036781	*CG13699*	enGFP	enGFP+Tai	0.139188	2.07725	3.89956
FBgn0035578	*CG13707*	enGFP	enGFP+Tai	0.751781	3.45219	2.19912
FBgn0035555	*CG13720*	enGFP	enGFP+Tai	0.0912839	0.698627	2.93609
FBgn0035553	*CG13722*	enGFP	enGFP+Tai	0.451253	95.5166	7.72567
FBgn0036717	*CG13731*	enGFP	enGFP+Tai	2.1046	45.1367	4.42269
FBgn0036382	*CG13737*	enGFP	enGFP+Tai	11.0446	43.3297	1.97201
FBgn0033374	*CG13741*	enGFP	enGFP+Tai	0.0853976	0.223901	1.39059
FBgn0263026	*CG13776*	enGFP	enGFP+Tai	0.351404	1.15814	1.72061
FBgn0031939	*CG13796*	enGFP	enGFP+Tai	0.151177	0.655687	2.11677
FBgn0039040	*CG13833*	enGFP	enGFP+Tai	0.142888	0.437428	1.61416
FBgn0038993	*CG13843*	enGFP	enGFP+Tai	0.127101	0.291825	1.19912
FBgn0038967	*CG13847*	enGFP	enGFP+Tai	0.247527	11.3664	5.52105
FBgn0038959	*CG13856*	enGFP	enGFP+Tai	0.505539	7.73813	3.93609
FBgn0038958	*CG13857*	enGFP	enGFP+Tai	0.100858	0.308759	1.61416
FBgn0034501	*CG13868*	enGFP	enGFP+Tai	0.328088	0.941483	1.52085
FBgn0035104	*CG13875*	enGFP	enGFP+Tai	1.26001	2.25009	0.836554
FBgn0035138	*CG13884*	enGFP	enGFP+Tai	0.220019	0.505163	1.19912
FBgn0035168	*CG13889*	enGFP	enGFP+Tai	0.0209184	0.0800477	1.93609
FBgn0035287	*CG13937*	enGFP	enGFP+Tai	0.185312	0.496397	1.42154
FBgn0033405	*CG13954*	enGFP	enGFP+Tai	0.122758	1.03346	3.07359
FBgn0031763	*CG13996*	enGFP	enGFP+Tai	0.44241	1.01577	1.19912
FBgn0031677	*CG14036*	enGFP	enGFP+Tai	1.16414	2.67288	1.19912
FBgn0036690	*CG14059*	enGFP	enGFP+Tai	0.188082	1.29551	2.78409
FBgn0036870	*CG14095*	enGFP	enGFP+Tai	0.302093	2.31202	2.93609
FBgn0036351	*CG14107*	enGFP	enGFP+Tai	0.521974	90.8162	7.44283
FBgn0036364	*CG14109*	enGFP	enGFP+Tai	0.18581	0.426621	1.19912
FBgn0036352	*CG14110*	enGFP	enGFP+Tai	0.708681	3.47122	2.29223
FBgn0036323	*CG14118*	enGFP	enGFP+Tai	0.0865351	0.529826	2.61416
FBgn0036935	*CG14186*	enGFP	enGFP+Tai	0.0748409	0.257752	1.78409
FBgn0030981	*CG14191*	enGFP	enGFP+Tai	0.215776	14.3673	6.05711
FBgn0030994	*CG14193*	enGFP	enGFP+Tai	0.613965	1.09641	0.836554
FBgn0039429	*CG14238*	enGFP	enGFP+Tai	0.362715	0.693995	0.93609
FBgn0039479	*CG14257*	enGFP	enGFP+Tai	10.5547	20.273	0.941682
FBgn0039482	*CG14258*	enGFP	enGFP+Tai	0.537942	3.84259	2.83655
FBgn0039504	*CG14260*	enGFP	enGFP+Tai	0.872424	1.73601	0.992674
FBgn0039503	*CG14262*	enGFP	enGFP+Tai	0.441476	0.788378	0.836554
FBgn0262562	*CG14318*	enGFP	enGFP+Tai	0.317291	5.25403	4.04955
FBgn0262871	*CG14333*	enGFP	enGFP+Tai	5.03971	9.64266	0.93609
FBgn0038207	*CG14356*	enGFP	enGFP+Tai	0.234701	1.97588	3.07359
FBgn0038170	*CG14367*	enGFP	enGFP+Tai	0.1988	0.38034	0.935971
FBgn0038073	*CG14395*	enGFP	enGFP+Tai	0.628624	1.39268	1.1476
FBgn0032914	*CG14397*	enGFP	enGFP+Tai	0.40429	10.8296	4.74345
FBgn0030038	*CG1440*	enGFP	enGFP+Tai	47.5192	82.7544	0.800327
FBgn0032900	*CG14401*	enGFP	enGFP+Tai	0.361176	0.7371	1.02916
FBgn0030595	*CG14406*	enGFP	enGFP+Tai	0.272049	0.833	1.61445
FBgn0029922	*CG14431*	enGFP	enGFP+Tai	0.149545	0.515035	1.78409
FBgn0263109	*CG14470*	enGFP	enGFP+Tai	5.32087	15.4356	1.53653
FBgn0039651	*CG14508*	enGFP	enGFP+Tai	0.114669	0.26328	1.19912
FBgn0039612	*CG14523*	enGFP	enGFP+Tai	0.0611654	0.327705	2.42161
FBgn0031955	*CG14535*	enGFP	enGFP+Tai	0.0456623	0.104841	1.19912
FBgn0040602	*CG14545*	enGFP	enGFP+Tai	0.407278	0.77926	0.93609
FBgn0039408	*CG14551*	enGFP	enGFP+Tai	0.202212	0.619039	1.61416
FBgn0037126	*CG14567*	enGFP	enGFP+Tai	6.24055	11.0929	0.829891
FBgn0033063	*CG14589*	enGFP	enGFP+Tai	0.198388	0.455499	1.19912
FBgn0033054	*CG14591*	enGFP	enGFP+Tai	0.0902619	0.18158	1.00842
FBgn0037503	*CG14598*	enGFP	enGFP+Tai	13.324	50.7111	1.92827
FBgn0037487	*CG14608*	enGFP	enGFP+Tai	0.389385	0.943698	1.27713
FBgn0040358	*CG14625*	enGFP	enGFP+Tai	0.0598567	0.320673	2.42152
FBgn0037217	*CG14636*	enGFP	enGFP+Tai	0.196631	4.88919	4.63603
FBgn0037288	*CG14661*	enGFP	enGFP+Tai	0.283472	0.650854	1.19912
FBgn0037850	*CG14695*	enGFP	enGFP+Tai	0.136548	0.313514	1.19912

FBgn0033307	CG14752	enGFP	enGFP+Tai	0.378204	19.9722	5.72269
FBgn0038273	CG14860	enGFP	enGFP+Tai	6.65933	13.1912	0.986131
FBgn0031169	CG1494	enGFP	enGFP+Tai	0.0273634	0.146595	2.42152
FBgn0032405	CG14946	enGFP	enGFP+Tai	2.82855	5.43238	0.941524
FBgn0035428	CG14960	enGFP	enGFP+Tai	1.40167	3.44811	1.29866
FBgn0035508	CG15005	enGFP	enGFP+Tai	1.51813	5.34463	1.8158
FBgn0030929	CG15043	enGFP	enGFP+Tai	1.29173	17.2017	3.73518
FBgn0034391	CG15080	enGFP	enGFP+Tai	1.22275	10.6824	3.12703
FBgn0034396	CG15097	enGFP	enGFP+Tai	0.711099	2.13782	1.58801
FBgn0034417	CG15117	enGFP	enGFP+Tai	0.0616181	0.177657	1.52767
FBgn0032665	CG15152	enGFP	enGFP+Tai	0.803713	1.84533	1.19912
FBgn0030270	CG15199	enGFP	enGFP+Tai	0.545303	1.66936	1.61416
FBgn0030234	CG15211	enGFP	enGFP+Tai	1.04099	4.69708	2.17381
FBgn0040842	CG15212	enGFP	enGFP+Tai	15.8324	762.125	5.58907
FBgn0029681	CG15239	enGFP	enGFP+Tai	0.276697	18.6354	6.07359
FBgn0030161	CG15249	enGFP	enGFP+Tai	0.268475	2.67129	3.31467
FBgn0263216	CG15250	enGFP	enGFP+Tai	5.06517	42.6426	3.07361
FBgn0263216	CG15251	enGFP	enGFP+Tai	0.150763	15.6923	6.70162
FBgn0031088	CG15322	enGFP	enGFP+Tai	0.111474	0.981121	3.13772
FBgn0264978	CG15393	enGFP	enGFP+Tai	3.24093	6.82108	1.07359
FBgn0031463	CG15400	enGFP	enGFP+Tai	0.377021	0.769459	1.0292
FBgn0031542	CG15414	enGFP	enGFP+Tai	0.634247	1.94164	1.61416
FBgn0039804	CG15544	enGFP	enGFP+Tai	13.4676	31.0409	1.20468
FBgn0039806	CG15545	enGFP	enGFP+Tai	0.713611	5.02459	2.8158
FBgn0039807	CG15546	enGFP	enGFP+Tai	6.20265	17.1716	1.46907
FBgn0039821	CG15556	enGFP	enGFP+Tai	0.152063	0.310344	1.0292
FBgn0037409	CG15589	enGFP	enGFP+Tai	2.24319	18.9237	3.07657
FBgn0031632	CG15628	enGFP	enGFP+Tai	14.2267	35.2165	1.30765
FBgn0034639	CG15673	enGFP	enGFP+Tai	0.910389	1.59258	0.806807
FBgn0030493	CG15756	enGFP	enGFP+Tai	24.71	250.128	3.3395
FBgn0029814	CG15765	enGFP	enGFP+Tai	0.337419	1.51715	2.16875
FBgn0035308	CG15822	enGFP	enGFP+Tai	6.27489	11.5525	0.880548
FBgn0032136	CG15828	enGFP	enGFP+Tai	0.0470056	0.151095	1.68455
FBgn0029864	CG15894	enGFP	enGFP+Tai	0.334377	0.960114	1.52173
FBgn0033447	CG1625	enGFP	enGFP+Tai	0.0378141	0.231569	2.61444
FBgn0030027	CG1632	enGFP	enGFP+Tai	8.01987	16.5023	1.04102
FBgn0031558	CG16704	enGFP	enGFP+Tai	2.00372	197.057	6.61979
FBgn0037665	CG16733	enGFP	enGFP+Tai	60.6928	209.9	1.79011
FBgn0032835	CG16772	enGFP	enGFP+Tai	0.279292	0.641255	1.19912
FBgn0034538	CG16799	enGFP	enGFP+Tai	0.491913	1.12943	1.19912
FBgn0032462	CG16800	enGFP	enGFP+Tai	2.71615	8.16656	1.58817
FBgn0030484	CG1681	enGFP	enGFP+Tai	12.4271	35.2961	1.50601
FBgn0032522	CG16848	enGFP	enGFP+Tai	0.124909	0.573581	2.19912
FBgn0028938	CG16886	enGFP	enGFP+Tai	0.351156	4.5064	3.68179
FBgn0032533	CG16888	enGFP	enGFP+Tai	1.15955	2.95815	1.35113
FBgn0034483	CG16894	enGFP	enGFP+Tai	0.460755	1.41053	1.61416
FBgn0031816	CG16947	enGFP	enGFP+Tai	7.13019	15.3899	1.10997
FBgn0033443	CG1698	enGFP	enGFP+Tai	3.7797	11.5223	1.60809
FBgn0040554	CG17025	enGFP	enGFP+Tai	0.310475	0.950469	1.61416
FBgn0036552	CG17028	enGFP	enGFP+Tai	0.266013	0.83312	1.64703
FBgn0032291	CG17118	enGFP	enGFP+Tai	0.322037	0.985863	1.61416
FBgn0032299	CG17127	enGFP	enGFP+Tai	0.5456	269.674	8.94915
FBgn0039941	CG17167	enGFP	enGFP+Tai	1.50704	3.37827	1.16457
FBgn0040514	CG17169	enGFP	enGFP+Tai	0.387735	1.48373	1.93609
FBgn0036447	CG17173	enGFP	enGFP+Tai	0.0900814	0.206827	1.19912
FBgn0035144	CG17181	enGFP	enGFP+Tai	0.0471899	0.18058	1.93609
FBgn0038761	CG17190	enGFP	enGFP+Tai	0.799999	1.98987	1.3146
FBgn0032419	CG17217	enGFP	enGFP+Tai	0.32784	0.752721	1.19912
FBgn0031489	CG17224	enGFP	enGFP+Tai	1.31145	3.28482	1.32466
FBgn0031490	CG17264	enGFP	enGFP+Tai	0.341998	2.16873	2.66479
FBgn0038828	CG17270	enGFP	enGFP+Tai	0.107461	0.246731	1.19912
FBgn0035880	CG17352	enGFP	enGFP+Tai	4.08298	8.13011	0.993654
FBgn0033936	CG17386	enGFP	enGFP+Tai	0.213309	2.93854	3.78409
FBgn0039977	CG17454	enGFP	enGFP+Tai	77.3661	141.283	0.868811
FBgn0032869	CG17470	enGFP	enGFP+Tai	0.339817	0.780222	1.19912
FBgn0263780	CG17684	enGFP	enGFP+Tai	0.585201	1.03356	0.820613

FBgn0025835	*CG17707*	enGFP	enGFP+Tai	0.452046	6.38227	3.81953
FBgn0038009	*CG17738*	enGFP	enGFP+Tai	0.626417	3.35593	2.42152
FBgn0033756	*CG17760*	enGFP	enGFP+Tai	0.285055	0.581767	1.0292
FBgn0039167	*CG17786*	enGFP	enGFP+Tai	0.824984	19.8397	4.58788
FBgn0028394	*CG17834*	enGFP	enGFP+Tai	21.2114	41.565	0.970526
FBgn0032791	*CG18094*	enGFP	enGFP+Tai	3.35051	6.25679	0.901043
FBgn0030359	*CG18130*	enGFP	enGFP+Tai	0.278101	0.48689	0.807986
FBgn0031343	*CG18131*	enGFP	enGFP+Tai	0.157362	0.304011	0.950038
FBgn0036839	*CG18136*	enGFP	enGFP+Tai	0.0731624	0.167981	1.19912
FBgn0036024	*CG18180*	enGFP	enGFP+Tai	0.540304	3.03243	2.48863
FBgn0031869	*CG18304*	enGFP	enGFP+Tai	0.0658316	0.201533	1.61416
FBgn0033610	*CG18335*	enGFP	enGFP+Tai	0.229766	0.439619	0.93609
FBgn0037683	*CG18473*	enGFP	enGFP+Tai	0.231712	0.62068	1.42152
FBgn0033154	*CG1850*	enGFP	enGFP+Tai	2.6655	924.077	8.43746
FBgn0028527	*CG18507*	enGFP	enGFP+Tai	24.5758	45.9502	0.902833
FBgn0031469	*CG18558*	enGFP	enGFP+Tai	0.0770071	0.825106	3.42152
FBgn0038973	*CG18594*	enGFP	enGFP+Tai	0.286618	79.1885	8.11002
FBgn0038460	*CG18622*	enGFP	enGFP+Tai	0.14858	0.341139	1.19912
FBgn0031426	*CG18641*	enGFP	enGFP+Tai	0.680474	2.29148	1.75167
FBgn0042098	*CG18735*	enGFP	enGFP+Tai	0.978631	7.91779	3.01626
FBgn0042106	*CG18754*	enGFP	enGFP+Tai	1.36523	2.78629	1.0292
FBgn0035290	*CG1887*	enGFP	enGFP+Tai	0.102387	3.72212	5.18402
FBgn0250839	*CG2016*	enGFP	enGFP+Tai	41.8109	99.4263	1.24975
FBgn0262636	*CG2052*	enGFP	enGFP+Tai	0.0334393	0.0762307	1.18883
FBgn0033289	*CG2121*	enGFP	enGFP+Tai	0.29054	0.667166	1.19931
FBgn0003065	*CG2150*	enGFP	enGFP+Tai	0.388934	144.169	8.53402
FBgn0027544	*CG2217*	enGFP	enGFP+Tai	0.0322876	0.288356	3.1588
FBgn0029995	*CG2256*	enGFP	enGFP+Tai	0.13215	0.303417	1.19912
FBgn0033484	*CG2269*	enGFP	enGFP+Tai	0.0779645	0.185241	1.24851
FBgn0030396	*CG2556*	enGFP	enGFP+Tai	4.51672	9.33785	1.04782
FBgn0037518	*CG2641*	enGFP	enGFP+Tai	4.26125	7.82707	0.877196
FBgn0035090	*CG2736*	enGFP	enGFP+Tai	0.15868	1.3966	3.13772
FBgn0037534	*CG2781*	enGFP	enGFP+Tai	0.842399	9.18722	3.44705
FBgn0031646	*CG2837*	enGFP	enGFP+Tai	0.308531	3.75672	3.60599
FBgn0031273	*CG2839*	enGFP	enGFP+Tai	0.0543107	0.374092	2.78409
FBgn0035078	*CG2857*	enGFP	enGFP+Tai	0.125926	1.62313	3.68813
FBgn0028491	*CG2930*	enGFP	enGFP+Tai	0.945979	14.9083	3.97816
FBgn0031468	*CG2975*	enGFP	enGFP+Tai	1.91703	4.68367	1.28876
FBgn0050008	*CG30008*	enGFP	enGFP+Tai	0.173501	0.398359	1.19912
FBgn0050036	*CG30036*	enGFP	enGFP+Tai	0.322102	0.575204	0.836554
FBgn0050046	*CG30046*	enGFP	enGFP+Tai	0.202834	0.698562	1.78409
FBgn0050062	*CG30062*	enGFP	enGFP+Tai	0.623085	1.19109	0.934782
FBgn0050076	*CG30076*	enGFP	enGFP+Tai	0.111048	0.424945	1.93609
FBgn0029720	*CG3009*	enGFP	enGFP+Tai	1.13776	2.66169	1.22615
FBgn0050101	*CG30101*	enGFP	enGFP+Tai	0.371191	115.268	8.27861
FBgn0050108	*CG30108*	enGFP	enGFP+Tai	1.32417	8.34752	2.65625
FBgn0037519	*CG3014*	enGFP	enGFP+Tai	0.0370823	0.0677826	0.870186
FBgn0050154	*CG30154*	enGFP	enGFP+Tai	0.440456	1.34839	1.61416
FBgn0050161	*CG30161*	enGFP	enGFP+Tai	0.201308	0.616272	1.61416
FBgn0265187	*CG30194*	enGFP	enGFP+Tai	5.70522	11.3467	0.991922
FBgn0050197	*CG30197*	enGFP	enGFP+Tai	7.44701	31.347	2.07359
FBgn0050273	*CG30273*	enGFP	enGFP+Tai	0.83271	1.48704	0.836554
FBgn0050286	*CG30286*	enGFP	enGFP+Tai	0.28332	0.66465	1.23016
FBgn0050339	*CG30339*	enGFP	enGFP+Tai	0.456765	0.815682	0.836554
FBgn0050343	*CG30343*	enGFP	enGFP+Tai	0.119686	0.2748	1.19912
FBgn0050357	*CG30357*	enGFP	enGFP+Tai	1.03324	2.87554	1.47666
FBgn0031645	*CG3036*	enGFP	enGFP+Tai	14.2023	32.5711	1.19747
FBgn0050377	*CG30377*	enGFP	enGFP+Tai	0.924418	1.99383	1.10893
FBgn0050398	*CG30398*	enGFP	enGFP+Tai	0.470522	0.839945	0.836031
FBgn0050424	*CG30424*	enGFP	enGFP+Tai	0.186943	0.864299	2.20893
FBgn0050428	*CG30428*	enGFP	enGFP+Tai	14.7923	29.3119	0.986639
FBgn0050438	*CG30438*	enGFP	enGFP+Tai	1.78566	4.60988	1.36827
FBgn0050456	*CG30456*	enGFP	enGFP+Tai	0.219765	0.493976	1.16847
FBgn0050497	*CG30497*	enGFP	enGFP+Tai	6.07515	12.6285	1.05569
FBgn0029608	*CG3091*	enGFP	enGFP+Tai	0.245079	0.468942	0.936164
FBgn0029804	*CG3097*	enGFP	enGFP+Tai	20.6842	60.7097	1.55339

FBgn0051004	CG31004	enGFP	enGFP+Tai	0.0324477	0.397159	3.61353
FBgn0051005	CG31005	enGFP	enGFP+Tai	3.52226	18.6505	2.40464
FBgn0051029	CG31029	enGFP	enGFP+Tai	0.132956	0.407022	1.61416
FBgn0029807	CG3108	enGFP	enGFP+Tai	0.0366407	4.76721	7.02355
FBgn0051086	CG31086	enGFP	enGFP+Tai	0.606223	1.43506	1.24319
FBgn0051100	CG31100	enGFP	enGFP+Tai	0.312358	6.05614	4.27713
FBgn0051139	CG31139	enGFP	enGFP+Tai	0.583675	1.0721	0.877196
FBgn0051140	CG31140	enGFP	enGFP+Tai	1.1175	2.674	1.25872
FBgn0051145	CG31145	enGFP	enGFP+Tai	0.0857501	4.60372	5.74652
FBgn0051161	CG31161	enGFP	enGFP+Tai	0.0849231	0.584951	2.78409
FBgn0051176	CG31176	enGFP	enGFP+Tai	1.17718	5.32369	2.1771
FBgn0051183	CG31183	enGFP	enGFP+Tai	0.02871	0.109864	1.93609
FBgn0031466	CG3119	enGFP	enGFP+Tai	0.273595	0.841346	1.62066
FBgn0051226	CG31226	enGFP	enGFP+Tai	0.692898	4.24342	2.61451
FBgn0051313	CG31313	enGFP	enGFP+Tai	0.295565	0.678618	1.19912
FBgn0051523	CG31523	enGFP	enGFP+Tai	53.1567	94.4007	0.828546
FBgn0264907	CG31530	enGFP	enGFP+Tai	0.037127	0.0852437	1.19912
FBgn0051559	CG31559	enGFP	enGFP+Tai	3.52591	8.62461	1.29046
FBgn0051626	CG31626	enGFP	enGFP+Tai	0.553289	1.58143	1.51512
FBgn0051676	CG31676	enGFP	enGFP+Tai	1.4611	2.90741	0.992674
FBgn0031449	CG31689	enGFP	enGFP+Tai	0.619272	1.42128	1.19854
FBgn0262475	CG31763	enGFP	enGFP+Tai	1.29219	4.45017	1.78404
FBgn0051781	CG31781	enGFP	enGFP+Tai	0.351613	0.672758	0.936098
FBgn0051785	CG31785	enGFP	enGFP+Tai	0.928038	2.84104	1.61416
FBgn0051789	CG31789	enGFP	enGFP+Tai	0.402967	129.838	8.33184
FBgn0263079	CG31790	enGFP	enGFP+Tai	0.0510238	0.195251	1.93609
FBgn0062978	CG31808	enGFP	enGFP+Tai	0.978534	7.21356	2.88202
FBgn0051869	CG31869	enGFP	enGFP+Tai	29.7115	63.31	1.09141
FBgn0051871	CG31871	enGFP	enGFP+Tai	0.116485	7.48858	6.00648
FBgn0260479	CG31904	enGFP	enGFP+Tai	0.0367721	0.0844288	1.19912
FBgn0052040	CG32040	enGFP	enGFP+Tai	0.321262	0.737618	1.19912
FBgn0052055	CG32055	enGFP	enGFP+Tai	1.23937	17.0059	3.77835
FBgn0052152	CG32152	enGFP	enGFP+Tai	0.269652	0.550331	1.0292
FBgn0052182	CG32182	enGFP	enGFP+Tai	0.11774	0.360442	1.61416
FBgn0052225	CG32225	enGFP	enGFP+Tai	0.116624	0.26777	1.19912
FBgn0052246	CG32246	enGFP	enGFP+Tai	0.0830075	0.31766	1.93617
FBgn0052354	CG32354	enGFP	enGFP+Tai	3.43305	11.9348	1.79761
FBgn0052436	CG32436	enGFP	enGFP+Tai	0.142237	0.254004	0.836554
FBgn0031629	CG3244	enGFP	enGFP+Tai	7.63304	143.168	4.22931
FBgn0262509	CG32458	enGFP	enGFP+Tai	2.31709	4.28559	0.887181
FBgn0052462	CG32462	enGFP	enGFP+Tai	1.07718	2.8396	1.39843
FBgn0052506	CG32506	enGFP	enGFP+Tai	0.0750462	0.201024	1.42152
FBgn0052547	CG32547	enGFP	enGFP+Tai	0.0678861	0.2338	1.78409
FBgn0052572	CG32572	enGFP	enGFP+Tai	0.0598567	0.183242	1.61416
FBgn0052573	CG32573	enGFP	enGFP+Tai	0.000692875	0.421083	9.24729
FBgn0052645	CG32645	enGFP	enGFP+Tai	0.185579	17.4413	6.55433
FBgn0052668	CG32668	enGFP	enGFP+Tai	0.0518984	0.237752	2.1957
FBgn0052687	CG32687	enGFP	enGFP+Tai	0.288617	0.662666	1.19912
FBgn0052694	CG32694	enGFP	enGFP+Tai	1.91022	16.678	3.12614
FBgn0052736	CG32736	enGFP	enGFP+Tai	0.00187456	12.7229	12.7286
FBgn0052793	CG32793	enGFP	enGFP+Tai	1.08227	5.20643	2.26624
FBgn0052815	CG32815	enGFP	enGFP+Tai	0.0657035	0.402281	2.61416
FBgn0052855	CG32855	enGFP	enGFP+Tai	0.204667	6.05617	4.88706
FBgn0263037	CG32972	enGFP	enGFP+Tai	3.3354	41.3721	3.63273
FBgn0053056	CG33056	enGFP	enGFP+Tai	8.15345	21.218	1.3798
FBgn0053191	CG33191	enGFP	enGFP+Tai	0.108838	0.390881	1.84455
FBgn0069056	CG33226	enGFP	enGFP+Tai	0.563384	1.14981	1.0292
FBgn0053267	CG33267	enGFP	enGFP+Tai	1.11072	3.4003	1.61416
FBgn0053286	CG33286	enGFP	enGFP+Tai	0.0399723	0.214145	2.42152
FBgn0053293	CG33293	enGFP	enGFP+Tai	0.275705	0.633019	1.19912
FBgn0053460	CG33460	enGFP	enGFP+Tai	0.504848	1.03034	1.0292
FBgn0053465	CG33465	enGFP	enGFP+Tai	0.536562	1.50571	1.48863
FBgn0053468	CG33468	enGFP	enGFP+Tai	0.329596	0.756752	1.19912
FBgn0036459	CG3349	enGFP	enGFP+Tai	0.0609232	0.233133	1.93609
FBgn0053494	CG33494	enGFP	enGFP+Tai	0.884819	1.86225	1.07359
FBgn0250819	CG33521	enGFP	enGFP+Tai	0.503511	0.885337	0.814203

FBgn0031619	CG3355	enGFP	enGFP+Tai	8.30926	31.284	1.91263
FBgn0034997	CG3376	enGFP	enGFP+Tai	16.9147	35.2307	1.05855
FBgn0035240	CG33791	enGFP	enGFP+Tai	0.0669843	0.310401	2.21224
FBgn0263750	CG33937	enGFP	enGFP+Tai	0.399902	0.783018	0.969401
FBgn0053970	CG33970	enGFP	enGFP+Tai	9.5972	20.9331	1.1251
FBgn0054051	CG34051	enGFP	enGFP+Tai	0.221809	0.680518	1.61732
FBgn0083956	CG34120	enGFP	enGFP+Tai	2.47528	4.85324	0.971354
FBgn0083972	CG34136	enGFP	enGFP+Tai	0.250461	1.91686	2.93609
FBgn0083975	CG34139	enGFP	enGFP+Tai	0.0204136	0.062493	1.61416
FBgn0085194	CG34165	enGFP	enGFP+Tai	0.45012	1.03348	1.19912
FBgn0085195	CG34166	enGFP	enGFP+Tai	4.00187	9.62227	1.2657
FBgn0085222	CG34193	enGFP	enGFP+Tai	1.68797	2.95282	0.806807
FBgn0085234	CG34205	enGFP	enGFP+Tai	0.280096	1.07184	1.93609
FBgn0085236	CG34207	enGFP	enGFP+Tai	1.29981	3.96717	1.60981
FBgn0085261	CG34232	enGFP	enGFP+Tai	0.584098	7.48363	3.67946
FBgn0085263	CG34234	enGFP	enGFP+Tai	0.316869	0.727532	1.19912
FBgn0085276	CG34247	enGFP	enGFP+Tai	13.2614	48.0405	1.85702
FBgn0264746	CG34252	enGFP	enGFP+Tai	0.405921	0.724886	0.836554
FBgn0085294	CG34265	enGFP	enGFP+Tai	0.563436	1.72487	1.61416
FBgn0266566	CG34275	enGFP	enGFP+Tai	0.10458	0.399046	1.93195
FBgn0085305	CG34276	enGFP	enGFP+Tai	0.584834	1.79038	1.61416
FBgn0085325	CG34296	enGFP	enGFP+Tai	1.83274	3.27287	0.836554
FBgn0085334	CG34305	enGFP	enGFP+Tai	1.37445	4.20585	1.61355
FBgn0085345	CG34316	enGFP	enGFP+Tai	0.17776	0.408138	1.19912
FBgn0085360	CG34331	enGFP	enGFP+Tai	1.57623	3.37776	1.09959
FBgn0085384	CG34355	enGFP	enGFP+Tai	6.49741	19.9452	1.6181
FBgn0267336	CG34360	enGFP	enGFP+Tai	3.50195	10.609	1.59906
FBgn0263117	CG34377	enGFP	enGFP+Tai	0.270396	0.62083	1.19912
FBgn0085466	CG34437	enGFP	enGFP+Tai	0.186091	0.427266	1.19912
FBgn0024984	CG3457	enGFP	enGFP+Tai	0.543484	2.91163	2.42152
FBgn0038250	CG3505	enGFP	enGFP+Tai	0.390167	1.49304	1.93609
FBgn0029708	CG3556	enGFP	enGFP+Tai	0.613107	1.53567	1.32466
FBgn0031417	CG3597	enGFP	enGFP+Tai	0.12206	0.373666	1.61416
FBgn0031562	CG3604	enGFP	enGFP+Tai	0.59113	3.16689	2.42152
FBgn0029824	CG3726	enGFP	enGFP+Tai	2.02436	4.57751	1.1771
FBgn0032116	CG3759	enGFP	enGFP+Tai	0.398904	1.43496	1.8469
FBgn0024989	CG3777	enGFP	enGFP+Tai	42.4496	157.038	1.88729
FBgn0030421	CG3812	enGFP	enGFP+Tai	0.304034	0.63989	1.07359
FBgn0034804	CG3831	enGFP	enGFP+Tai	3.38503	16.8744	2.3176
FBgn0029866	CG3842	enGFP	enGFP+Tai	18.7942	86.9249	2.20948
FBgn0265185	CG3884	enGFP	enGFP+Tai	0.803087	3.50168	2.12442
FBgn0038291	CG3984	enGFP	enGFP+Tai	0.615701	17.0311	4.7898
FBgn0038292	CG3987	enGFP	enGFP+Tai	0.492978	3.01834	2.61416
FBgn0058178	CG40178	enGFP	enGFP+Tai	10.8515	20.1126	0.890205
FBgn0034885	CG4019	enGFP	enGFP+Tai	0.14137	0.433147	1.61538
FBgn0058470	CG40470	enGFP	enGFP+Tai	0.0893124	0.205062	1.19912
FBgn0085736	CG40472	enGFP	enGFP+Tai	1.01117	1.9347	0.93609
FBgn0069969	CG40498	enGFP	enGFP+Tai	0.121338	0.371456	1.61416
FBgn0037838	CG4089	enGFP	enGFP+Tai	8.04056	15.4886	0.945838
FBgn0263112	CG41130	enGFP	enGFP+Tai	0.646074	1.97785	1.61416
FBgn0038017	CG4115	enGFP	enGFP+Tai	8.79761	172.852	4.29628
FBgn0036793	CG4174	enGFP	enGFP+Tai	0.00355637	0.14993	5.39774
FBgn0250862	CG42237	enGFP	enGFP+Tai	0.202046	27.37	7.08177
FBgn0250867	CG42238	enGFP	enGFP+Tai	31.8882	61.4019	0.945261
FBgn0250869	CG42240	enGFP	enGFP+Tai	14.7400	27.5023	0.899748
FBgn0259098	CG42246	enGFP	enGFP+Tai	0.338664	1.03676	1.61416
FBgn0259099	CG42247	enGFP	enGFP+Tai	0.0328558	0.0590358	0.84544
FBgn0259145	CG42260	enGFP	enGFP+Tai	0.0410786	0.135459	1.7214
FBgn0259151	CG42266	enGFP	enGFP+Tai	0.212662	0.922291	2.11666
FBgn0259167	CG42272	enGFP	enGFP+Tai	8.66789	18.2016	1.07031
FBgn0259200	CG42304	enGFP	enGFP+Tai	0.00173771	0.198774	6.83779
FBgn0259222	CG42322	enGFP	enGFP+Tai	0.508972	2.66106	2.38634
FBgn0259224	CG42324	enGFP	enGFP+Tai	0.165533	0.541703	1.71038
FBgn0259226	CG42326	enGFP	enGFP+Tai	0.36257	5.62436	3.95536
FBgn0259233	CG42331	enGFP	enGFP+Tai	0.0554146	13.6379	7.94314
FBgn0259708	CG42362	enGFP	enGFP+Tai	0.436976	1.4715	1.75167

FBgn0259715	*CG42369*	enGFP	enGFP+Tai	0.104099	0.318681	1.61416
FBgn0264707	*CG42377*	enGFP	enGFP+Tai	0.594617	1.45373	1.28973
FBgn0259739	*CG42393*	enGFP	enGFP+Tai	0.133007	0.407178	1.61416
FBgn0259821	*CG42402*	enGFP	enGFP+Tai	0.369378	1.88465	2.35113
FBgn0259926	*CG42449*	enGFP	enGFP+Tai	0.12279	0.404543	1.7201
FBgn0259933	*CG42456*	enGFP	enGFP+Tai	12.4285	23.4876	0.918243
FBgn0034761	*CG4250*	enGFP	enGFP+Tai	1.8215	6.97029	1.93609
FBgn0260657	*CG42540*	enGFP	enGFP+Tai	0.0409675	0.0775068	0.919844
FBgn0260658	*CG42541*	enGFP	enGFP+Tai	0.127559	0.409898	1.6841
FBgn0031389	*CG4259*	enGFP	enGFP+Tai	0.512556	1.30759	1.35113
FBgn0264979	*CG4267*	enGFP	enGFP+Tai	0.222297	1.27599	2.52105
FBgn0261803	*CG42749*	enGFP	enGFP+Tai	6.31064	23.839	1.91747
FBgn0261837	*CG42769*	enGFP	enGFP+Tai	3.79406	6.81204	0.844345
FBgn0261845	*CG42777*	enGFP	enGFP+Tai	19.7515	38.9308	0.978949
FBgn0263354	*CG42784*	enGFP	enGFP+Tai	0.0361255	0.082966	1.1995
FBgn0261859	*CG42788*	enGFP	enGFP+Tai	3.90164	7.20828	0.885574
FBgn0261932	*CG42798*	enGFP	enGFP+Tai	0.862397	5.9402	2.78409
FBgn0038799	*CG4288*	enGFP	enGFP+Tai	0.22901	1.22691	2.42155
FBgn0030747	*CG4301*	enGFP	enGFP+Tai	0.0314618	0.216709	2.78409
FBgn0027073	*CG4302*	enGFP	enGFP+Tai	0.079545	0.365271	2.19912
FBgn0039078	*CG4374*	enGFP	enGFP+Tai	4.49358	14.4391	1.68405
FBgn0032132	*CG4382*	enGFP	enGFP+Tai	86.4128	395.144	2.19306
FBgn0039075	*CG4393*	enGFP	enGFP+Tai	0.0555292	0.148744	1.42152
FBgn0030432	*CG4404*	enGFP	enGFP+Tai	0.73833	1.44407	0.967799
FBgn0034128	*CG4409*	enGFP	enGFP+Tai	0.351963	0.808108	1.19912
FBgn0038740	*CG4562*	enGFP	enGFP+Tai	0.314149	3.06109	3.28452
FBgn0038366	*CG4576*	enGFP	enGFP+Tai	1.60981	5.6929	1.82227
FBgn0036427	*CG4613*	enGFP	enGFP+Tai	0.120506	0.368911	1.61416
FBgn0035587	*CG4623*	enGFP	enGFP+Tai	0.267504	0.477716	0.836596
FBgn0032549	*CG4650*	enGFP	enGFP+Tai	0.163804	0.376094	1.19912
FBgn0029838	*CG4666*	enGFP	enGFP+Tai	0.29084	11.1295	5.25802
FBgn0033815	*CG4676*	enGFP	enGFP+Tai	0.13272	0.4063	1.61416
FBgn0030778	*CG4678*	enGFP	enGFP+Tai	0.562208	17.2919	4.94285
FBgn0037992	*CG4702*	enGFP	enGFP+Tai	1.37657	156.328	6.82736
FBgn0039024	*CG4721*	enGFP	enGFP+Tai	0.0617568	0.141632	1.19748
FBgn0028514	*CG4793*	enGFP	enGFP+Tai	0.0485869	0.334667	2.78409
FBgn0031220	*CG4822*	enGFP	enGFP+Tai	0.439917	1.17815	1.42122
FBgn0030796	*CG4829*	enGFP	enGFP+Tai	0.655653	1.79593	1.45372
FBgn0270925	*CG4836*	enGFP	enGFP+Tai	0.165968	0.380088	1.19543
FBgn0036436	*CG4914*	enGFP	enGFP+Tai	81.6922	278.327	1.76851
FBgn0027556	*CG4928*	enGFP	enGFP+Tai	7.87366	28.5293	1.85734
FBgn0034137	*CG4945*	enGFP	enGFP+Tai	0.0644501	0.128445	0.994898
FBgn0036587	*CG4950*	enGFP	enGFP+Tai	1.29108	2.65553	1.04043
FBgn0036612	*CG4998*	enGFP	enGFP+Tai	0.316998	69.186	7.76986
FBgn0034275	*CG5002*	enGFP	enGFP+Tai	0.0692132	0.317827	2.19912
FBgn0028743	*CG5036*	enGFP	enGFP+Tai	0.0465123	0.177987	1.93609
FBgn0032637	*CG5050*	enGFP	enGFP+Tai	0.23914	0.640577	1.42152
FBgn0034145	*CG5065*	enGFP	enGFP+Tai	7.79193	41.5507	2.41482
FBgn0037005	*CG5078*	enGFP	enGFP+Tai	0.217967	0.583862	1.42152
FBgn0032470	*CG5142*	enGFP	enGFP+Tai	0.112647	0.47417	2.07359
FBgn0034154	*CG5267*	enGFP	enGFP+Tai	0.484329	0.926387	0.935627
FBgn0036568	*CG5389*	enGFP	enGFP+Tai	0.0675792	0.310324	2.19912
FBgn0038353	*CG5399*	enGFP	enGFP+Tai	4.77061	19.4291	2.02598
FBgn0034887	*CG5428*	enGFP	enGFP+Tai	0.248556	3.04366	3.61416
FBgn0265052	*CG5431*	enGFP	enGFP+Tai	1.8133	8.75387	2.2713
FBgn0034364	*CG5493*	enGFP	enGFP+Tai	0.128965	0.296105	1.19912
FBgn0039564	*CG5527*	enGFP	enGFP+Tai	0.0577505	0.132595	1.19912
FBgn0039527	*CG5639*	enGFP	enGFP+Tai	4.24967	19.047	2.16414
FBgn0032192	*CG5731*	enGFP	enGFP+Tai	23.6677	41.4289	0.807721
FBgn0034301	*CG5756*	enGFP	enGFP+Tai	0.150146	5.86994	5.2889
FBgn0032666	*CG5758*	enGFP	enGFP+Tai	47.3665	113.736	1.26375
FBgn0038682	*CG5835*	enGFP	enGFP+Tai	9.97061	44.0236	2.14252
FBgn0038897	*CG5849*	enGFP	enGFP+Tai	0.0435232	0.166582	1.93638
FBgn0038511	*CG5873*	enGFP	enGFP+Tai	11.2041	63.0586	2.49266
FBgn0029835	*CG5921*	enGFP	enGFP+Tai	0.648519	9.42968	3.86199
FBgn0029836	*CG5928*	enGFP	enGFP+Tai	0.626453	7.35167	3.55279

FBgn0032587	*CG5953*	enGFP	enGFP+Tai	2.63334	6.852	1.37963
FBgn0036997	*CG5955*	enGFP	enGFP+Tai	0.224732	0.601983	1.42152
FBgn0039387	*CG5959*	enGFP	enGFP+Tai	0.134201	0.308125	1.19912
FBgn0031914	*CG5973*	enGFP	enGFP+Tai	5.29805	25.3824	2.26029
FBgn0063649	*CG6006*	enGFP	enGFP+Tai	0.0479237	0.141859	1.56564
FBgn0034736	*CG6018*	enGFP	enGFP+Tai	0.141938	0.271575	0.93609
FBgn0036202	*CG6024*	enGFP	enGFP+Tai	0.211442	0.475932	1.1705
FBgn0038676	*CG6026*	enGFP	enGFP+Tai	0.386958	15.4846	5.32251
FBgn0264894	*CG6043*	enGFP	enGFP+Tai	2.62953	11.3146	2.10531
FBgn0031918	*CG6055*	enGFP	enGFP+Tai	1.55731	168.052	6.75371
FBgn0264894	*CG6108*	enGFP	enGFP+Tai	0.0917067	2.03504	4.47189
FBgn0038339	*CG6118*	enGFP	enGFP+Tai	0.197547	68.0639	8.42855
FBgn0039415	*CG6142*	enGFP	enGFP+Tai	0.632394	2.32316	1.8772
FBgn0036154	*CG6168*	enGFP	enGFP+Tai	1.02156	1.78705	0.806807
FBgn0027611	*CG6206*	enGFP	enGFP+Tai	7.18691	15.3266	1.09259
FBgn0033862	*CG6209*	enGFP	enGFP+Tai	0.0651471	0.548453	3.07359
FBgn0036139	*CG6216*	enGFP	enGFP+Tai	0.286775	1.09739	1.93609
FBgn0036125	*CG6279*	enGFP	enGFP+Tai	0.299691	0.572402	0.933551
FBgn0033866	*CG6280*	enGFP	enGFP+Tai	2.76888	16.308	2.55821
FBgn0035914	*CG6282*	enGFP	enGFP+Tai	0.0797073	0.213517	1.42157
FBgn0263776	*CG6327*	enGFP	enGFP+Tai	0.0631342	0.918604	3.86295
FBgn0039464	*CG6330*	enGFP	enGFP+Tai	4.27515	10.8116	1.33853
FBgn0033875	*CG6357*	enGFP	enGFP+Tai	4.90955	42.8975	3.12723
FBgn0034162	*CG6426*	enGFP	enGFP+Tai	7.47529	28.0518	1.90789
FBgn0035922	*CG6486*	enGFP	enGFP+Tai	0.523131	0.92026	0.814869
FBgn0034224	*CG6520*	enGFP	enGFP+Tai	0.568589	1.45053	1.35113
FBgn0037852	*CG6608*	enGFP	enGFP+Tai	9.81277	18.9046	0.946002
FBgn0036687	*CG6652*	enGFP	enGFP+Tai	0.0637886	0.184951	1.53577
FBgn0030947	*CG6696*	enGFP	enGFP+Tai	2.89454	15.5071	2.42152
FBgn0033889	*CG6701*	enGFP	enGFP+Tai	8.73253	24.4037	1.48263
FBgn0031926	*CG6739*	enGFP	enGFP+Tai	8.09933	20.9773	1.37295
FBgn0038070	*CG6753*	enGFP	enGFP+Tai	1.86452	7.19199	1.94759
FBgn0030876	*CG6762*	enGFP	enGFP+Tai	5.97479	12.5968	1.0761
FBgn0035903	*CG6765*	enGFP	enGFP+Tai	0.0823788	0.342122	2.05417
FBgn0036834	*CG6836*	enGFP	enGFP+Tai	0.900572	1.7231	0.93609
FBgn0030884	*CG6847*	enGFP	enGFP+Tai	4.47788	12.4533	1.47564
FBgn0038290	*CG6912*	enGFP	enGFP+Tai	1.44881	35.6407	4.62059
FBgn0036945	*CG6981*	enGFP	enGFP+Tai	0.190744	0.583849	1.61396
FBgn0034191	*CG6984*	enGFP	enGFP+Tai	7.17229	12.8877	0.845488
FBgn0038941	*CG7080*	enGFP	enGFP+Tai	0.127893	0.293644	1.19912
FBgn0035888	*CG7120*	enGFP	enGFP+Tai	0.0460943	0.14111	1.61416
FBgn0031948	*CG7149*	enGFP	enGFP+Tai	0.163727	0.29238	0.836554
FBgn0037107	*CG7166*	enGFP	enGFP+Tai	0.0378578	0.115895	1.61416
FBgn0037099	*CG7173*	enGFP	enGFP+Tai	3.43547	7.42137	1.11118
FBgn0031940	*CG7214*	enGFP	enGFP+Tai	0.295731	0.565833	0.93609
FBgn0031971	*CG7224*	enGFP	enGFP+Tai	26.7453	61.005	1.18964
FBgn0031970	*CG7227*	enGFP	enGFP+Tai	0.120122	0.229834	0.93609
FBgn0031968	*CG7231*	enGFP	enGFP+Tai	4.16621	8.11028	0.961017
FBgn0036782	*CG7320*	enGFP	enGFP+Tai	0.148621	0.568726	1.93609
FBgn0036939	*CG7365*	enGFP	enGFP+Tai	0.256183	1.04568	2.0292
FBgn0262562	*CG7397*	enGFP	enGFP+Tai	0.238903	6.94794	4.86209
FBgn0035815	*CG7422*	enGFP	enGFP+Tai	0.977593	4.15659	2.08809
FBgn0030982	*CG7423*	enGFP	enGFP+Tai	0.323532	0.990439	1.61416
FBgn0031979	*CG7429*	enGFP	enGFP+Tai	2.28232	4.36684	0.93609
FBgn0038727	*CG7432*	enGFP	enGFP+Tai	1.92813	7.16238	1.89323
FBgn0036927	*CG7433*	enGFP	enGFP+Tai	1.28995	2.31964	0.846585
FBgn0037140	*CG7442*	enGFP	enGFP+Tai	0.131618	0.251829	0.93609
FBgn0037144	*CG7458*	enGFP	enGFP+Tai	0.0631097	0.2898	2.19912
FBgn0035575	*CG7509*	enGFP	enGFP+Tai	0.141205	0.432277	1.61416
FBgn0035798	*CG7526*	enGFP	enGFP+Tai	0.0507067	0.162387	1.67918
FBgn0039681	*CG7582*	enGFP	enGFP+Tai	0.12883	0.887385	2.78409
FBgn0036727	*CG7589*	enGFP	enGFP+Tai	0.0709281	0.325702	2.19912
FBgn0032025	*CG7778*	enGFP	enGFP+Tai	0.482025	0.922276	0.93609
FBgn0036116	*CG7888*	enGFP	enGFP+Tai	0.38731	11.2063	4.85468
FBgn0036416	*CG7924*	enGFP	enGFP+Tai	3.98237	44.3026	3.47569
FBgn0028533	*CG7953*	enGFP	enGFP+Tai	0.14211	7.61082	5.74297

FBgn0033387	*CG8008*	enGFP	enGFP+Tai	0.0998815	0.229345	1.19923
FBgn0031012	*CG8051*	enGFP	enGFP+Tai	0.0523252	0.280324	2.42152
FBgn0032010	*CG8086*	enGFP	enGFP+Tai	0.302694	0.868053	1.51992
FBgn0037616	*CG8136*	enGFP	enGFP+Tai	0.352066	1.48282	2.07442
FBgn0033365	*CG8170*	enGFP	enGFP+Tai	7.24972	25.2091	1.79794
FBgn0033362	*CG8172*	enGFP	enGFP+Tai	1.65893	11.4501	2.78704
FBgn0034021	*CG8180*	enGFP	enGFP+Tai	14.2988	27.8392	0.961223
FBgn0033359	*CG8213*	enGFP	enGFP+Tai	0.501358	19.6264	5.29081
FBgn0030684	*CG8260*	enGFP	enGFP+Tai	0.357318	0.729254	1.02921
FBgn0031999	*CG8419*	enGFP	enGFP+Tai	0.0411344	0.125926	1.61416
FBgn0037664	*CG8420*	enGFP	enGFP+Tai	15.1979	108.291	2.83297
FBgn0038126	*CG8483*	enGFP	enGFP+Tai	17.421	30.5805	0.811787
FBgn0035777	*CG8563*	enGFP	enGFP+Tai	0.626641	2.4579	1.97171
FBgn0030841	*CG8568*	enGFP	enGFP+Tai	0.656507	11.5563	4.13772
FBgn0040837	*CG8620*	enGFP	enGFP+Tai	0.230712	0.66996	1.53798
FBgn0033308	*CG8736*	enGFP	enGFP+Tai	1.11403	8.0145	2.84682
FBgn0033760	*CG8785*	enGFP	enGFP+Tai	0.196273	5.16491	4.71781
FBgn0028955	*CG8788*	enGFP	enGFP+Tai	7.6614	16.4529	1.10266
FBgn0033234	*CG8791*	enGFP	enGFP+Tai	0.306494	0.586427	0.93609
FBgn0033702	*CG8854*	enGFP	enGFP+Tai	1.43594	3.7365	1.3797
FBgn0038405	*CG8927*	enGFP	enGFP+Tai	4.89521	131.998	4.753
FBgn0030815	*CG8945*	enGFP	enGFP+Tai	0.211269	0.831556	1.97673
FBgn0030688	*CG8952*	enGFP	enGFP+Tai	0.179053	0.822214	2.19912
FBgn0035077	*CG9083*	enGFP	enGFP+Tai	0.391906	141.89	8.50005
FBgn0030617	*CG9095*	enGFP	enGFP+Tai	5.13172	23.516	2.19613
FBgn0031762	*CG9098*	enGFP	enGFP+Tai	0.0894082	0.478997	2.42154
FBgn0035189	*CG9119*	enGFP	enGFP+Tai	0.866447	2.27356	1.39177
FBgn0035199	*CG9134*	enGFP	enGFP+Tai	15.6777	42.3563	1.43386
FBgn0035208	*CG9184*	enGFP	enGFP+Tai	0.184418	3.35804	4.18656
FBgn0035193	*CG9192*	enGFP	enGFP+Tai	14.2648	27.8782	0.966678
FBgn0036428	*CG9238*	enGFP	enGFP+Tai	10.5316	32.4421	1.62314
FBgn0038181	*CG9297*	enGFP	enGFP+Tai	0.0324011	0.396915	3.61472
FBgn0038179	*CG9312*	enGFP	enGFP+Tai	7.88694	14.8457	0.912503
FBgn0035094	*CG9380*	enGFP	enGFP+Tai	0.0961867	0.664036	2.78735
FBgn0030569	*CG9411*	enGFP	enGFP+Tai	1.49227	40.9519	4.77835
FBgn0033110	*CG9447*	enGFP	enGFP+Tai	0.376785	0.69208	0.877196
FBgn0036875	*CG9449*	enGFP	enGFP+Tai	0.215268	1.44227	2.74413
FBgn0036877	*CG9452*	enGFP	enGFP+Tai	0.171264	0.393223	1.19912
FBgn0030594	*CG9509*	enGFP	enGFP+Tai	0.174068	0.666138	1.93617
FBgn0266434	*CG9517*	enGFP	enGFP+Tai	0.352426	3.50643	3.31461
FBgn0030590	*CG9518*	enGFP	enGFP+Tai	0.356022	7.30237	4.35833
FBgn0030588	*CG9521*	enGFP	enGFP+Tai	0.372679	3.08046	3.04714
FBgn0030587	*CG9522*	enGFP	enGFP+Tai	0.500261	1.5315	1.6142
FBgn0031821	*CG9542*	enGFP	enGFP+Tai	0.781577	2.63194	1.75167
FBgn0031089	*CG9572*	enGFP	enGFP+Tai	0.339828	3.98483	3.55164
FBgn0036862	*CG9619*	enGFP	enGFP+Tai	1.23395	3.48696	1.49868
FBgn0031515	*CG9664*	enGFP	enGFP+Tai	0.111928	0.642305	2.52069
FBgn0030775	*CG9673*	enGFP	enGFP+Tai	0.181696	0.417249	1.19938
FBgn0030159	*CG9689*	enGFP	enGFP+Tai	73.5602	163.642	1.15354
FBgn0039759	*CG9733*	enGFP	enGFP+Tai	0.883116	1.72725	0.967799
FBgn0039758	*CG9737*	enGFP	enGFP+Tai	0.518846	3.44145	2.72964
FBgn0039756	*CG9743*	enGFP	enGFP+Tai	0.0814396	0.623285	2.93609
FBgn0039754	*CG9747*	enGFP	enGFP+Tai	28.1835	70.0774	1.3141
FBgn0036259	*CG9760*	enGFP	enGFP+Tai	0.134788	0.257896	0.93609
FBgn0034860	*CG9812*	enGFP	enGFP+Tai	6.02692	13.2367	1.13505
FBgn0034861	*CG9815*	enGFP	enGFP+Tai	0.902568	4.82432	2.41822
FBgn0263072	*CG9817*	enGFP	enGFP+Tai	0.0195751	0.0449691	1.19992
FBgn0034490	*CG9864*	enGFP	enGFP+Tai	0.440437	0.943783	1.09952
FBgn0034649	*CG9865*	enGFP	enGFP+Tai	0.000849775	4.20187	12.2717
FBgn0034829	*CG9899*	enGFP	enGFP+Tai	0.0470277	0.143968	1.61416
FBgn0030756	*CG9903*	enGFP	enGFP+Tai	0.261258	0.59985	1.19912
FBgn0039916	*CG9935*	enGFP	enGFP+Tai	0.28194	0.621223	1.13972
FBgn0086758	*chinmo*	enGFP	enGFP+Tai	1.25388	2.45421	0.96886
FBgn0032598	*ChLD3*	enGFP	enGFP+Tai	0.840446	2.25128	1.42152
FBgn0038180	*Cht5*	enGFP	enGFP+Tai	47.2873	146.295	1.62936
FBgn0263132	*Cht6*	enGFP	enGFP+Tai	10.1	25.1794	1.31789

FBgn0035427	*ckd*	enGFP	enGFP+Tai	6.45288	14.9832	1.21533
FBgn0051116	*ClC-a*	enGFP	enGFP+Tai	0.0362819	0.0833067	1.19918
FBgn0000337	*cn*	enGFP	enGFP+Tai	0.0717968	0.219794	1.61416
FBgn0039805	*Cpr100A*	enGFP	enGFP+Tai	0.528993	361.699	9.41732
FBgn0053302	*Cpr31A*	enGFP	enGFP+Tai	1.33735	7.4438	2.47666
FBgn0028871	*Cpr35B*	enGFP	enGFP+Tai	9.18051	50.4606	2.45851
FBgn0033600	*Cpr47Ec*	enGFP	enGFP+Tai	2.71174	19.1973	2.82362
FBgn0033725	*Cpr49Ac*	enGFP	enGFP+Tai	205.257	428.516	1.06192
FBgn0033942	*Cpr51A*	enGFP	enGFP+Tai	34.7036	955.737	4.78346
FBgn0035512	*Cpr64Ac*	enGFP	enGFP+Tai	0.364468	1.25523	1.78409
FBgn0035513	*Cpr64Ad*	enGFP	enGFP+Tai	0.166687	24.2386	7.18402
FBgn0035737	*Cpr65Ec*	enGFP	enGFP+Tai	40.976	361.726	3.14204
FBgn0052029	*Cpr66D*	enGFP	enGFP+Tai	15.9905	28.5555	0.836554
FBgn0036617	*Cpr72Ea*	enGFP	enGFP+Tai	3.13625	242.21	6.27107
FBgn0036618	*Cpr72Eb*	enGFP	enGFP+Tai	0.560193	182.212	8.34548
FBgn0036619	*Cpr72Ec*	enGFP	enGFP+Tai	0.100858	0.231569	1.19912
FBgn0037069	*Cpr78Cc*	enGFP	enGFP+Tai	0.816627	30.9371	5.24352
FBgn0037114	*Cpr78E*	enGFP	enGFP+Tai	16.4812	53.5123	1.69905
FBgn0039480	*Cpr97Ea*	enGFP	enGFP+Tai	1.13846	32.6013	4.83977
FBgn0039481	*Cpr97Eb*	enGFP	enGFP+Tai	0.585833	20.6245	5.13772
FBgn0050009	*CR30009*	enGFP	enGFP+Tai	0.129508	0.297351	1.19912
FBgn0035636	*Cralbp*	enGFP	enGFP+Tai	7.52816	13.5037	0.842981
FBgn0025456	*CREG*	enGFP	enGFP+Tai	10.1491	29.971	1.56222
FBgn0010383	*Cyp18a1*	enGFP	enGFP+Tai	2.34271	65.9587	4.81531
FBgn0033753	*Cyp301a1*	enGFP	enGFP+Tai	5.49949	22.4659	2.03037
FBgn0001992	*Cyp303a1*	enGFP	enGFP+Tai	1.17123	19.9594	4.09098
FBgn0038095	*Cyp304a1*	enGFP	enGFP+Tai	0.737359	1.63026	1.14466
FBgn0033524	*Cyp49a1*	enGFP	enGFP+Tai	0.0881582	0.807283	3.19491
FBgn0005670	*Cyp4d1*	enGFP	enGFP+Tai	0.178594	0.45646	1.3538
FBgn0015034	*Cyp4e1*	enGFP	enGFP+Tai	0.959501	3.30452	1.78409
FBgn0015714	*Cyp6a17*	enGFP	enGFP+Tai	11.0097	37.8822	1.78274
FBgn0033978	*Cyp6a23*	enGFP	enGFP+Tai	1.43645	3.42025	1.25159
FBgn0025454	*Cyp6g1*	enGFP	enGFP+Tai	0.19956	0.661832	1.72964
FBgn0033696	*Cyp6g2*	enGFP	enGFP+Tai	0.624323	6.58324	3.39843
FBgn0033697	*Cyp6t3*	enGFP	enGFP+Tai	0.416006	5.79458	3.80003
FBgn0015039	*Cyp9b2*	enGFP	enGFP+Tai	0.339927	1.04063	1.61416
FBgn0030001	*cyr*	enGFP	enGFP+Tai	0.274582	1.47103	2.42152
FBgn0086907	*Cyt-c-d*	enGFP	enGFP+Tai	0.1878	0.862358	2.19909
FBgn0039286	*dan*	enGFP	enGFP+Tai	0.118228	0.452418	1.93609
FBgn0034136	*Dat*	enGFP	enGFP+Tai	0.489952	2.09939	2.09926
FBgn0031461	*daw*	enGFP	enGFP+Tai	4.62672	16.3135	1.818
FBgn0000422	*Ddc*	enGFP	enGFP+Tai	1.59662	5.98985	1.9075
FBgn0263118	*dei*	enGFP	enGFP+Tai	0.372904	21.4047	5.84298
FBgn0043043	*desat2*	enGFP	enGFP+Tai	0.21511	0.576209	1.42152
FBgn0013810	*Dhc36C*	enGFP	enGFP+Tai	0.0518006	0.190295	1.8772
FBgn0013813	*Dhc98D*	enGFP	enGFP+Tai	0.00787801	0.0964689	3.61416
FBgn0011274	*Dif*	enGFP	enGFP+Tai	3.48639	8.23768	1.24051
FBgn0033885	*DJ-1alpha*	enGFP	enGFP+Tai	0.236505	1.44804	2.61416
FBgn0051361	*dpr17*	enGFP	enGFP+Tai	0.451654	0.806264	0.836034
FBgn0028408	*Drep-2*	enGFP	enGFP+Tai	0.294578	0.625356	1.08603
FBgn0283461	*Drs*	enGFP	enGFP+Tai	3.08138	5.89572	0.93609
FBgn0261799	*dsx-c73A*	enGFP	enGFP+Tai	0.901394	2.55823	1.50492
FBgn0004511	*dy*	enGFP	enGFP+Tai	2.00314	81.7051	5.35009
FBgn0066365	*dyl*	enGFP	enGFP+Tai	0.0495553	64.2149	10.3397
FBgn0036819	*dysb*	enGFP	enGFP+Tai	2.83464	5.22274	0.881642
FBgn0000527	*e*	enGFP	enGFP+Tai	0.167675	1.12287	2.74345
FBgn0020445	*E23*	enGFP	enGFP+Tai	4.5187	20.5583	2.18574
FBgn0000451	*ect*	enGFP	enGFP+Tai	1.56421	262.912	7.393
FBgn0260746	*Ect3*	enGFP	enGFP+Tai	0.864477	6.33259	2.8729
FBgn0000551	*Edg78E*	enGFP	enGFP+Tai	0.327172	317.878	9.92421
FBgn0004554	*Edg91*	enGFP	enGFP+Tai	9.75783	42.8142	2.13346
FBgn0000557	*Ef1alpha100E*	enGFP	enGFP+Tai	12.8931	24.9946	0.95502
FBgn0004592	*Eig71Ee*	enGFP	enGFP+Tai	0.096812	0.889123	3.19912
FBgn0264490	*Eip93F*	enGFP	enGFP+Tai	0.0525396	3.21919	5.93715
FBgn0052072	*Elo68alpha*	enGFP	enGFP+Tai	0.172046	0.526691	1.61416
FBgn0036128	*Elo68beta*	enGFP	enGFP+Tai	0.203639	0.623408	1.61416

FBgn0036319	*Ent3*	enGFP	enGFP+Tai	0.188183	0.396062	1.07359
FBgn0085421	*Epac*	enGFP	enGFP+Tai	0.516459	1.45757	1.49684
FBgn0013953	*Esp*	enGFP	enGFP+Tai	0.114053	1.67729	3.87835
FBgn0037090	*Est-Q*	enGFP	enGFP+Tai	0.381456	0.700659	0.877196
FBgn0262111	*f*	enGFP	enGFP+Tai	0.958167	1.87579	0.96915
FBgn0028379	*fan*	enGFP	enGFP+Tai	0.184973	0.566264	1.61416
FBgn0266084	*Fhos*	enGFP	enGFP+Tai	10.5129	18.3635	0.804682
FBgn0032773	*fon*	enGFP	enGFP+Tai	0.625711	1.4345	1.19698
FBgn0004650	*fs(1)N*	enGFP	enGFP+Tai	0.038645	0.118305	1.61416
FBgn0001078	*ftz-f1*	enGFP	enGFP+Tai	2.69368	12.5792	2.2234
FBgn0026718	*fu12*	enGFP	enGFP+Tai	0.109856	0.269459	1.29445
FBgn0001089	*Gal*	enGFP	enGFP+Tai	2.05697	3.64332	0.824729
FBgn0026077	*Gasp*	enGFP	enGFP+Tai	90.9218	328.121	1.85153
FBgn0030011	*Gbeta5*	enGFP	enGFP+Tai	0.646175	1.20103	0.89427
FBgn0004623	*Gbeta76C*	enGFP	enGFP+Tai	0.195314	0.373701	0.93609
FBgn0035245	*GC*	enGFP	enGFP+Tai	0.170374	0.391238	1.19934
FBgn0035574	*Gef64C*	enGFP	enGFP+Tai	6.95692	17.7035	1.34752
FBgn0267252	*Ggamma30A*	enGFP	enGFP+Tai	0.305257	0.934513	1.61419
FBgn0004618	*gl*	enGFP	enGFP+Tai	0.0441417	0.709477	4.00654
FBgn0001114	*Glt*	enGFP	enGFP+Tai	5.64994	11.6116	1.03926
FBgn0024963	*GluClalpha*	enGFP	enGFP+Tai	0.0592802	0.321144	2.4376
FBgn0041229	*Gr93a*	enGFP	enGFP+Tai	0.298899	0.61002	1.0292
FBgn0001142	*Gs1*	enGFP	enGFP+Tai	5.243	12.6598	1.27179
FBgn0042206	*GstD10*	enGFP	enGFP+Tai	2.96626	5.44843	0.877196
FBgn0010038	*GstD2*	enGFP	enGFP+Tai	0.473921	1.81354	1.93609
FBgn0010039	*GstD3*	enGFP	enGFP+Tai	67.3986	124.081	0.880498
FBgn0010041	*GstD5*	enGFP	enGFP+Tai	0.282022	0.863363	1.61416
FBgn0063492	*GstE8*	enGFP	enGFP+Tai	1.67484	5.67661	1.761
FBgn0063491	*GstE9*	enGFP	enGFP+Tai	0.201638	0.617281	1.61416
FBgn0027790	*GV1*	enGFP	enGFP+Tai	77.1421	146.749	0.92776
FBgn0038435	*Gyc-89Da*	enGFP	enGFP+Tai	0.758478	27.39	5.1744
FBgn0261509	*haf*	enGFP	enGFP+Tai	5.79648	17.182	1.56765
FBgn0045852	*ham*	enGFP	enGFP+Tai	0.079097	0.27241	1.78409
FBgn0005619	*Hdc*	enGFP	enGFP+Tai	0.120622	0.46158	1.93609
FBgn0033448	*hebe*	enGFP	enGFP+Tai	0.211808	4.33468	4.3551
FBgn0041629	*Hexo2*	enGFP	enGFP+Tai	2.62109	5.67555	1.11459
FBgn0041150	*hoe1*	enGFP	enGFP+Tai	0.208234	0.642109	1.62461
FBgn0000448	*Hr46*	enGFP	enGFP+Tai	14.0332	34.8933	1.3141
FBgn0001223	*Hsp22*	enGFP	enGFP+Tai	12.5853	44.7586	1.83043
FBgn0001225	*Hsp26*	enGFP	enGFP+Tai	421.366	898.887	1.09306
FBgn0001229	*Hsp67Bc*	enGFP	enGFP+Tai	3.08355	15.7744	2.35492
FBgn0001230	*Hsp68*	enGFP	enGFP+Tai	22.0086	85.3426	1.9552
FBgn0013277	*Hsp70Ba*	enGFP	enGFP+Tai	0.272274	0.583466	1.09959
FBgn0051354	*Hsp70Bbb*	enGFP	enGFP+Tai	0.207187	1.82353	3.13772
FBgn0013279	*Hsp70Bc*	enGFP	enGFP+Tai	0.623554	11.2365	4.17154
FBgn0020416	*Idgf1*	enGFP	enGFP+Tai	0.191963	0.587664	1.61416
FBgn0020414	*Idgf3*	enGFP	enGFP+Tai	0.518836	3.63595	2.80898
FBgn0013467	*igl*	enGFP	enGFP+Tai	0.144435	0.331595	1.199
FBgn0263397	*Ih*	enGFP	enGFP+Tai	0.229993	5.03841	4.45331
FBgn0001253	*ImpE1*	enGFP	enGFP+Tai	121.927	395.956	1.69932
FBgn0001256	*ImpL1*	enGFP	enGFP+Tai	4.38943	538.287	6.9382
FBgn0001258	*ImpL3*	enGFP	enGFP+Tai	9.63411	29.1727	1.59839
FBgn0001263	*inaD*	enGFP	enGFP+Tai	0.532496	1.13205	1.08809
FBgn0085351	*inaF-A*	enGFP	enGFP+Tai	0.0404531	0.181785	2.16791
FBgn0260812	*inaF-D*	enGFP	enGFP+Tai	0.0750036	0.1723	1.19989
FBgn0036816	*Indy*	enGFP	enGFP+Tai	44.7988	85.5117	0.932661
FBgn0011603	*ine*	enGFP	enGFP+Tai	0.299142	0.914673	1.61243
FBgn0025885	*Inos*	enGFP	enGFP+Tai	68.1117	124.298	0.867823
FBgn0027106	*inx7*	enGFP	enGFP+Tai	1.1908	2.30015	0.9498
FBgn0031634	*Ir25a*	enGFP	enGFP+Tai	0.132384	0.270181	1.0292
FBgn0034456	*Ir56b*	enGFP	enGFP+Tai	0.121578	4.83847	5.3146
FBgn0036150	*Ir68a*	enGFP	enGFP+Tai	0.6477	1.14013	0.815796
FBgn0037630	*Ir85a*	enGFP	enGFP+Tai	0.76767	1.99765	1.37974
FBgn0259193	*Ir94d*	enGFP	enGFP+Tai	0.0785301	0.240407	1.61416
FBgn0032706	*Irk3*	enGFP	enGFP+Tai	0.382616	1.22995	1.68464
FBgn0027654	*jdp*	enGFP	enGFP+Tai	0.805614	5.4629	2.76151

FBgn0028841	*jhamt*	enGFP	enGFP+Tai	0.157717	0.603533	1.93609
FBgn0034406	*Jheh3*	enGFP	enGFP+Tai	0.545277	2.0866	1.93609
FBgn0030334	*Karl*	enGFP	enGFP+Tai	3.00314	8.30563	1.46762
FBgn0011236	*ken*	enGFP	enGFP+Tai	19.1965	39.354	1.03567
FBgn0002522	*lab*	enGFP	enGFP+Tai	0.143719	0.25665	0.836554
FBgn0020637	*Lcp65Ag2*	enGFP	enGFP+Tai	1.46336	23.5191	4.00648
FBgn0286075	*lig3*	enGFP	enGFP+Tai	7.76017	13.951	0.846206
FBgn0023496	*Lip1*	enGFP	enGFP+Tai	0.267504	8.87162	5.05157
FBgn0032264	*Lip4*	enGFP	enGFP+Tai	0.181295	0.414869	1.19431
FBgn0035610	*Lkr*	enGFP	enGFP+Tai	0.226485	0.901353	1.99267
FBgn0002562	*Lsp1alpha*	enGFP	enGFP+Tai	0.605431	1.30582	1.10893
FBgn0002563	*Lsp1beta*	enGFP	enGFP+Tai	1.23636	5.00712	2.01788
FBgn0002576	*lz*	enGFP	enGFP+Tai	0.0851402	0.390973	2.19915
FBgn0002577	*m*	enGFP	enGFP+Tai	5.3511	26.1633	2.28964
FBgn0002578	*m1*	enGFP	enGFP+Tai	0.272049	0.832833	1.61416
FBgn0002645	*Map205*	enGFP	enGFP+Tai	53.4403	99.025	0.889864
FBgn0023549	*Mct1*	enGFP	enGFP+Tai	0.314648	0.65363	1.05473
FBgn0004513	*Mdr65*	enGFP	enGFP+Tai	0.283301	0.505914	0.836554
FBgn0260401	*MED9*	enGFP	enGFP+Tai	0.0338245	45.2911	10.3869
FBgn0004228	*mex1*	enGFP	enGFP+Tai	0.23381	1.34454	2.5237
FBgn0260745	*mfas*	enGFP	enGFP+Tai	78.7062	300.772	1.93412
FBgn0033438	*Mmp2*	enGFP	enGFP+Tai	16.3625	34.2641	1.0663
FBgn0259749	*mmy*	enGFP	enGFP+Tai	21.459	53.5169	1.31841
FBgn0086711	*mol*	enGFP	enGFP+Tai	2.03873	7.44207	1.86803
FBgn0033773	*mos*	enGFP	enGFP+Tai	0.218742	0.418526	0.93609
FBgn0261529	*ms(2)34Fe*	enGFP	enGFP+Tai	0.0799573	0.346766	2.11666
FBgn0011666	*Msi*	enGFP	enGFP+Tai	0.0787648	0.180709	1.19804
FBgn0086681	*Mst36Fa*	enGFP	enGFP+Tai	0.461554	1.05973	1.19912
FBgn0261349	*Mst36Fb*	enGFP	enGFP+Tai	0.366494	0.701227	0.93609
FBgn0035623	*mthl2*	enGFP	enGFP+Tai	0.0675421	0.620308	3.19912
FBgn0010431	*mtrm*	enGFP	enGFP+Tai	0.281527	0.538657	0.93609
FBgn0038642	*Muc91C*	enGFP	enGFP+Tai	0.300598	0.525846	0.806807
FBgn0038492	*Mur89F*	enGFP	enGFP+Tai	1.48391	17.5878	3.5671
FBgn0264272	*mwh*	enGFP	enGFP+Tai	1.29165	3.61526	1.48488
FBgn0029762	*NAAT1*	enGFP	enGFP+Tai	0.108335	0.20728	0.93609
FBgn0266347	*nAcRalpha-80B*	enGFP	enGFP+Tai	0.394265	0.991446	1.33037
FBgn0031261	*nAcRbeta-21C*	enGFP	enGFP+Tai	1.04279	1.95719	0.908339
FBgn0004118	*nAcRbeta-96A*	enGFP	enGFP+Tai	0.0730322	0.376114	2.36457
FBgn0002930	*nec*	enGFP	enGFP+Tai	0.525121	1.27268	1.27714
FBgn0261673	*nemy*	enGFP	enGFP+Tai	7.00932	12.3261	0.814367
FBgn0015773	*NetA*	enGFP	enGFP+Tai	7.92848	14.1274	0.83338
FBgn0015774	*NetB*	enGFP	enGFP+Tai	8.24269	15.337	0.895831
FBgn0265140	*Neu3*	enGFP	enGFP+Tai	18.6053	35.2648	0.922518
FBgn0027929	*nimB1*	enGFP	enGFP+Tai	0.119222	0.638715	2.42152
FBgn0028543	*nimB2*	enGFP	enGFP+Tai	0.100528	0.384688	1.93609
FBgn0028542	*nimB4*	enGFP	enGFP+Tai	0.390628	1.34532	1.78409
FBgn0259896	*nimC1*	enGFP	enGFP+Tai	0.539449	3.66412	2.76391
FBgn0028939	*nimC2*	enGFP	enGFP+Tai	0.116761	0.223393	0.936025
FBgn0053126	*NLaz*	enGFP	enGFP+Tai	0.175981	1.34685	2.93609
FBgn0010399	*Nmdar1*	enGFP	enGFP+Tai	0.0619889	0.142327	1.19912
FBgn0011676	*Nos*	enGFP	enGFP+Tai	0.117896	0.510807	2.11527
FBgn0002962	*nos*	enGFP	enGFP+Tai	0.0578015	0.220925	1.93438
FBgn0038198	*Npc2b*	enGFP	enGFP+Tai	1.00163	7.81911	2.96466
FBgn0004108	*Nrt*	enGFP	enGFP+Tai	28.2188	56.9553	1.01317
FBgn0032946	*nrv3*	enGFP	enGFP+Tai	0.168567	0.383744	1.18682
FBgn0013342	*n-syb*	enGFP	enGFP+Tai	0.103474	0.827647	2.99974
FBgn0261526	*NT1*	enGFP	enGFP+Tai	5.86457	14.7215	1.32783
FBgn0029147	*NtR*	enGFP	enGFP+Tai	1.18255	2.20604	0.899564
FBgn0032123	*Oatp30B*	enGFP	enGFP+Tai	8.75146	15.7757	0.85011
FBgn0284250	*Oaz*	enGFP	enGFP+Tai	0.528656	1.29673	1.29448
FBgn0034470	*Obp56d*	enGFP	enGFP+Tai	1.64358	296.861	7.49681
FBgn0046875	*Obp83g*	enGFP	enGFP+Tai	9.4831	52.1482	2.45919
FBgn0031097	*obst-A*	enGFP	enGFP+Tai	116.742	326.392	1.48328
FBgn0031737	*obst-E*	enGFP	enGFP+Tai	0.158123	7.23951	5.51678
FBgn0015522	*olf186-M*	enGFP	enGFP+Tai	0.804812	1.53988	0.936093
FBgn0026396	*Or22c*	enGFP	enGFP+Tai	0.123778	0.378927	1.61416

FBgn0036019	*Or67b*	enGFP	enGFP+Tai	0.107367	0.574797	2.42051
FBgn0036474	*Or71a*	enGFP	enGFP+Tai	0.133439	0.612754	2.19912
FBgn0037417	*Osi10*	enGFP	enGFP+Tai	0.0811696	0.807599	3.31463
FBgn0040279	*Osi14*	enGFP	enGFP+Tai	5.0102	63.8015	3.67065
FBgn0037410	*Osi2*	enGFP	enGFP+Tai	9.07761	55.4705	2.61134
FBgn0027527	*Osi6*	enGFP	enGFP+Tai	0.0925189	513.499	12.4383
FBgn0037414	*Osi7*	enGFP	enGFP+Tai	0.248426	1132.6	12.1545
FBgn0037416	*Osi9*	enGFP	enGFP+Tai	0.750264	32.9756	5.45786
FBgn0262728	*Pal*	enGFP	enGFP+Tai	0.56128	1.07392	0.93609
FBgn0011279	*Pbprp1*	enGFP	enGFP+Tai	0.371358	1.70528	2.19912
FBgn0030840	*p-cup*	enGFP	enGFP+Tai	0.222128	1.13335	2.35113
FBgn0264815	*Pde1c*	enGFP	enGFP+Tai	0.715307	9.47119	3.72691
FBgn0016694	*Pdp1*	enGFP	enGFP+Tai	5.75782	16.7146	1.53752
FBgn0011695	*PebIII*	enGFP	enGFP+Tai	0.963001	3.93076	2.0292
FBgn0022770	*Peritrophin-A*	enGFP	enGFP+Tai	1.6904	5.45211	1.68945
FBgn0031530	*pgant2*	enGFP	enGFP+Tai	3.38703	13.0515	1.94612
FBgn0035975	*PGRP-LA*	enGFP	enGFP+Tai	1.1608	2.60681	1.16717
FBgn0037906	*PGRP-LB*	enGFP	enGFP+Tai	0.138112	0.408546	1.56466
FBgn0035976	*PGRP-LC*	enGFP	enGFP+Tai	4.54833	23.5148	2.37016
FBgn0260458	*PGRP-LD*	enGFP	enGFP+Tai	0.000299075	0.338997	10.1465
FBgn0030310	*PGRP-SA*	enGFP	enGFP+Tai	0.402061	1.84627	2.19912
FBgn0043575	*PGRP-SC2*	enGFP	enGFP+Tai	0.361542	0.830101	1.19912
FBgn0035089	*Phk-3*	enGFP	enGFP+Tai	455.321	1437.2	1.6583
FBgn0032749	*Phlpp*	enGFP	enGFP+Tai	0.0464421	0.142175	1.61416
FBgn0004959	*phm*	enGFP	enGFP+Tai	1.17795	3.12882	1.40934
FBgn0024315	*Picot*	enGFP	enGFP+Tai	0.437629	0.843786	0.94717
FBgn0003089	*pip*	enGFP	enGFP+Tai	18.358	46.7353	1.34811
FBgn0004872	*piwi*	enGFP	enGFP+Tai	0.689969	2.97032	2.10602
FBgn0000489	*Pka-C3*	enGFP	enGFP+Tai	3.7107	16.7771	2.17673
FBgn0003091	*Pkc53E*	enGFP	enGFP+Tai	0.147212	1.91431	3.70085
FBgn0038603	*PKD*	enGFP	enGFP+Tai	38.4002	71.1567	0.889887
FBgn0005626	*ple*	enGFP	enGFP+Tai	0.239918	7.94798	5.04997
FBgn0063127	*pncr002:3R*	enGFP	enGFP+Tai	141.459	547.946	1.95365
FBgn0020258	*ppk*	enGFP	enGFP+Tai	0.931916	5.32823	2.51538
FBgn0029723	*Proc-R*	enGFP	enGFP+Tai	0.100258	0.177007	0.820091
FBgn0004595	*pros*	enGFP	enGFP+Tai	0.226526	0.592357	1.38679
FBgn0262867	*Ptr*	enGFP	enGFP+Tai	1.96998	19.6225	3.31626
FBgn0262867	*ptr*	enGFP	enGFP+Tai	2.00028	6.75403	1.75555
FBgn0013323	*Ptth*	enGFP	enGFP+Tai	0.153012	0.585527	1.93609
FBgn0031888	*Pvf2*	enGFP	enGFP+Tai	17.0845	29.7772	0.801514
FBgn0028572	*qtc*	enGFP	enGFP+Tai	0.421296	2.11412	2.32715
FBgn0003187	*qua*	enGFP	enGFP+Tai	0.563356	1.75004	1.63527
FBgn0033389	*Rad51D*	enGFP	enGFP+Tai	0.856334	1.52922	0.836554
FBgn0243486	*rdo*	enGFP	enGFP+Tai	29.5938	56.5171	0.933391
FBgn0016715	*Reg-2*	enGFP	enGFP+Tai	4.97185	8.7377	0.813471
FBgn0015801	*Reg-5*	enGFP	enGFP+Tai	27.9628	77.2919	1.46681
FBgn0011829	*Ret*	enGFP	enGFP+Tai	0.982232	1.85839	0.919916
FBgn0004795	*retn*	enGFP	enGFP+Tai	0.0905573	0.161785	0.837173
FBgn0051719	*RluA-1*	enGFP	enGFP+Tai	0.0429999	0.0987525	1.19948
FBgn0022981	*rpk*	enGFP	enGFP+Tai	6.01484	13.2897	1.14371
FBgn0037742	*Rpt3R*	enGFP	enGFP+Tai	4.59888	8.2908	0.850229
FBgn0003292	*rt*	enGFP	enGFP+Tai	14.3372	38.2506	1.41572
FBgn0003295	*ru*	enGFP	enGFP+Tai	1.16166	2.13377	0.877209
FBgn0003312	*sad*	enGFP	enGFP+Tai	1.97459	3.56648	0.852949
FBgn0003319	*Sb*	enGFP	enGFP+Tai	21.1749	54.196	1.35583
FBgn0033033	*scaf*	enGFP	enGFP+Tai	32.6065	74.523	1.19253
FBgn0025391	*Scgdelta*	enGFP	enGFP+Tai	3.38653	6.66395	0.976571
FBgn0020907	*Scp2*	enGFP	enGFP+Tai	0.11553	0.353676	1.61416
FBgn0260653	*serp*	enGFP	enGFP+Tai	91.0813	261.982	1.52424
FBgn0010414	*SerT*	enGFP	enGFP+Tai	0.954705	1.96963	1.0448
FBgn0003366	*sev*	enGFP	enGFP+Tai	0.20171	0.407994	1.01626
FBgn0003372	*Sgs1*	enGFP	enGFP+Tai	0.0329438	0.075639	1.19912
FBgn0003373	*Sgs3*	enGFP	enGFP+Tai	0.274925	1.57807	2.52105
FBgn0003374	*Sgs4*	enGFP	enGFP+Tai	0.185736	0.42645	1.19912
FBgn0003375	*Sgs5*	enGFP	enGFP+Tai	0.292059	0.670568	1.19912
FBgn0003382	*sha*	enGFP	enGFP+Tai	0.0790868	2.28127	4.85025

FBgn0005564	*Shal*	enGFP	enGFP+Tai	0.154739	0.518555	1.74466
FBgn0003388	*shd*	enGFP	enGFP+Tai	0.685084	1.72276	1.33037
FBgn0016061	*Side*	enGFP	enGFP+Tai	0.0623741	0.143211	1.19912
FBgn0029761	*SK*	enGFP	enGFP+Tai	0.85696	2.97355	1.79489
FBgn0037203	*slif*	enGFP	enGFP+Tai	1.36074	2.80385	1.04302
FBgn0033657	*Sln*	enGFP	enGFP+Tai	0.0332553	0.229063	2.78409
FBgn0002941	*slou*	enGFP	enGFP+Tai	0.192073	0.477751	1.3146
FBgn0035539	*slow*	enGFP	enGFP+Tai	29.4941	52.0538	0.819578
FBgn0003435	*sm*	enGFP	enGFP+Tai	7.86392	27.5383	1.80812
FBgn0003448	*sna*	enGFP	enGFP+Tai	0.252505	0.515335	1.0292
FBgn0065088	*snmRNA:641*	enGFP	enGFP+Tai	114.704	234.099	1.0292
FBgn0083008	*snoRNA:Psi28S-1135e*	enGFP	enGFP+Tai	26.7092	61.3244	1.19912
FBgn0083006	*snoRNA:Psi28S-1153*	enGFP	enGFP+Tai	60.7296	116.196	0.93609
FBgn0082989	*snoRNA:Psi28S-2442a*	enGFP	enGFP+Tai	44.4171	101.982	1.19912
FBgn0034070	*SP2353*	enGFP	enGFP+Tai	0.19888	0.418576	1.07359
FBgn0260470	*SP555*	enGFP	enGFP+Tai	0.117379	0.232938	0.988773
FBgn0003475	*spir*	enGFP	enGFP+Tai	4.09521	7.67213	0.90569
FBgn0039795	*Spn100A*	enGFP	enGFP+Tai	74.7426	269.879	1.85231
FBgn0003486	*spo*	enGFP	enGFP+Tai	0.59375	1.32194	1.15473
FBgn0003495	*spz*	enGFP	enGFP+Tai	1.92811	4.74228	1.29839
FBgn0031959	*spz3*	enGFP	enGFP+Tai	10.4885	18.515	0.819888
FBgn0032362	*spz4*	enGFP	enGFP+Tai	0.158578	12.3792	6.28659
FBgn0035056	*spz6*	enGFP	enGFP+Tai	12.8216	26.5407	1.04963
FBgn0014033	*Sr-CI*	enGFP	enGFP+Tai	0.474096	1.86604	1.97673
FBgn0003507	*srp*	enGFP	enGFP+Tai	0.466224	1.08659	1.22071
FBgn0003527	*stil*	enGFP	enGFP+Tai	0.127233	0.292126	1.19912
FBgn0004242	*Syt1*	enGFP	enGFP+Tai	0.26146	0.949707	1.86089
FBgn0041092	*tai*	enGFP	enGFP+Tai	27.1148	879.1	5.01887
FBgn0259730	*tal-1A*	enGFP	enGFP+Tai	0.332533	53.7417	7.3364
FBgn0259733	*tal-AA*	enGFP	enGFP+Tai	17.5923	181.326	3.36558
FBgn0266579	*tau*	enGFP	enGFP+Tai	0.262254	0.702492	1.42152
FBgn0050446	*Tdc2*	enGFP	enGFP+Tai	0.0592802	0.136107	1.19912
FBgn0026760	*Tehao*	enGFP	enGFP+Tai	0.0309555	0.0710738	1.19912
FBgn0041183	*TepI*	enGFP	enGFP+Tai	0.122925	0.235197	0.93609
FBgn0014073	*Tie*	enGFP	enGFP+Tai	4.54605	9.57378	1.07447
FBgn0025879	*Timp*	enGFP	enGFP+Tai	6.95643	13.0471	0.907312
FBgn0003710	*tipE*	enGFP	enGFP+Tai	0.054492	0.382696	2.81208
FBgn0028397	*Tob*	enGFP	enGFP+Tai	0.0462661	0.519306	3.48856
FBgn0028396	*TotA*	enGFP	enGFP+Tai	0.333164	3.05978	3.19912
FBgn0050035	*Tret1-1*	enGFP	enGFP+Tai	1.00778	4.8036	2.25294
FBgn0033644	*Tret1-2*	enGFP	enGFP+Tai	0.0936693	0.358575	1.93663
FBgn0051721	*Trim9*	enGFP	enGFP+Tai	4.59815	11.56	1.33002
FBgn0003751	*trk*	enGFP	enGFP+Tai	0.869199	1.66307	0.93609
FBgn0022355	*Tsf1*	enGFP	enGFP+Tai	13.4673	27.0296	1.00508
FBgn0034094	*Tsf3*	enGFP	enGFP+Tai	1.26399	7.29927	2.52977
FBgn0032074	*Tsp29Fa*	enGFP	enGFP+Tai	0.600116	1.95205	1.70168
FBgn0032075	*Tsp29Fb*	enGFP	enGFP+Tai	0.136054	2.18717	4.00682
FBgn0029507	*Tsp42Ed*	enGFP	enGFP+Tai	0.782571	1.91657	1.29223
FBgn0029837	*Tsp5D*	enGFP	enGFP+Tai	0.41905	1.60355	1.93607
FBgn0035936	*Tsp66E*	enGFP	enGFP+Tai	22.877	57.5285	1.33038
FBgn0043550	*Tsp68C*	enGFP	enGFP+Tai	1.81938	3.32068	0.868034
FBgn0033658	*TwdlBeta*	enGFP	enGFP+Tai	1.2372	64.5766	5.70586
FBgn0031957	*TwdlE*	enGFP	enGFP+Tai	9.58206	280.589	4.87198
FBgn0029170	*TwdlT*	enGFP	enGFP+Tai	1.66642	205.066	6.94319
FBgn0031758	*Ucp4B*	enGFP	enGFP+Tai	0.866027	2.63316	1.60431
FBgn0031757	*Ucp4C*	enGFP	enGFP+Tai	0.129508	0.396468	1.61416
FBgn0026315	*Ugt35a*	enGFP	enGFP+Tai	1.02154	1.92448	0.913722
FBgn0040260	*Ugt36Bc*	enGFP	enGFP+Tai	0.215095	0.384148	0.836688
FBgn0053519	*Unc-89*	enGFP	enGFP+Tai	0.198509	0.349433	0.815812
FBgn0030904	*upd2*	enGFP	enGFP+Tai	0.411011	1.25824	1.61416
FBgn0053542	*upd3*	enGFP	enGFP+Tai	0.367723	0.797388	1.11666
FBgn0034225	*veil*	enGFP	enGFP+Tai	0.401508	1.84373	2.19912
FBgn0053200	*VepD*	enGFP	enGFP+Tai	0.930876	3.20594	1.78409
FBgn0261341	*verm*	enGFP	enGFP+Tai	258.856	720.115	1.47608
FBgn0043841	*vir-1*	enGFP	enGFP+Tai	25.1021	57.5679	1.19745
FBgn0016076	*vri*	enGFP	enGFP+Tai	27.1431	53.1575	0.969688

FBgn0037750	*Whamy*	enGFP	enGFP+Tai	0.0756789	0.231684	1.61419
FBgn0030805	*wus*	enGFP	enGFP+Tai	30.7068	61.22	0.995445
FBgn0052677	*X11Lbeta*	enGFP	enGFP+Tai	0.235893	0.464238	0.976732
FBgn0004034	*y*	enGFP	enGFP+Tai	0.0675921	1.08496	4.00464
FBgn0032601	*yellow-b*	enGFP	enGFP+Tai	7.4991	17.2832	1.20458
FBgn0041712	*yellow-d*	enGFP	enGFP+Tai	3.59176	6.87224	0.93609
FBgn0041710	*yellow-f*	enGFP	enGFP+Tai	0.402112	1.69263	2.07359
FBgn0039896	*yellow-h*	enGFP	enGFP+Tai	5.3541	11.1954	1.06419
FBgn0265575	*yin*	enGFP	enGFP+Tai	0.902413	7.61696	3.07736
FBgn0005391	*Yp2*	enGFP	enGFP+Tai	0.275898	0.492692	0.836554

Table 4. Overlap between the group of candidate Tai-induced mRNAs and the predicted *Drosophila* secretome (supporting Fig. 3). Alphabetical gene list of mRNAs with FPKM log[2]Δ>0.8 between *en>GFP* and *en>tai,GFP* that are also present in the predicted *Drosophila* secretome (from reference [44]).

Flybase id	Gene	Sample 1	Sample 2	value 1 (FPKM)	value 2 (FPKM)	log2(Δ)
FBgn0000551	*Edg78E*	enGFP	enGFP+Tai	0.327172	317.878	9.92421
FBgn0039805	*Cpr100A*	enGFP	enGFP+Tai	0.528993	361.699	9.41732
FBgn0036618	*Cpr72Eb*	enGFP	enGFP+Tai	0.560193	182.212	8.34548
FBgn0034470	*Obp56d*	enGFP	enGFP+Tai	1.64358	296.861	7.49681
FBgn0035513	*Cpr64Ad*	enGFP	enGFP+Tai	0.166687	24.2386	7.18402
FBgn0250862	*CG42237*	enGFP	enGFP+Tai	0.202046	27.37	7.08177
FBgn0029170	*TwdlT*	enGFP	enGFP+Tai	1.66642	205.066	6.94319
FBgn0001256	*ImpL1*	enGFP	enGFP+Tai	4.38943	538.287	6.9382
FBgn0004780	*Ccp84Ad*	enGFP	enGFP+Tai	0.241138	25.4681	6.72269
FBgn0032362	*spz4*	enGFP	enGFP+Tai	0.158578	12.3792	6.28659
FBgn0036617	*Cpr72Ea*	enGFP	enGFP+Tai	3.13625	242.21	6.27107
FBgn0051145	*CG31145*	enGFP	enGFP+Tai	0.0857501	4.60372	5.74652
FBgn0033658	*TwdlBeta*	enGFP	enGFP+Tai	1.2372	64.5766	5.70586
FBgn0031737	*obst-E*	enGFP	enGFP+Tai	0.158123	7.23951	5.51678
FBgn0033359	*CG8213*	enGFP	enGFP+Tai	0.501358	19.6264	5.29081
FBgn0034301	*CG5756*	enGFP	enGFP+Tai	0.150146	5.86994	5.2889
FBgn0029838	*CG4666*	enGFP	enGFP+Tai	0.29084	11.1295	5.25802
FBgn0037069	*Cpr78Cc*	enGFP	enGFP+Tai	0.816627	30.9371	5.24352
FBgn0039481	*Cpr97Eb*	enGFP	enGFP+Tai	0.585833	20.6245	5.13772
FBgn0039297	*CG11852*	enGFP	enGFP+Tai	1.95275	67.7126	5.11585
FBgn0004783	*Ccp84Aa*	enGFP	enGFP+Tai	0.445613	15.3469	5.10602
FBgn0037290	*CG1124*	enGFP	enGFP+Tai	0.13402	4.5131	5.07359
FBgn0023496	*Lip1*	enGFP	enGFP+Tai	0.267504	8.87162	5.05157
FBgn0031957	*TwdlE*	enGFP	enGFP+Tai	9.58206	280.589	4.87198
FBgn0039480	*Cpr97Ea*	enGFP	enGFP+Tai	1.13846	32.6013	4.83977
FBgn0033942	*Cpr51A*	enGFP	enGFP+Tai	34.7036	955.737	4.78346
FBgn0020637	*Lcp65Ag2*	enGFP	enGFP+Tai	1.46336	23.5191	4.00648
FBgn0004034	*y*	enGFP	enGFP+Tai	0.0675921	1.08496	4.00464
FBgn0259226	*CG42326*	enGFP	enGFP+Tai	0.36257	5.62436	3.95536
FBgn0264815	*Pde1c*	enGFP	enGFP+Tai	0.715307	9.47119	3.72691
FBgn0051004	*CG31004*	enGFP	enGFP+Tai	0.0324477	0.397159	3.61353
FBgn0038492	*Mur89F*	enGFP	enGFP+Tai	1.48391	17.5878	3.5671
FBgn0051973	*Cda5*	enGFP	enGFP+Tai	1.5626	16.5565	3.40537
FBgn0030493	*CG15756*	enGFP	enGFP+Tai	24.71	250.128	3.3395
FBgn0004782	*Ccp84Ab*	enGFP	enGFP+Tai	0.396776	3.94766	3.3146
FBgn0004592	*Eig71Ee*	enGFP	enGFP+Tai	0.096812	0.889123	3.19912
FBgn0028396	*TotA*	enGFP	enGFP+Tai	0.333164	3.05978	3.19912
FBgn0035623	*mthl2*	enGFP	enGFP+Tai	0.0675421	0.620308	3.19912
FBgn0035737	*Cpr65Ec*	enGFP	enGFP+Tai	40.976	361.726	3.14204
FBgn0034788	*CG13532*	enGFP	enGFP+Tai	0.0765759	0.644668	3.07359
FBgn0038198	*Npc2b*	enGFP	enGFP+Tai	1.00163	7.81911	2.96466
FBgn0039203	*CG13618*	enGFP	enGFP+Tai	0.763163	5.84075	2.93609
FBgn0053126	*NLaz*	enGFP	enGFP+Tai	0.175981	1.34685	2.93609
FBgn0040601	*CG13643*	enGFP	enGFP+Tai	0.102472	0.745044	2.86209
FBgn0039482	*CG14258*	enGFP	enGFP+Tai	0.537942	3.84259	2.83655
FBgn0037664	*CG8420*	enGFP	enGFP+Tai	15.1979	108.291	2.83297
FBgn0033600	*Cpr47Ec*	enGFP	enGFP+Tai	2.71174	19.1973	2.82362
FBgn0020414	*Idgf3*	enGFP	enGFP+Tai	0.518836	3.63595	2.80898
FBgn0036690	*dIlp8*	enGFP	enGFP+Tai	0.188082	1.29551	2.78409
FBgn0036875	*CG9449*	enGFP	enGFP+Tai	0.215268	1.44227	2.74413
FBgn0263109	*CG12551*	enGFP	enGFP+Tai	3.57902	21.0001	2.55276
FBgn0034094	*Tsf3*	enGFP	enGFP+Tai	1.26399	7.29927	2.52977
FBgn0003373	*Sgs3*	enGFP	enGFP+Tai	0.274925	1.57807	2.52105
FBgn0264979	*CG4267*	enGFP	enGFP+Tai	0.222297	1.27599	2.52105
FBgn0053302	*Cpr31A*	enGFP	enGFP+Tai	1.33735	7.4438	2.47666
FBgn0046875	*Obp83g*	enGFP	enGFP+Tai	9.4831	52.1482	2.45919
FBgn0028871	*Cpr35B*	enGFP	enGFP+Tai	9.18051	50.4606	2.45851
FBgn0024963	*GluClalpha*	enGFP	enGFP+Tai	0.0592802	0.321144	2.4376

FBgn0027929	*nimB1*	enGFP	enGFP+Tai	0.119222	0.638715	2.42152
FBgn0039299	*CG11854*	enGFP	enGFP+Tai	0.772745	4.02158	2.3797
FBgn0002577	*m*	enGFP	enGFP+Tai	5.3511	26.1633	2.28964
FBgn0011279	*Pbprp1*	enGFP	enGFP+Tai	0.371358	1.70528	2.19912
FBgn0030310	*PGRP-SA*	enGFP	enGFP+Tai	0.402061	1.84627	2.19912
FBgn0039527	*CG5639*	enGFP	enGFP+Tai	4.24967	19.047	2.16414
FBgn0004554	*Edg91*	enGFP	enGFP+Tai	9.75783	42.8142	2.13346
FBgn0038498	*beat-IIa*	enGFP	enGFP+Tai	0.221992	0.951431	2.09959
FBgn0041710	*yellow-f*	enGFP	enGFP+Tai	0.402112	1.69263	2.07359
FBgn0050197	*CG30197*	enGFP	enGFP+Tai	7.44701	31.347	2.07359
FBgn0002563	*Lsp1beta*	enGFP	enGFP+Tai	1.23636	5.00712	2.01788
FBgn0013323	*Ptth*	enGFP	enGFP+Tai	0.153012	0.585527	1.93609
FBgn0028543	*nimB2*	enGFP	enGFP+Tai	0.100528	0.384688	1.93609
FBgn0034200	*CG11395*	enGFP	enGFP+Tai	0.0946531	0.362206	1.93609
FBgn0036459	*CG3349*	enGFP	enGFP+Tai	0.0609232	0.233133	1.93609
FBgn0037036	*CG10586*	enGFP	enGFP+Tai	0.368285	1.40931	1.93609
FBgn0038173	*Adgf-C*	enGFP	enGFP+Tai	0.0807451	0.308985	1.93609
FBgn0038250	*CG3505*	enGFP	enGFP+Tai	0.390167	1.49304	1.93609
FBgn0034005	*alphaPS4*	enGFP	enGFP+Tai	0.0786319	0.300775	1.9355
FBgn0260745	*mfas*	enGFP	enGFP+Tai	78.7062	300.772	1.93412
FBgn0034162	*CG6426*	enGFP	enGFP+Tai	7.47529	28.0518	1.90789
FBgn0036752	*Adgf-A*	enGFP	enGFP+Tai	0.67538	2.46474	1.86766
FBgn0039795	*Spn100A*	enGFP	enGFP+Tai	74.7426	269.879	1.85231
FBgn0026077	*Gasp*	enGFP	enGFP+Tai	90.9218	328.121	1.85153
FBgn0031461	*daw*	enGFP	enGFP+Tai	4.62672	16.3135	1.818
FBgn0052354	*CG32354*	enGFP	enGFP+Tai	3.43305	11.9348	1.79761
FBgn0028542	*nimB4*	enGFP	enGFP+Tai	0.390628	1.34532	1.78409
FBgn0035512	*Cpr64Ac*	enGFP	enGFP+Tai	0.364468	1.25523	1.78409
FBgn0031426	*CG18641*	enGFP	enGFP+Tai	0.680474	2.29148	1.75167
FBgn0086782	*amn*	enGFP	enGFP+Tai	0.0987785	0.327594	1.72964
FBgn0037114	*Cpr78E*	enGFP	enGFP+Tai	16.4812	53.5123	1.69905
FBgn0022770	*Peritrophin-A*	enGFP	enGFP+Tai	1.6904	5.45211	1.68945
FBgn0032136	*CG15828*	enGFP	enGFP+Tai	0.0470056	0.151095	1.68455
FBgn0035089	*Phk-3*	enGFP	enGFP+Tai	455.321	1437.2	1.6583
FBgn0038180	*Cht5*	enGFP	enGFP+Tai	47.2873	146.295	1.62936
FBgn0054051	*CG34051*	enGFP	enGFP+Tai	0.221809	0.680518	1.61732
FBgn0002578	*m1*	enGFP	enGFP+Tai	0.272049	0.832833	1.61416
FBgn0004650	*fs(1)N*	enGFP	enGFP+Tai	0.038645	0.118305	1.61416
FBgn0020416	*Idgf1*	enGFP	enGFP+Tai	0.191963	0.587664	1.61416
FBgn0030270	*CG15199*	enGFP	enGFP+Tai	0.545303	1.66936	1.61416
FBgn0030904	*upd2*	enGFP	enGFP+Tai	0.411011	1.25824	1.61416
FBgn0031869	*CG18304*	enGFP	enGFP+Tai	0.0658316	0.201533	1.61416
FBgn0037107	*CG7166*	enGFP	enGFP+Tai	0.0378578	0.115895	1.61416
FBgn0037906	*PGRP-LB*	enGFP	enGFP+Tai	0.138112	0.408546	1.56466
FBgn0263109	*CG14470*	enGFP	enGFP+Tai	5.32087	15.4356	1.53653
FBgn0034417	*CG15117*	enGFP	enGFP+Tai	0.0616181	0.177657	1.52767
FBgn0260653	*serp*	enGFP	enGFP+Tai	91.0813	261.982	1.52424
FBgn0038494	*beat-IIb*	enGFP	enGFP+Tai	0.834953	2.39009	1.5173
FBgn0261799	*dsx-c73A*	enGFP	enGFP+Tai	0.901394	2.55823	1.50492
FBgn0031097	*obst-A*	enGFP	enGFP+Tai	116.742	326.392	1.48328
FBgn0261341	*verm*	enGFP	enGFP+Tai	258.856	720.115	1.47608
FBgn0030884	*CG6847*	enGFP	enGFP+Tai	4.47788	12.4533	1.47564
FBgn0032598	*ChLD3*	enGFP	enGFP+Tai	0.840446	2.25128	1.42152
FBgn0261526	*NT1*	enGFP	enGFP+Tai	5.86457	14.7215	1.32783
FBgn0029708	*CG3556*	enGFP	enGFP+Tai	0.613107	1.53567	1.32466
FBgn0263132	*Cht6*	enGFP	enGFP+Tai	10.1	25.1794	1.31789
FBgn0003495	*spz*	enGFP	enGFP+Tai	1.92811	4.74228	1.29839
FBgn0022770	*CG31559*	enGFP	enGFP+Tai	3.52591	8.62461	1.29046
FBgn0002930	*nec*	enGFP	enGFP+Tai	0.525121	1.27268	1.27714
FBgn0037487	*CG14608*	enGFP	enGFP+Tai	0.389385	0.943698	1.27713
FBgn0250839	*CG2016*	enGFP	enGFP+Tai	41.8109	99.4263	1.24975
FBgn0029720	*CG3009*	enGFP	enGFP+Tai	1.13776	2.66169	1.22615
FBgn0035427	*ckd*	enGFP	enGFP+Tai	6.45288	14.9832	1.21533
FBgn0003372	*Sgs1*	enGFP	enGFP+Tai	0.0329438	0.075639	1.19912
FBgn0003374	*Sgs4*	enGFP	enGFP+Tai	0.185736	0.42645	1.19912
FBgn0003375	*Sgs5*	enGFP	enGFP+Tai	0.292059	0.670568	1.19912

FBgn0010399	*Nmdar1*	enGFP	enGFP+Tai	0.0619889	0.142327	1.19912
FBgn0032612	*CG13282*	enGFP	enGFP+Tai	0.251816	0.57817	1.19912
FBgn0033868	*CG13340*	enGFP	enGFP+Tai	0.0645323	0.148166	1.19912
FBgn0036619	*Cpr72Ec*	enGFP	enGFP+Tai	0.100858	0.231569	1.19912
FBgn0036877	*CG9452*	enGFP	enGFP+Tai	0.171264	0.393223	1.19912
FBgn0039798	*CG11313*	enGFP	enGFP+Tai	0.103486	0.237604	1.19912
FBgn0043575	*PGRP-SC2*	enGFP	enGFP+Tai	0.361542	0.830101	1.19912
FBgn0032773	*fon*	enGFP	enGFP+Tai	0.625711	1.4345	1.19698
FBgn0033033	*scaf*	enGFP	enGFP+Tai	32.6065	74.523	1.19253
FBgn0053542	*upd3*	enGFP	enGFP+Tai	0.367723	0.797388	1.11666
FBgn0041629	*Hexo2*	enGFP	enGFP+Tai	2.62109	5.67555	1.11459
FBgn0002562	*Lsp1alpha*	enGFP	enGFP+Tai	0.605431	1.30582	1.10893
FBgn0027611	*CG6206*	enGFP	enGFP+Tai	7.18691	15.3266	1.09259
FBgn0034070	*SP2353*	enGFP	enGFP+Tai	0.19888	0.418576	1.07359
FBgn0033438	*Mmp2*	enGFP	enGFP+Tai	16.3625	34.2641	1.0663
FBgn0033725	*Cpr49Ac*	enGFP	enGFP+Tai	205.257	428.516	1.06192
FBgn0035056	*spz6*	enGFP	enGFP+Tai	12.8216	26.5407	1.04963
FBgn0001114	*Glt*	enGFP	enGFP+Tai	5.64994	11.6116	1.03926
FBgn0031634	*Ir25a*	enGFP	enGFP+Tai	0.132384	0.270181	1.0292
FBgn0034638	*CG10433*	enGFP	enGFP+Tai	2.45838	5.01521	1.0286
FBgn0022355	*Tsf1*	enGFP	enGFP+Tai	13.4673	27.0296	1.00508
FBgn0003751	*trk*	enGFP	enGFP+Tai	0.869199	1.66307	0.93609
FBgn0041183	*TepI*	enGFP	enGFP+Tai	0.122925	0.235197	0.93609
FBgn0283461	*Drs*	enGFP	enGFP+Tai	3.08138	5.89572	0.93609
FBgn0034154	*CG5267*	enGFP	enGFP+Tai	0.484329	0.926387	0.93563
FBgn0265140	*Neu3*	enGFP	enGFP+Tai	18.6053	35.2648	0.92252
FBgn0025879	*Timp*	enGFP	enGFP+Tai	6.95643	13.0471	0.90731
FBgn0015774	*NetB*	enGFP	enGFP+Tai	8.24269	15.337	0.89583
FBgn0005391	*Yp2*	enGFP	enGFP+Tai	0.275898	0.492692	0.83655
FBgn0052029	*Cpr66D*	enGFP	enGFP+Tai	15.9905	28.5555	0.83655
FBgn0015773	*NetA*	enGFP	enGFP+Tai	7.92848	14.1274	0.83338
FBgn0031959	*spz3*	enGFP	enGFP+Tai	10.4885	18.515	0.81989
FBgn0038126	*CG8483*	enGFP	enGFP+Tai	17.421	30.5805	0.81179
FBgn0036154	*CG6168*	enGFP	enGFP+Tai	1.02156	1.78705	0.80681
FBgn0038642	*Muc91C*	enGFP	enGFP+Tai	0.300598	0.525846	0.80681